CHAPTER 2

MODELING THE AIRCRAFT

2.1 INTRODUCTION

Model building is a fundamental process. An aircraft designer has a mental model of the type of aircraft that is needed, uses physical models to gather wind tunnel data, and designs with mathematical models that incorporate the experimental data. The modeling process is often iterative; a mathematical model based on the laws of physics will suggest what experimental data should be taken, and the model may then undergo considerable refinement in order to fit the data. In building the mathematical model we recognize the onset of the law of diminishing returns and build a model that is good enough for our purposes but has known limitations. Some of these limitations involve uncertainty in the values of parameters. Later we attempt to characterize this uncertainty mathematically and allow for it in control system design.

Actually, because of the high cost of building and flight testing a real aircraft, the importance of the mathematical models goes far beyond design. The mathematical model is used, in conjunction with computer simulation, to evaluate the performance of the prototype aircraft and hence improve the design. It can also be used to drive training simulators, to reconstruct the flight conditions involved in accidents, and to study the effects of modifications to the design. Furthermore, mathematical models are used in all aspects of the aircraft design (e.g., structural models for studying stress distribution and predicting fatigue life).

All of the chapters following this one will make use of the mathematical models presented in this chapter in some form and thus demonstrate the importance of modeling in the design of aircraft control systems. The rigid-body equations of motion that were derived in Chapter 1 form the skeleton of the aircraft model. In this chapter we add some muscles to the skeleton by modeling the aerodynamic forces and moments

Aircraft Control and Simulation: Dynamics, Controls Design, and Autonomous Systems, Third Edition.
Brian L. Stevens, Frank L. Lewis, Eric N. Johnson.

that drive the equations. By the end of the chapter we will have the capability, given the basic aerodynamic data, to build mathematical models that can be used for computer simulation or for control systems design. We start by considering some basic elements of aerodynamics.

2.2 BASIC AERODYNAMICS

In the aerospace industry it is necessary for a wide range of specialists to work together; thus flight control engineers must be able to work with the aerodynamicists as well as with structural and propulsion engineers. Each must have some understanding of the terms and mathematical models used by the other. This is becoming increasingly important as designers seek to widen aircraft performance envelopes by integrating the many parts of the whole design process. Furthermore, at the prototype stage the controls designer must work closely with the test pilots to make the final adjustments to the control systems. This may take many hours of simulator time and flight testing.

Airfoil Section Aerodynamics

The mathematical model used by the control engineer will usually contain aerodynamic data for the aircraft as a whole. However, to gain the necessary insight, we start by examining the aerodynamic forces on an airfoil.

Figure 2.2-1 shows the cross section of an airfoil (a theoretical body of infinite length shaped to produce lift when placed in an airflow) and defines some of the terms used. The flowfield around the airfoil is represented by the *streamlines* shown in the figure (for a steady flow, the flow direction at any point is tangential to the streamline passing through that point). The figure illustrates attached flow, that is, the streamlines follow the surface of the airfoil and do not reverse direction anywhere over the surface. This is a two-dimensional situation; the cross section is constant and the length of this airfoil is infinite, so that the flowfield does not change in the direction perpendicular to the plane of the diagram. The initial direction of the flowfield is defined

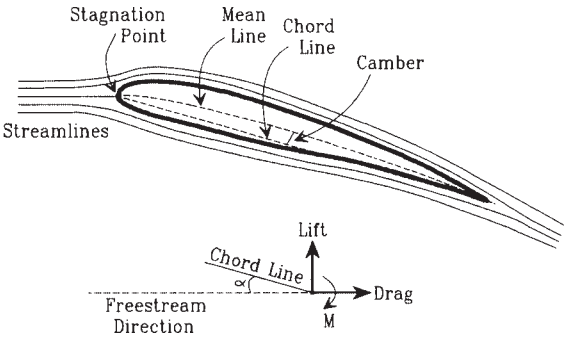

Figure 2.2-1 Definitions associated with an airfoil.

by the freestream velocity vector. This is the velocity measured ahead of the airfoil at a sufficient distance that the flow there is unaffected by the presence of the airfoil.

The shape of the airfoil determines its aerodynamic properties, and some of the important geometrical parameters are shown in the figure. The *chord line* is a straight line drawn from the leading edge to the trailing edge and is the reference line for describing the shape. An airfoil may be symmetric or, more usually, asymmetric with respect to the chord line. The *mean line* (or *camber line*) is a line joining the leading edge to the trailing edge and having a desired shape. The airfoil is constructed on this camber line by drawing perpendiculars and placing the upper and lower surfaces equal distances above and below the camber line according to a chosen distribution of airfoil thickness. The shape of the camber line, the thickness distribution, and the leading-edge radius combine to determine the aerodynamic properties and the useful speed range.

Two different physical mechanisms contribute to producing an aerodynamic force. First, each element of surface area, multiplied by the pressure at that position, leads to an elemental force normal to the airfoil surface. When this calculation is integrated over the whole surface, the resultant force is, in general, nonzero, except, for example, in the idealized case of laminar flow around a symmetrical airfoil pointed directly into the flow. Second, for each element of surface area there is a layer of the fluid (air) in contact with the surface and not moving relative to the surface. When the flow is laminar, we can visualize layers of fluid farther from the surface moving progressively faster, and the molecular forces between layers, per unit area, constitute the *shear stress*. Shear stress multiplied by the element of area leads to an elemental force tangential to the surface. When the shear forces are integrated over the whole surface, the resultant force is defined to be the *skin friction*. The skin friction force will be proportional to the *wetted area* (area in contact with the fluid) of the airfoil. When the flow is *turbulent* (i.e., the motion at any point is irregular and eddies are formed) over some or all of the airfoil surface, the physical mechanism is harder to visualize but we still define a skin friction force, although the mathematical model is different. The combination of the pressure force and the skin friction force is the resultant aerodynamic force on the airfoil.

Now imagine that the airfoil is pivoted about an axis perpendicular to the cross section, passing through the chord line at an arbitrary distance back from the leading edge. The angle that the chord line makes with the freestream velocity vector is the airfoil *angle of attack*, usually denoted by α (hereinafter referred to as "alpha") and shown as a positive quantity in the figure. In our hypothetical experiment, let the freestream velocity vector be constant in magnitude and direction and the ambient temperature and pressure be constant. In this situation, the only remaining variable that influences the aerodynamic forces is alpha. Also, elementary mechanics tells us that in this situation the aerodynamic effects can be represented by a force acting at the axis and normal to it (because of symmetry) and a couple acting around the axis.

The aerodynamic force is conventionally resolved into two perpendicular components, the *lift* and *drag* components, shown in the figure. Lift is defined to be perpendicular to the freestream velocity vector, and drag is parallel to it. Lift and

drag normally increase as alpha is increased. An aerodynamic moment is also indicated in the figure, and the positive reference direction is shown there. By definition, the moment is zero when the axis is chosen to pass through the center of pressure (cp) of the airfoil (i.e., the cp is the point through which the total force can be thought to be acting). This is not a particularly convenient location for the axis since experiments show that the location of the cp changes significantly with alpha. There is another special location for the axis: the *aerodynamic center* (ac) of the airfoil. The ac is a point at which the aerodynamic moment tends to be invariant with respect to alpha (within some range of alpha). It is normally close to the chord line, about one quarter-chord back from the leading edge, and moves back to the half-chord position at supersonic speeds. As alpha is varied through positive and negative values, the cp moves in such a way that the moment about the ac remains constant. For the cambered airfoil shown in Figure 2.2-1, the moment about the ac will be a nose-down (negative) moment, as shown in Figure 2.2-2, curve 1.

The aerodynamic center is important when we come to consider the stability of the airfoil in an airflow. It is obvious (by reductio ad absurdum) that if we move the pivot axis forward of the ac we will measure a negative pitching moment that becomes more negative as alpha is increased. This is shown in curve 2 of Figure 2.2-2; point *B* on this curve is the angle of attack where the pitching moment becomes zero. If we attempt to increase alpha away from point *B*, a negative pitching moment is generated; conversely, decreasing alpha generates a positive moment. These are restoring moments that tend to hold alpha at the value *B*. Therefore, neglecting any moment due to its weight, the airfoil will settle into a *stable equilibrium* condition at point *B* when allowed to pivot freely about a point forward of the aerodynamic center.

When the axis is at the aerodynamic center, as in curve 1 of the figure, there is a stable equilibrium at point *A*. This point is at a large negative value of alpha outside the normal range of operation. When we place the pivot axis behind the ac, as in curve 3, the pitching moment increases with alpha. There is an equilibrium condition

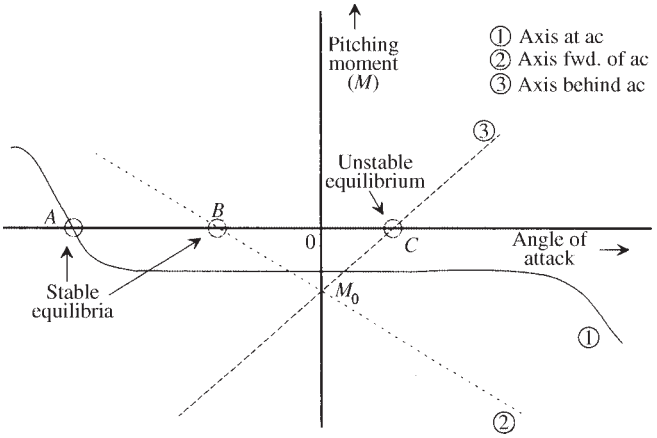

Figure 2.2-2 Airfoil moment about different axes.

at point C, but this is an *unstable equilibrium* because any small perturbation in alpha creates a moment that drives the angle of attack out of this region. With the sign conventions we have chosen, we see that a stable equilibrium is associated with a negative slope to the pitching moment curve and unstable equilibrium with a positive slope. If the airfoil had to support the weight of an aircraft, a stable equilibrium point would normally have to occur at a positive angle of attack. This would require curve 2 to be shifted upward (i.e., M_0 positive); in practice, the horizontal tail of the aircraft provides the additional positive pitching moment required.

The stability of this hypothetical experiment has been analyzed by considering the *static* balance of the pitching moment and the effect of small perturbations. The condition of a steady-state moment tending to restore equilibrium is known as *positive stiffness* and, in this case, positive pitch stiffness is associated with a *negative slope* of the pitching moment–alpha curve. In this experiment only a single degree of freedom was involved: rotation around a fixed axis. The static analysis was sufficient to determine whether the equilibrium was stable or unstable (and to determine the stability boundary), but not sufficient to determine the dynamics of the motion when the equilibrium was disturbed.

The motion of an airplane in the vertical plane involves three degrees of freedom, one rotational (the pitching motion described above) and two translational (horizontal and vertical velocity components). An analysis of the stability of the motion requires that a steady-state trajectory be defined and an analysis of small perturbations in the motion be performed. From this analysis the *dynamic modes* (i.e., the time-dependent behavior of the system in response to an impulsive input) can be determined. A pilot's ability to control an airplane is linked to the stability of the modes, so *dynamic stability* is of critical importance. Dynamic stability analyses will be performed in later chapters. Here we simply note that positive stiffness is not sufficient to ensure dynamic stability, but the aircraft dynamic stability conditions will later be seen to be dominated by the static stability condition.

We must now describe the mathematical models for the forces and moments on an airfoil and include the situation where the parameters of the flowfield may vary. It is shown in textbooks on aerodynamics (Kuethe and Chow, 1984) that, for a body of given shape with a given orientation to the freestream flow, the forces and moments are proportional to the product of freestream mass density, ρ, the square of the freestream airspeed, V_T, and a characteristic area for the body. The product of the first two quantities has the dimensions of pressure and it is convenient to define the *dynamic pressure*, $\overline{q}$, by

$$\overline{q} = \frac{1}{2}\rho V_T^2 \qquad \text{(pressure units)} \tag{2.2-1}$$

and note that this is also the kinetic energy per unit volume. In the *standard atmosphere* model (U.S. Standard Atmosphere, 1976) the mass density ρ is 2.3769×10^{-3} slugs/ft^3 at sea level (1.2250 kg/m^3) and, as an example, the dynamic pressure at 300 mph (440 ft/s) at sea level is

$$\overline{q} = 0.5 \times 0.002377 \times 440^2 = 230 \text{ lb/ft}^2 \text{ (psf)}$$

This dynamic pressure of about 1.6 lb/in.^{2} (psi) is to be compared with the static pressure of approximately 14.7 psi at sea level. By dividing a measured (or calculated) aerodynamic force by the product of dynamic pressure and an arbitrarily chosen reference area, we determine dimensionless coefficients that represent the ability of the airfoil to produce lift or drag. In the case of an aerodynamic moment we must also divide by an arbitrarily chosen reference length. The dimensionless coefficients are called *aerodynamic coefficients* and depend on the shape of the airfoil and its angle of attack.

An aerodynamic coefficient is also a function of the freestream viscosity, which is a measure of a fluid's resistance to rate of change of shape. In addition, the aerodynamic coefficient depends on how much the fluid is compressed in the flow around the airfoil. If this dependence is expressed in terms of two appropriate parameters, then *geometrically similar* airfoils (i.e., same shape, same definition of reference area, but not necessarily the same size) will have the same aerodynamic coefficient when they are at the same angle of attack in two different flowfields, providing that the two *similarity parameters* are the same for each. This assumes that the effect of surface roughness is negligible and that there is no effect from turbulence in the freestream airflow. Matching of the two sets of similarity parameters is required for wind tunnel results to carry over to full-sized aircraft. The two conventional similarity parameters will now be described.

The nature of the boundary layer viscous flow is determined by a single freestream dimensionless parameter, the *Reynolds number*, R_e, given by

$$R_e = (\rho \ell V_T)/\mu, \tag{2.2-2}$$

where ℓ is some characteristic length and μ is the viscosity of the fluid. Note that the viscosity varies greatly with the temperature of the fluid but is practically independent of the pressure. The characteristic length is usually the airfoil chord or, for an aircraft, the mean chord of the wing. Reynolds numbers obtained in practice vary from a few hundred thousand to several million. The flow in the boundary layer is laminar at low Reynolds numbers and, at some critical Reynolds number of the order of a few hundred thousand, it transitions to turbulent flow with a corresponding increase in the skin friction drag.

For most airplanes in flight, the boundary layer flow is turbulent over most of the wing airfoil, except for close to the leading edge. The NACA 6-series airfoils, designed in the 1930s and 1940s to promote laminar flow, showed a significant drag reduction in wind tunnel tests, but this usually could not be maintained in the face of the surface contamination and production roughness of practical wings.

The dynamic pressure is an increment of pressure on top of the static pressure. The fractional change in volume, which is a measure of how much the fluid is compressed, is given by dividing the dynamic pressure by the bulk modulus of elasticity (which has the units of pressure). Physics texts show that the speed of sound in a fluid is given by the square root of the quotient of the modulus of elasticity over the mass density. Therefore, when the dynamic pressure is divided by the modulus of elasticity, we obtain a dimensionless quantity equal to one-half of the square of the *freestream Mach number*, M, defined by

$$M = V_T/a, \tag{2.2-3}$$

where a is the speed of sound at the ambient conditions. At sea level in the standard atmosphere, a is equal to 1117 ft/s (340 m/s, 762 mph). Freestream Mach number is the second similarity parameter, and the aerodynamic coefficients are written as functions of alpha, Reynolds number, and Mach number. The Mach number ranges of interest in aerodynamics are

$$\begin{aligned} &\text{subsonic speeds:} && M < 1.0 \\ &\text{transonic speeds:} && 0.8 \leq M \leq 1.2 \\ &\text{supersonic speeds:} && 1.0 < M < 5.0 \\ &\text{hypersonic speeds:} && 5.0 \leq M \end{aligned} \tag{2.2-4}$$

The *compressibility effects*, described above, may begin to have a noticeable influence on an aerodynamic coefficient at a freestream Mach number as low as 0.3. By definition pressure disturbances propagate through a fluid at the speed of sound, and an approaching low-speed aircraft can be heard when it is still some distance from the observer. When the Mach number reaches unity at some point in the flow, pressure disturbances at that point can no longer propagate ahead. The wavefront remains fixed to the aerodynamic body at that point and is called a *shock wave*. At still higher Mach numbers the wavefront is inclined backward in the flow and forms a *Mach cone* with its apex at the source of the pressure disturbance. The Mach number will in general reach unity at some point on the airfoil surface when the freestream velocity is still subsonic. This freestream Mach number, called the *critical Mach number*, defines the beginning of *transonic flow* for an airfoil or wing. Because of the formation of shock waves and their interaction with the boundary layer, the aerodynamic coefficients can vary with Mach number in a complex manner in the transonic regime. For example, at a freestream Mach number slightly greater than the critical Mach number, a sharp increase in drag coefficient occurs. This is called the *drag divergence Mach number*. In the supersonic regime the aerodynamic coefficients tend to change less erratically with Mach number, and in the hypersonic regime the aerodynamic effects eventually become invariant with Mach number.

We are now in a position to write down the mathematical models for the magnitudes of the forces and moments shown in Figure 2.2-1. The measurements are typically made at some point in the airfoil close to the ac (usually at the quarter-chord point). The force components and the moment of the couple are modeled by the following equations, involving lift, drag, and moment *section coefficients* C_ℓ, C_d, and C_m, respectively:

$$\begin{aligned} \text{lift per unit span} &= \overline{q}\, c\, C_\ell\, (\alpha, M, R_e) \\ \text{drag per unit span} &= \overline{q}\, c\, C_d\, (\alpha, M, R_e) \\ \text{pitching moment per unit span} &= \overline{q}\, c^2\, C_m\, (\alpha, M, R_e) \end{aligned} \tag{2.2-5}$$

The reference length for this infinitely long airfoil section is the chord length, c, and the product $\overline{q}c$ has the dimensions of force per unit length.

Consider first the variation of section aerodynamic coefficients with alpha. The dimensionless *lift coefficient*, C_ℓ, measures the effectiveness of the airfoil at producing lift. This coefficient is linear in alpha at low values of alpha and positive at zero angle of attack for cambered airfoils. The *lift-curve slope* has a theoretical value of 2π per radian for thin airfoils at low subsonic Mach numbers. The drag equation has the same form as the lift equation, and the *drag coefficient*, C_d, is usually parabolic in alpha, in the region where the lift coefficient is linear in alpha. The drag coefficient is commonly presented as a function of lift coefficient. Typical plots of lift and drag coefficients, with representative values, are shown, respectively, in Figures 2.2-3*a* and *b*. The moment equation is different from the lift and drag equations in that it requires an additional length variable to make it dimensionally correct. The airfoil chord, c, is used once again for this purpose. A typical plot of the *pitching moment coefficient*, C_m, is also shown in Figure 2.2-3*a*.

Now consider the variation of these coefficients at higher values of alpha. Wind tunnel flow visualization studies show that, at high values of alpha, the flow can no longer follow the upper surface of the airfoil and becomes detached. There is a region above the upper surface, near the trailing edge, where the velocity is low and the flow reverses direction in places in a turbulent motion. As the angle of attack is increased farther, the beginning of the region of separated flow moves toward the leading edge of the airfoil. The pressure distribution over the airfoil is changed in such a way that the lift component of the aerodynamic force falls off rapidly and the drag component increases rapidly. The airfoil is said to be *stalled*, and this condition is normally avoided in flight. The pitching moment (about the axis through the aerodynamic center) also changes rapidly, typically becoming more negative.

Next consider the effect of Reynolds number. The lift-curve slope is essentially independent of R_e when $R_e \approx 10^6$ to 10^7 (where normal, manned aircraft fly) but is significantly reduced when $R_e \approx 10^5$ (which may be reached by miniature and

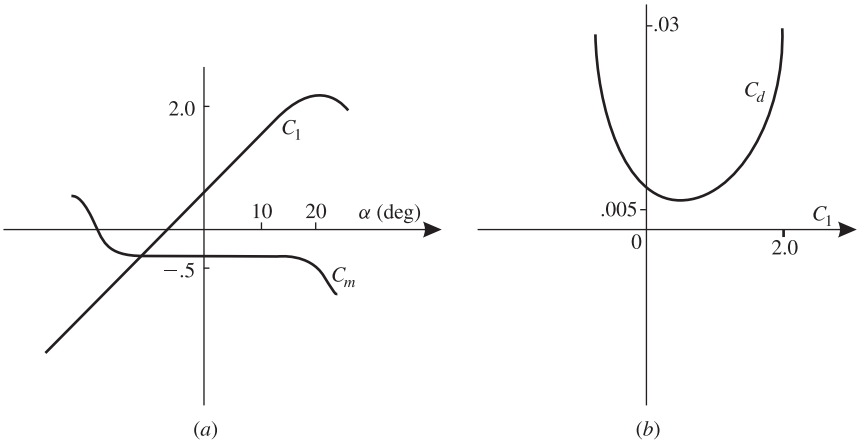

Figure 2.2-3 Typical plots of lift, drag, and moment coefficients.

unmanned vehicles). The maximum (stall) lift coefficient tends to increase with R_e, even at high values. The drag curve is affected by R_e in that its minimum value is larger at lower R_e; also, near stall the drag coefficient is increased by lower R_e. The pitching moment is similar to the lift coefficient in that it is independent of Reynolds number in the linear region, at high R_e, but not independent in the stall region.

Finally, consider the effect of Mach number on the aerodynamic coefficients. In the case of the lift coefficient, both the lift-curve slope and the maximum lift are changed when compressibility effects begin to occur. The theoretical values for lift-curve slope are modified by the Prandtl-Glauert correction (Anderson, 1991; Kuethe and Chow, 1984):

$$\frac{\partial C_L}{\partial \alpha} = \frac{2\pi}{\sqrt{(1 - M^2)}}, \qquad M < 1 \tag{2.2-6a}$$

$$\frac{\partial C_L}{\partial \alpha} = \frac{4}{\sqrt{(M^2 - 1)}}, \qquad M > 1 \tag{2.2-6b}$$

In the transonic region, the lift-curve slope of a thin airfoil will generally pass through a smooth peak, while that of a thick airfoil will show a more complicated variation. The maximum lift coefficient falls with increasing Mach number in the supersonic regime. For the drag coefficient, the effect of increasing subsonic Mach number is to bodily raise the drag curve shown in Figure 2.2-3*b*; the drag coefficient then falls off somewhat with increasing supersonic Mach number.

The effect of Mach number on the pitching moment coefficient is due to a rearward shift of the airfoil cp with Mach number. This causes a shift in position of the airfoil aerodynamic center. At low subsonic Mach numbers it is usually at a distance back from the leading edge equal to about 25% of the chord. In the transonic region its position may change erratically, and at higher speeds it tends to shift aft to the 50% chord position. Therefore, if the pitching moment is measured at the quarter-chord position, the slope, with alpha, changes from zero to a negative value as the Mach number is increased from subsonic to supersonic values.

Finite Wings

Real wings are finite in length and involve "three-dimensional" aerodynamics. When a wing is producing lift, the air tends to flow around the tip, from the high-pressure region under the wing to the low-pressure region above the upper surface. This circulation of the air creates a vortex motion at the tips so that, behind the wing, the sheet of air that is deflected downward by airfoil action curls up at the edges to form a *vortex sheet*. The energy that goes into creating the vortex motion leads to an increase in the force needed to push the wing through the air, that is, an increase in drag. In addition, the leakage around the tips creates a spanwise component of flow and reduces the lift-curve slope compared to that of a "two-dimensional" airfoil. Thus, there is a decrease in the *lift-over-drag* ratio compared to the airfoil. Many aircraft use wing-tip devices and aerodynamic "fences" on the wing to reduce these detrimental effects.

A complete wing may have straight or curved leading and trailing edges or it may consist of two identical halves that are swept back toward the tips. The chord may be constant or reduced toward the wing tip (wing taper), and different airfoil sections may be used over different parts of the span. The "planform" of a wing has a large impact on its aerodynamic properties. Among the most important parameters of the planform are the aspect ratio and the leading-edge sweep angle. These and other parameters are defined in Table 2.2-1.

An explanation of the calculation of the mean aerodynamic chord can be found in various aerodynamics texts (e.g., Dommasch et al., 1967). The aspect ratio is equivalent to a measure of span relative to chord; for complete aircraft, values range from about 30 (some sailplanes), through 14 (Lockheed U-2) and 7 (Boeing 747), down to about 3 (fighter aircraft), and even lower for delta wings. High-aspect-ratio wings act more like the "two-dimensional" airfoil, while low-aspect wings have greatly reduced lift-curve slope and lift-over-drag ratio. High lift-over-drag ratio is needed for efficient cruise performance (passenger jets), long-duration flight (military reconnaissance), and shallow glide angle (sailplanes). A low aspect ratio simplifies structural design problems for high-g aircraft, permits very high roll rates, and reduces *supersonic wave drag* (described later).

Prandtl's lifting line theory (Anderson, 1991) provides a simple expression for the lift-curve slope of a straight high-aspect-ratio finite wing in incompressible flow, in terms of aspect ratio and the lift-curve slope of the corresponding airfoil section. This formula can be combined with the Prandtl-Glauert corrections of Equations (2.2-6) to give a formula that applies to subsonic compressible flow. The transonic lift-curve slope is hard to predict but, in the supersonic regime, the lift-curve slope can be approximated as a constant (4.0) divided by the Prandtl-Glauert correction factor, as in Equation (2.2-6*b*). For low-aspect-ratio wings ($AR < 4$), slightly more complicated formulas are available (Anderson, 1999). Wing sweep further complicates the picture. A lift-curve slope formula can be derived for subsonic swept wings by introducing the cosine of the sweep angle into the above-described formulas. For supersonic swept wings the behavior of the lift-curve slope depends on whether the sweep of the wing puts its leading edge inside or outside of the shock wave from the apex of the swept wing, and no convenient formulas are available. The above facts are clearly described in much more detail by Anderson (1999).

Delta-shaped wing planforms behave in a fundamentally different way than conventional wings. When producing lift, a delta wing has a strong vortex rolling over the full length of each leading edge. The vortices are stable, in the sense that they remain

TABLE 2.2-1 Important Wing Planform Parameters

b = wing span (i.e., tip to tip)	λ = taper ratio (tip chord/root chord)
c = wing chord (varies along span)	
$\overline{c}$ = mean aerodynamic chord (mac)	Λ = leading-edge sweep angle
S = wing area (total)	$AR = b^2/S$ = aspect ratio

in place over a wide range of alpha, and contribute to lower pressure over the upper surface. The lift curve of the delta wing is slightly nonlinear, with the slope increasing at first as alpha increases. The average lift-curve slope is only about half that of a conventional wing, but the stall angle of attack is about twice as big. A delta wing has been used on various fighter aircraft because it can provide the large sweep angle needed for supersonic flight and can also attain a normal peak lift coefficient through the *vortex lift*. A degree of vortex lift similar to that of a delta wing can be obtained from a conventional swept wing if, near the wing root, the leading edge is carried forward with a sharp-edged extension having a sweep angle near 90°. This leading-edge extension generates a vortex that trails back over the inboard wing panels and keeps the flow attached to the wing at high alpha.

Aircraft Configurations

A conventional aircraft uses airfoil sections for the wings, horizontal tail, vertical tail, and possibly additional surfaces such as horizontal canards [notable exceptions to this configuration are the flying wing aircraft, such as the Northrop YB series (Anderson, 1976) and the more modern B-2 bomber]. The close proximity of the wings and fuselage, and of the wing and tail surfaces, creates interference effects, so that the total aerodynamic force is not given by the sum of the forces that would be obtained from the individual surfaces acting alone. In addition, the fuselage of the airplane provides some lift and a considerable amount of drag. Therefore, the aerodynamic coefficients of a complete aircraft must be found from wind tunnel measurements and computational fluid dynamics (CFD). Anderson (1999) cites a study that measured the subsonic lift-curve slope of a wing-fuselage combination as a function of the ratio of fuselage diameter to wingspan (d/b). The study showed that for a range of d/b from zero to 0.6, the lift-curve slope was within 5% of that of the wing alone. This was because of the lift of the fuselage, and because of favorable cross-flows induced on the wing by the fuselage. A further conclusion was that the lift of the wing-body combination could be approximated by using the lift coefficient of the wing alone, with a reference area given by the planform area of the wing projected through the fuselage. This is the usual definition of the wing planform reference area.

Figure 2.2-4 shows a number of distinctive planforms. Low-speed aircraft, ranging from light general aviation types to military heavy-lift transport aircraft, have stiff moderate-aspect-ratio wings with no sweepback (cf. Figure 2.2-4*d*). Aircraft designed to reach transonic speeds and beyond have highly swept wings. The effect of the sweep is to postpone the *transonic drag rise*, since the component of the airflow perpendicular to the leading edge has its speed reduced by the cosine of the sweep angle. Large jet airliners designed to cruise efficiently at high subsonic Mach numbers have swept wings with a high aspect ratio (Figure 2.2-4*e*). This produces the highest ratio of lift to induced drag (the increase in drag that occurs when lift is produced). In the case of high-speed fighter aircraft, the requirement for low supersonic wave drag and high maneuverability causes a dramatic change to very-low-aspect-ratio wings (Figure 2.2-4*b*). The stubby wings allow the aircraft structure to be designed to withstand very high lift forces during maneuvers. They also reduce the moment of inertia

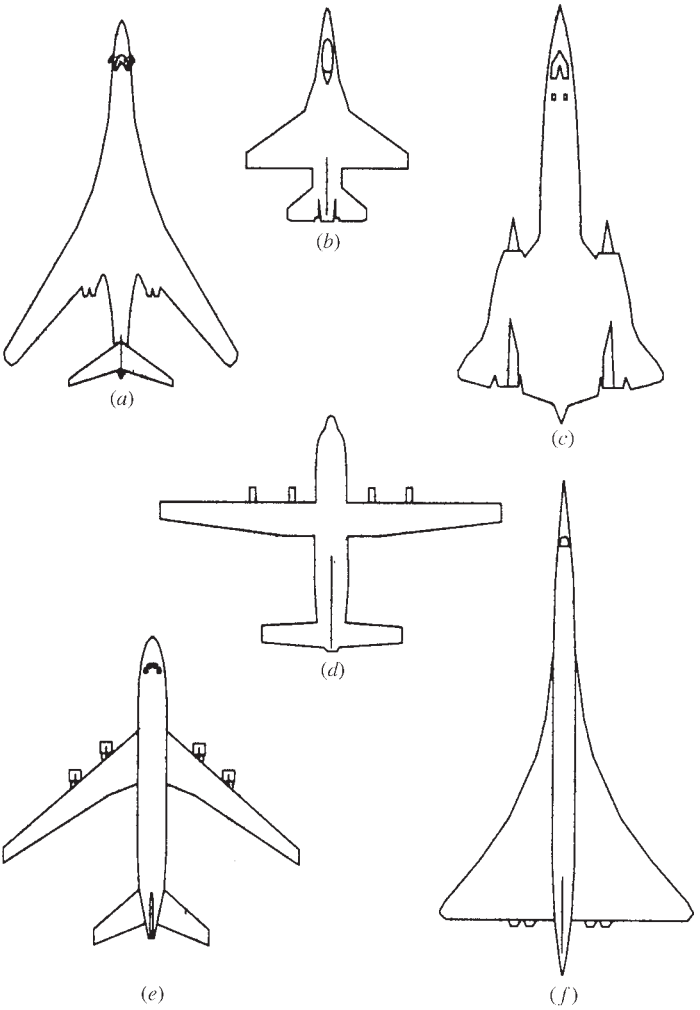

Figure 2.2-4 Types of aircraft wing planform.

about the longitudinal axis and the aerodynamic damping moments during rolling, thus promoting a high roll acceleration and a high maximum roll rate.

Wing sweep has the disadvantage of reducing the lift-curve slope of the wing (i.e., less lift at a given alpha) and producing suboptimal performance at low speeds. A way to overcome this when a high lift-to-drag ratio is required over a wide envelope is to use a variable-sweep wing, as exemplified by the F-14 and B-1B aircraft (Figure 2.2-4*a*). This is a heavy and costly solution. For commercial aircraft that are usually optimized for one cruise condition, the most common method of achieving adequate lift at low speeds is to increase the camber and area of the wing by means of leading- and trailing-edge devices (slats and flaps). These may then be

deployed manually for landing. More specialized solutions are to use an automatic maneuvering flap, as in the case of the F-16 leading-edge flap, which is deployed automatically as a function of angle of attack when the Mach number is low. More recently the concept has been taken to its logical conclusion in the *mission adaptive wing* (DeCamp et al., 1987), tested on an F-111 aircraft.

Wing planforms that create vortex lift are shown in Figures 2.2-4*b*, *c*, and *f*, representing the F-16, SR-71, and Concorde aircraft, respectively.

The F-16 has sharp-edged, highly swept forebody *strakes* to generate the vortices. The design goal was to achieve maximum maneuverability through the use of vortex lift. The Concorde has an *ogee* wing with very large initial sweep angle, with the design aim of increasing the lift at low speed and reducing the movement of the aerodynamic center between low-speed and supersonic cruise conditions. The high angle of attack needed to get the low-speed vortex lift would obscure the pilot's view of the runway, and this problem was solved by using the droop nose. Some description of the design of these wings can be found in the American Institute of Aeronautics and Astronautics (AIAA) case studies (Droste and Walker, no date; Rech and Leyman, no date). The SR-71 Mach 3-plus, high-altitude, strategic reconnaisance aircraft (Drendel, 1982) has a blended wing-body with chines. This blending reduces wing-body wave interference drag at cruise speed, while vortex lift effects may be useful during takeoff and landing.

Vortices are also shed from a conventional forebody at high alpha, and a long forebody overhang (as in the case of the shark nose on the F-5) presents difficult design problems. This is because any slight asymmetry in the shed vortices causes pressure differentials at the nose and leads to a relatively large (and unpredictable) yawing moment because of the long lever arm from the aircraft center of mass.

2.3 AIRCRAFT FORCES AND MOMENTS

The equations of motion derived in Chapter 1 are driven by the aerodynamic forces and moments acting at the cm of the complete rigid aircraft. In Section 2.2 we have covered enough basic aerodynamics to understand how these forces and moments come about. We now begin to examine how they can be measured and expressed.

Definition of Axes and Angles

The aerodynamic forces and moments on an aircraft are produced by the relative motion with respect to the air and depend on the orientation of the aircraft with respect to the airflow. In a uniform airflow these forces and moments are unchanged after a rotation around the freestream velocity vector. Therefore, only two orientation angles (with respect to the relative wind) are needed to specify the aerodynamic forces and moments. The angles that are used are the *angle of attack* (alpha) and the *sideslip angle* (beta). They are known as the *aerodynamic angles* and will now be formally defined for an aircraft. Note that the aerodynamic forces and moments are also dependent on angular rates, but for the moment we are concerned only with orientation.

Figure 2.3-1 shows an aircraft with the relative wind on its right side (i.e., sideslip-ping), with three *frd* (forward, right, down) coordinate systems with a common origin at the aircraft cm, and with aerodynamic angles α and β. The *body-fixed coordinate system, bf,* has its x-axis parallel to the fuselage reference line (used in the blueprints) and its z-axis in the (conventional) aircraft plane of symmetry. The angle of attack is denoted by α_{frl} when measured to the fuselage reference line from the projection of the relative wind on the body x–z plane. It is positive when the relative wind is on the underside of the aircraft. The sideslip angle is measured to the relative wind vector from the same projection. It is positive when the relative wind is on the right side of the airplane.

The angle of attack is also given the symbol α_0 when measured to the aircraft zero-lift line (where aircraft lift is zero, with neutral controls and no sideslip). We will simply write "α" throughout and mean α_{frl} unless otherwise stated. For an aircraft in steady-state flight (Section 2.6) the "equilibrium" angle of attack will be denoted by α_e, and the equilibrium sideslip angle is normally zero.

In Figure 2.3-1, α_e defines the orientation of the *stability-axes* coordinate system, s, which is used for analyzing the effect of perturbations from steady-state flight. As can be seen from the figure, it is obtained from the body-fixed system by a left-handed rotation, through α_e, around the body y-axis. The *wind-axes system, w,* is obtained from the stability-axes system by a rotation around the z-axis that aligns the wind x-axis directly into the relative wind. A left-handed wind-axes system, aligned back-ward, left, and "up" relative to the aircraft, has been used in the past for wind tunnel

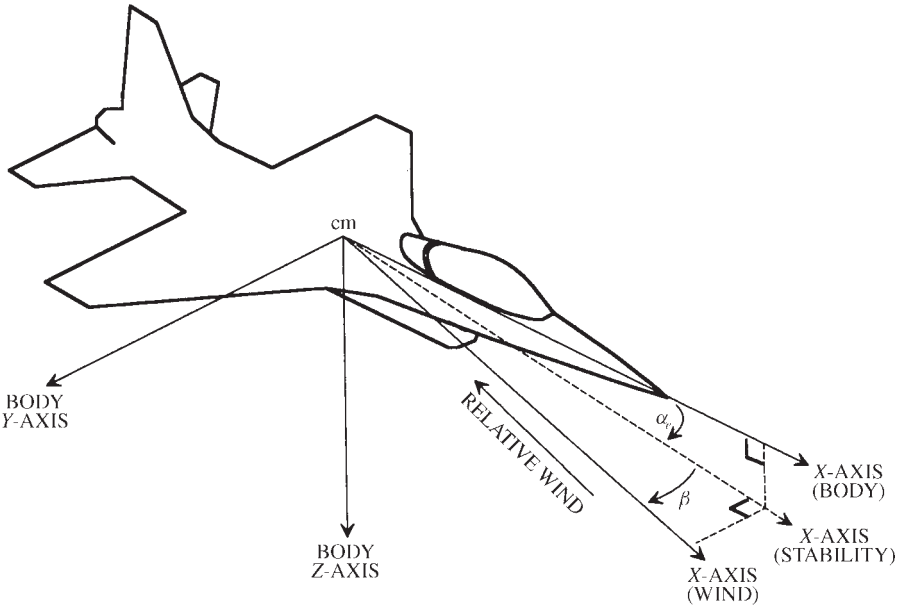

Figure 2.3-1 Definitions of axes and aerodynamic angles.

data (Pope, 1954). *Lift L*, *drag D*, and *cross-wind force C* were defined naturally in these axes as the aerodynamic force components along the respective positive axes. The notation for our right-handed coordinate systems is given in Table 2.3-1, in the next subsection.

Following the rules for finding rotation matrices, the rotation matrices from body fixed to stability and stability to wind axes are

$$C_{s/bf} = \begin{bmatrix} \cos\alpha_e & 0 & \sin\alpha_e \\ 0 & 1 & 0 \\ -\sin\alpha_e & 0 & \cos\alpha_e \end{bmatrix} \tag{2.3-1a}$$

$$C_{w/s} = \begin{bmatrix} \cos\beta & \sin\beta & 0 \\ -\sin\beta & \cos\beta & 0 \\ 0 & 0 & 1 \end{bmatrix} \tag{2.3-1b}$$

and the combined rotation from body fixed to wind is

$$C_{w/bf} = \begin{bmatrix} \cos\alpha_e\cos\beta & \sin\beta & \sin\alpha_e\cos\beta \\ -\cos\alpha_e\sin\beta & \cos\beta & -\sin\alpha_e\sin\beta \\ -\sin\alpha_e & 0 & \cos\alpha_e \end{bmatrix} \tag{2.3-2}$$

This transformation will also be used without the subscript e when converting instantaneous wind-axes components into body axes, and vice-versa.

Definition of Forces and Moments

Table 2.3-1 defines the symbols that will be needed for aircraft force, moment, and velocity components. The subscripts A or T on the force and moment vectors indicate, respectively, aerodynamic or thrust effects. In the case of the aerodynamic forces, there are no specific symbols for stability-axes components but, as indicated in (2.3-3*b*), the stability axes have two components that are unchanged from the other axes. These dimensionless coefficients are defined in the next section. Note that C_N and C_X are, respectively, the *normal force* and *axial force* coefficients; C_N is the negative of the body-axes force coefficient C_Z.

A useful notation scheme is to use lowercase symbols to indicate small perturbations on the "uppercase" variables. Unfortunately, aircraft moments are almost universally denoted by lowercase symbols, as shown in (2.3-4) and (2.3-5). Also, the same symbols are commonly used for the dimensionless moment coefficients regardless of coordinate system, and the coordinate system must be explicitly stated.

Thrust components are shown in (2.3-5); note that a sideforce component can be produced by unbalanced engine power because in a multiengine aircraft the engines may be toed-in to align them with the airflow from the forebody. Also, the thrust axis is often slightly tilted with respect to the body x-axis, and so a z-component of thrust can result. In the case of VTOL or V/STOL aircraft, the z-component of thrust will

TABLE 2.3-1 Force, Moment, and Velocity Definitions

Aerodynamic forces:

$$\mathbf{F}_A^w \equiv \begin{bmatrix} -D \\ -C \\ -L \end{bmatrix} = C_{w/bf} \begin{bmatrix} X_A \\ Y_A \\ Z_A \end{bmatrix} \equiv C_{w/bf} \mathbf{F}_A^{bf} \tag{2.3-3a}$$

Dimensionless force coefficients:

$$\begin{array}{rcccc} & x & y & z & \\ \text{Wind}: & C_D & C_C & C_L & \\ \text{Stability}: & * & C_Y & C_L & \\ \text{Body}: & C_X & C_Y & C_Z & (-C_N) \end{array} \tag{2.3-3b}$$

Aerodynamic moments:

$$\mathbf{M}_A^{bf} \equiv \begin{bmatrix} \ell \\ m \\ n \end{bmatrix}, \quad \mathbf{M}_A^s \equiv \begin{bmatrix} \ell_s \\ m \\ n_s \end{bmatrix}, \quad \mathbf{M}_A^w \equiv \begin{bmatrix} \ell_w \\ m_w \\ n_w \end{bmatrix} \quad (n_w = n_s) \tag{2.3-4a}$$

Dimensionless moment coefficients:

$$C_\ell, C_m, C_n$$

(same notation in all systems) (2.3-4*b*)

Thrust force and moment:

$$\mathbf{F}_T^{bf} \equiv \begin{bmatrix} X_T \\ Y_T \\ Z_T \end{bmatrix}, \quad \mathbf{M}_T^{bf} \equiv \begin{bmatrix} m_{x,T} \\ m_{y,T} \\ m_{z,T} \end{bmatrix} \tag{2.3-5}$$

Relative velocity components:

$$\mathbf{v}_{rel}^{bf} \equiv \begin{bmatrix} U' \\ V' \\ W' \end{bmatrix} = C_{bf/w} v_{rel}^w \equiv C_{bf/w} \begin{bmatrix} V_T \\ 0 \\ 0 \end{bmatrix} = \begin{bmatrix} V_T \cos\alpha \ \cos\beta \\ V_T \sin\beta \\ V_T \sin\alpha \ \cos\beta \end{bmatrix} \tag{2.3-6a}$$

Aerodynamic angles:

$$\tan\alpha = \frac{W'}{U'}, \quad \sin\beta = \frac{V'}{V_T}, \quad V_T = |\mathbf{v}_{rel}| \tag{2.3-6b}$$

Absolute velocity components:

$$\mathbf{v}_{cm/e}^{bf} \equiv \begin{bmatrix} U \\ V \\ W \end{bmatrix} \tag{2.3-6c}$$

Angular velocity components (r denotes any ref. frame):

$$\boldsymbol{\omega}_{b/r}^{bf} \equiv \begin{bmatrix} P \\ Q \\ R \end{bmatrix}, \quad \boldsymbol{\omega}_{b/r}^s \equiv \begin{bmatrix} P_s \\ Q \\ R_s \end{bmatrix}, \quad \boldsymbol{\omega}_{b/r}^w \equiv \begin{bmatrix} P_w \\ Q_w \\ R_w \end{bmatrix} \quad (R_w = R_s) \tag{2.3-7}$$

Control surface deflections:

Elevator: δ_e Aileron: δ_a Rudder: δ_r Flap: δ_F

Throttle position: δ_t

Control vector: $\overline{U} = \begin{bmatrix} \delta_t & \delta_e & \delta_a & \delta_r & \delta_F & \dots \end{bmatrix}^T$

be particularly important. Models of propeller-driven aircraft must include several important force and moment effects.

In Equation (2.3-6) primes are used to denote velocity components relative to the atmosphere, as opposed to "inertial" components. In the wind system the relative velocity vector $\mathbf{v}_{rel}$ has only an x-component V_T, and so $V_T = |\mathbf{v}_{rel}|$. In (2.3-6*b*) the aerodynamic angles have been found from the interrelationships of the components in (2.3-6*a*). The control vector of the nonlinear state-space model has been denoted by $\overline{U}$, in this chapter only, to distinguish it from a velocity component.

Force and Moment Coefficients

The forces and moments acting on the complete aircraft are defined in terms of dimensionless aerodynamic coefficients in the same manner as for the airfoil section. The situation is now three dimensional, and the coefficients are functions of the two aerodynamic angles, as well as Mach and Reynolds numbers. Furthermore, an aircraft is a flexible structure and its shape is deformed by the influence of high dynamic pressure, with consequent changes in the aerodynamic coefficients. If Mach and altitude are specified, together with a temperature and density model of the atmosphere, then Reynolds number and dynamic pressure can be determined. Therefore, the aircraft aerodynamic coefficients are, in practice, specified as functions of the aerodynamic angles, Mach, and altitude (in the standard atmosphere). In addition, control surface deflections and propulsion system effects cause changes in the coefficients. A control surface deflection, δ_s, effectively changes the camber of a wing, which changes the lift, drag, and moment. Consequently, we write the dependence of an aerodynamic coefficient as

$$C_{(\,)} = C_{(\,)}(\alpha, \beta, M, h, \delta_s, T_c), \tag{2.3-8a}$$

where T_c is a *thrust coefficient* (defined later). Other factors that change the coefficients are configuration changes (e.g., landing gear, external tanks, etc.) and ground proximity effects. In terms of wind-axes components, we have the following coefficients:

$$\begin{aligned} \text{drag}, D &= \overline{q}\, S\, C_D \\ \text{lift}, L &= \overline{q}\, S\, C_L \\ \text{crosswind force}, C &= \overline{q}\, S\, C_C \\ \text{rolling moment}, \ell_w &= \overline{q}\, S\, b\, C_\ell \\ \text{pitching moment}, m_w &= \overline{q}\, S\, \overline{c}\, C_m \\ \text{yawing moment}, n_w &= \overline{q}\, S\, b\, C_n \end{aligned} \tag{2.3-8b}$$

Exactly equivalent definitions are used for body- or stability-axes components, with the symbols given in Table 2.3-1. In Equation (2.3-8*a*), as a rough generality, *longitudinal coefficients* (lift, drag, pitching moment) are primarily dependent on alpha, and in the *lateral-directional coefficients* (roll, yaw, and sideforce) beta is equally as important as alpha.

Equation (2.3-8*a*) implies a complicated functional dependence that would have to be modeled as a "lookup-table" in a computer. The vast majority of aircraft have flight envelopes restricted to small angles of attack and/or low Mach numbers. For these aircraft, the functional dependence will be simpler and any given coefficient might be broken down into a sum of simpler terms, with linearity assumed in some terms.

The coefficients considered so far are *static coefficients*, that is, they would be obtained from measurements on a stationary model in a wind tunnel (other methods are considered later). It is also necessary to model the aerodynamic effects when an airplane maneuvers. In general terms this requires a differential equation model of the aerodynamic force or moment. To determine if this level of complexity is warranted, we examine maneuvering flight more closely, in two categories. First, consider maneuvers that are slow enough that the flowfield around the aircraft is able to adjust in step with the maneuver and so the maneuver-induced translational velocities of points on the aircraft cause changes in the local aerodynamic angles that are still in the linear regime. The aerodynamic forces or moments can then be modeled as linearly proportional to the angular rate that produced them. Linearization is usually associated with taking a partial derivative, and in this case the coefficient of proportionality is called an *aerodynamic derivative*. The aerodynamic derivatives will be described in the next subsection.

In the second category are maneuvers in which an airplane can significantly change its orientation in a time interval that is comparable with the time required for the flowfield around the aircraft to readjust. These *unsteady aerodynamic effects* lead to time dependence in the aerodynamic coefficients and much more complicated mathematical models. For example, when a very maneuverable aircraft is pitched up rapidly and the angle of attack reaches a value near to stall, the lift generated by the wing may briefly exceed that predicted by the static lift curve. This *dynamic lift* occurs because flow separation takes a finite time to progress from the trailing edge of the wing to the leading edge. The effect can be modeled by making the lift coefficient satisfy a first-order differential equation involving angle-of-attack rate, "alpha-dot" (Goman and Khrabrov, 1994). Another example of possible unsteady aerodynamic behavior is *wing-rock* (McCormick, 1995).

The Aerodynamic Derivatives

The aerodynamic derivatives can be subdivided into two categories. First, when the body frame has a constant angular velocity vector, every point on the aircraft has a different translational velocity in the geographic frame and, taking body-axes components, the aerodynamic angles could be computed at any point using the equivalent of Equation (2.3-6*b*). For example, a roll rate P would create translational velocity components $\pm Pb/2$ at the wing tips. When $P > 0$ this would cause the angle of attack to be reduced by approximately $Pb/(2V_T)$ at the left wing tip and increased by the same amount at the right wing tip. This would in turn create a skew-symmetric variation in lift across the full span of the wings and, assuming that the wing is not stalled across most of the span, produce a negative rolling moment. Because the moment

opposes the roll rate P, the coefficient relating the rolling moment to the roll rate is called a *damping derivative*.

The quantity $Pb/(2V_T)$ is given the symbol $\hat{p}$ and is thought of as a dimensionless roll rate. In a continuous roll, with the aircraft cm moving in a straight line, the wing tips move along a helical path and $Pb/(2V_T)$ is the *helix angle*. The helix angle is a useful figure of merit for roll control power and has been evaluated and compared for a variety of aircraft (Perkins and Hage, 1949; Stinton, 1996). The mathematical model for the dimensionless damping force, or moment ΔC, is of the form

$$\Delta C_{(\ )} = C_{(\ )}(\alpha, \beta, M, h, \delta_s, T_c) \times \frac{k}{2V_T} \times \text{rate} \tag{2.3-9a}$$

The constant k in the dimensionless rate, in Equation (2.3-9a), is either the wingspan (for roll and yaw rates) or the wing mean aerodynamic chord (for pitch rate). The coefficient $C_{(\ )}$ is one of the following p, q, or r derivatives,

$$C_{\ell_p}\ C_{m_q}\ C_{n_r} \tag{2.3-9b}$$

$$C_{\ell_r}\ C_{n_p} \tag{2.3-9c}$$

$$C_{L_q}\ C_{Y_p}\ C_{Y_r}, \tag{2.3-9d}$$

which relate the increments in the moments or forces to the yawing, pitching, and rolling rates. Names are given to the derivatives later. The dimensionless forces and moments are converted to actual forces and moments as in Equations (2.3-8b). Some possible derivatives have been omitted, for example, the effect of pitch rate on drag is usually insignificant. The moment derivatives are the source of the important damping effects on the natural modes of the aircraft.

The second category of aerodynamic derivatives is the *acceleration derivatives*. When the aircraft has translational acceleration, the aerodynamic angles have nonzero first derivatives that can be found by differentiating Equations (2.3-6b). Thus,

$$\dot{\alpha} = \frac{U'\,\dot{W}' - W'\,\dot{U}'}{(U')^2 + (W')^2} \tag{2.3-10a}$$

and

$$\dot{\beta} = \frac{\dot{V}'\,V_T - V'\,\dot{V}_T}{V_T\,[(U')^2 + (W')^2]^{1/2}} \tag{2.3-10b}$$

where

$$\dot{V}_T = \frac{U'\,\dot{U}' + V'\,\dot{V}' + W'\,\dot{W}'}{V_T} \tag{2.3-10c}$$

The main steady aerodynamic effect of the changing aerodynamic angles is that, as the flowfield around the wings and fuselage changes, there is a small airspeed-dependent delay before the changes in downwash and sidewash are felt at

the tail. A first-order approximation in modeling these effects is to make the resulting force and moment increments directly proportional to the aerodynamic angle rates. Therefore, the following acceleration derivatives are commonly used:

$$\text{alpha-dot derivatives:} \qquad C_{L_{\dot{\alpha}}}\ C_{m_{\dot{\alpha}}} \tag{2.3-11}$$

These derivatives are used in an equation of exactly the same form as Equation (2.3-9*a*). The beta-dot derivatives, used to model the delay in the change in sidewash at the vertical tail, are less commonly used.

Aerodynamic Coefficient Measurement and Estimation

The static aerodynamic coefficients can be measured in a wind tunnel using an aircraft scale model mounted on a rigid "sting," to which strain gages have been attached. An older wind tunnel may use a "balance" rather than strain gages. Rigid mounting in a wind tunnel allows *untrimmed coefficients* to be measured, that is, nonzero aerodynamic moments can be measured as the aerodynamic angles are changed or control surfaces are moved.

Specially equipped wind tunnels allow the model to be subjected to an oscillatory motion (Queijo, 1971) so that damping and acceleration derivatives can be measured. Unfortunately, as might be expected, the results are dependent on the frequency of the oscillation. Empirical criteria have been formulated to determine frequency limits below which a quasi-steady assumption (i.e., instantaneous flowfield readjustment) can be made about the flow (Duncan, 1952).

The second important method of measuring aerodynamic coefficients is through *flight test*. In this case *trimmed coefficients* are measured by using the control surfaces to make perturbations from the trimmed steady-state flight condition (Maine and Iliffe, 1980). The typical results are curves of a coefficient plotted against Mach, with altitude as a parameter, for a specified aircraft weight and cm position. The dependence on altitude comes about through the variation of alpha with altitude for a given Mach number, through aeroelastic effects changing with dynamic pressure and, possibly, through Reynolds number effects. To convert to untrimmed coefficients, which are functions of the aerodynamic angles, Mach, and altitude, the trimmed angle of attack must also be recorded in the same form. The flight test results can then be cross-plotted to obtain untrimmed coefficients. The untrimmed coefficients are required when building an aircraft model that is intended to function over a wide range of flight conditions; the trimmed coefficients are used to build small-perturbation models for control systems design or *handling qualities* studies.

Other ways of determining aerodynamic coefficients include the use of CFD computer codes or a combination of empirical data and theory built into a computer program such as the Stability and Control Datcom (Hoak et al., 1970). The input data must include a geometrical description of the aircraft. There are also simple formulas based on assumptions of linearity that can be used to estimate the aerodynamic derivatives. Some of these will be described in subsequent sections.

Component Buildup

The aerodynamic coefficients have a complex dependence on a large number of variables, and this creates both modeling problems and measurement problems. For example, a computer model might be created in the form of a data lookup table in five dimensions (five independent variables). It would be difficult to design an interpolation algorithm for this table or to set up a data measurement system (e.g., wind tunnel measurements), and very little physical insight would be available to help. It is advantageous to build up an aerodynamic coefficient from a sum of components that provide physical insight, require just a single type of test and wind tunnel model, and are convenient to handle mathematically (e.g., fewer dimensions, linearizable, etc.). We will now take each of the aerodynamic coefficients in turn and examine their functional dependence and how this can be modeled.

Drag Coefficient, C_D

The drag coefficient of the complete aircraft is of paramount importance to the aircraft designer. Low drag provides better performance in terms of range, fuel economy, and maximum speed, and designers take pains to estimate the total drag accurately. By the same token we should understand how to make a good mathematical model of the drag. In general, the drag force is a combination of friction drag and drag caused when the integral of pressure over the whole surface area of the body is nonzero. Table 2.3-2 shows the total drag of an aircraft, composed of friction drag and various constituent parts of the pressure drag.

This is not a linear superposition of independent effects; the proportions of the three components will change with flight conditions, and they cannot necessarily be separated and measured individually. The *parasite drag* is called *profile drag* when applied to an airfoil section; it is the sum of skin friction and *form drag*. Form drag is simply the pressure drag caused by flow separation at high alpha. *Induced drag* (also called *vortex drag*) is the pressure drag caused by the tip vortices of a finite wing when it is producing lift. *Wave drag* is the pressure drag when shock waves are present over the surface of the aircraft. The total drag may be broken down into other different components according to the experimental situation. The resulting components will only be meaningful when used in the correct context. For example, *interference drag* is the difference between the summed drag of separate parts of the aircraft and the total drag when these parts are combined. It is a result of mutual interference between the flows over the different parts of the aircraft. Other terms include *drag due to lift* and *zero-lift drag* used for the complete aircraft.

TABLE 2.3-2 Aircraft Drag Components

Parasite Drag	= Friction Drag + Form Drag	(flow separation)
+ Induced Drag		(effect of wing-tip vortices, finite wing)
+ Wave Drag		(effect of shock waves on pressure distribution)
Total Drag		

Now consider, one by one, the drag terms from Table 2.3-2. The aircraft parasite drag is virtually all skin friction drag when the aircraft wing is not stalled. The amount of skin friction drag will depend on the wetted area of the aircraft. The wetted area can range from several times the wing planform area, down to approximately twice the planform area in the case of a flying-wing aircraft. However, as we have already seen, the value of the airplane drag coefficient is calculated based on the wing planform area. The flow in the boundary layer will ordinarily be mostly turbulent in normal flight, but this will depend to a small extent on the lift coefficient. In laminar flow the drag coefficient for skin friction is inversely proportional to the square root of the Reynolds number; in turbulent flow it decreases more slowly as the Reynolds number increases. The Reynolds number increases in proportion to airspeed, but dynamic pressure increases with the square of airspeed. Therefore, we expect to see an increase in skin friction drag with airspeed, although it will become a smaller fraction of the total drag at higher speeds. For example, the skin friction of a supersonic fighter may be about 50% of the total drag at subsonic speed and about 25% at supersonic speed (Whitford, 1987). The skin friction drag coefficient is found to vary parabolically with lift coefficient (Perkins and Hage, 1949).

Turning now to induced drag, the drag coefficient for the induced drag of a high-aspect unswept wing, in subsonic flow, can be modeled as (Perkins and Hage, 1949; Anderson, 1999)

$$C_{D_i} = C_L^2/(\pi\, e\, AR) \tag{2.3-12}$$

The *efficiency factor*, e, is close to unity, and aspect ratio is the important design parameter. This equation provides a guide to minimizing the induced drag of a complete aircraft, but the difficulties of constructing a light, high-aspect wing tend to limit the aspect ratio to values of 10 or lower, with the exceptions mentioned earlier.

Finally, consider wave drag. As in the case of an airfoil, an airplane will have a critical Mach number when the flow reaches supersonic speed at some point on the surface, and the airplane drag coefficient begins to rise. The drag divergence Mach number is the corner point or "knee" of the increasing drag coefficient curve and is reached next. A shock wave pattern is now established over the airplane and the total drag now includes wave drag. The drag coefficient continues to rise, peaks at about the end of the transonic regime, and falls off in the manner of the Prandtl-Glauert formula. Figure 2.3-2*a* shows the transonic drag rise for a particular fighter aircraft. The peak drag can be minimized by using a combination of three techniques. First, wing sweep (up to about 70°) is used to reduce the component of the relative wind that is normal to the leading edge of the wing. This has the effect of shifting the drag rise curve to the right and merging it into the supersonic part. The drag rise becomes less steep, the peak of the curve becomes less sharp, and its height is reduced. Second, supersonic aircraft use thin airfoils, with thickness-over-chord ratios down to about 5%; these airfoils have lower wave drag and higher critical Mach numbers than thick airfoils. Finally, if the cross-sectional area of the complete airplane is made to vary smoothly with the distance from nose or tail, then the drag peak can be significantly reduced. This is R. T. Whitcomb's famous *area rule* (Anderson, 1999), and it leads to a fighter fuselage with a pinched waist at the point where the wings begin.

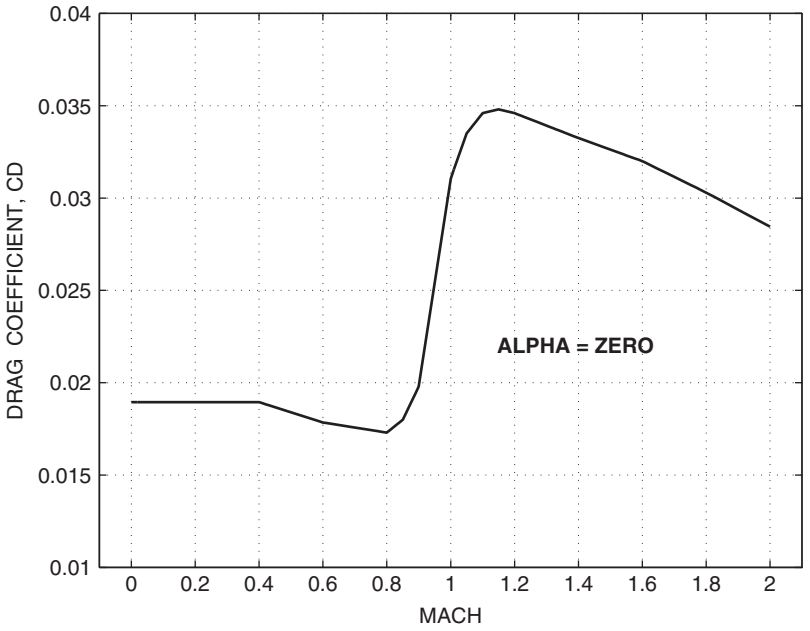

Figure 2.3-2*a* Transonic drag rise for a fighter aircraft.

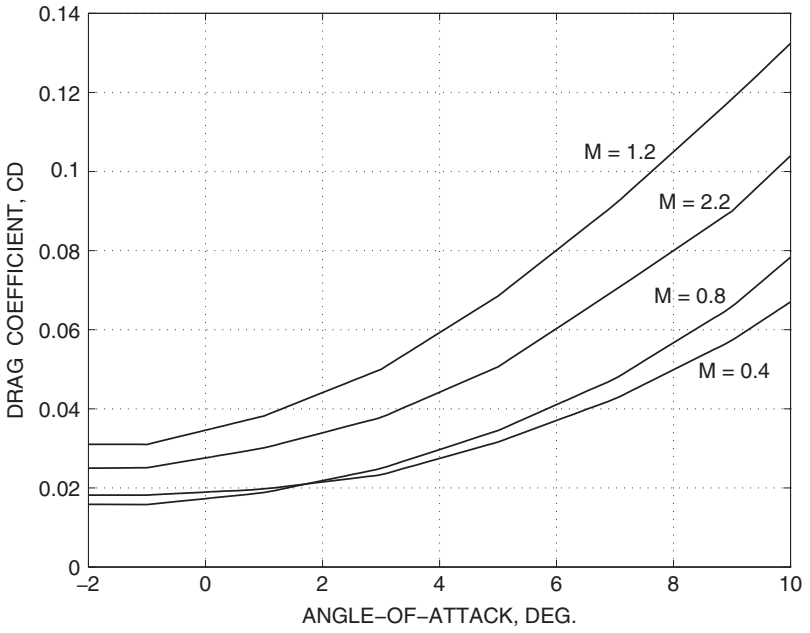

Figure 2.3-2*b* Drag coefficient of a fighter aircraft.

At constant Mach and below stall, the three types of drag described above each have a component that varies with the square of lift coefficient and a component that is independent of lift coefficient. Therefore, below stall, the complete airplane drag can be written as

$$C_D(C_L, M) = k\,(M)\,(C_L - C_{L_{DM}})^2 + C_{DM}(M), \tag{2.3-13}$$

where $k\,(M)$ is a proportionality constant that changes with Mach. This parabolic equation matches the actual drag variation quite accurately; it is known as the *drag polar*. Note that the minimum drag C_{DM} can occur at a nonzero value $C_{L_{DM}}$ of the lift coefficient.

If we consider lift beyond the stall, up to an angle of attack of 90°, two or possibly three values of alpha can correspond to a given lift coefficient, and the drag is in general different for each of these values of alpha. Therefore, for high-alpha simulation, we model drag as a function of alpha. Because lift is quite linear as a function of alpha below stall, the plot of drag coefficient is still parabolic in this region. Figure 2.3-2*b* shows the untrimmed baseline drag coefficient of the same supersonic fighter aircraft as used for Figure 2.3-2*a*, plotted against alpha with Mach as a parameter. In the figure, the drag varies parabolically with alpha and varies with Mach number in the same way as in Figure 2.3-2*a*.

In addition to the above effects, we can expect the drag coefficient to be dependent on altitude, sideslip, control surface and flap deflections, landing gear extension, and possibly ground effect. Altitude dependence (with Mach) allows for the effect of Reynolds number on the skin friction drag.

With the above facts and Equation (2.3-8*a*) in mind, we might expect a drag coefficient model consisting of a "baseline" component plus drag increments for control surfaces and gear of the form

$$\begin{aligned} C_D = {} & C_D(\alpha, \beta, M, h) + \Delta C_D(M, \delta_e) + \Delta C_D(M, \delta_r) + \Delta C_D(\delta_F) \\ & + \Delta C_D(\text{gear}) + \cdots \end{aligned} \tag{2.3-14}$$

With aircraft that operate with little sideslip, the sideslip dependence can be treated as a separate increment.

Lift Coefficient, C_L

The lift coefficient of the complete aircraft is determined by the wings, fuselage, and horizontal tail and their mutual interference effects. Nevertheless, it varies with alpha and Mach in a way similar to that described earlier for the finite wing. The variation of lift coefficient with alpha is usually quite linear until near the stall, when it drops sharply and then may rise again, before falling to zero when alpha is near 90°. The peak value of the lift coefficient may be as great as 3 for a highly cambered wing, but the increased drag of a highly cambered wing is not acceptable for high-speed aircraft. These aircraft use thin wings with not much camber and get their lift from the

higher dynamic pressure or from effectively increasing the camber with leading- and trailing-edge flaps to get lift at low speed. Ground effect produces greater lift for a given drag; it is usually negligible beyond one wingspan above the ground.

The slope of the lift curve increases with aspect ratio and with reduction in the wing leading-edge sweep angle. Light aviation aircraft and large passenger jets can have wing aspect ratios greater than 7, compared to 3 to 4 for a fighter aircraft. Increasing the wing sweep angle has the desirable (for high-speed aircraft) effect of delaying the transonic drag rise, and the sweep angle may lie between roughly 25° and 60°. Since lift-curve slope is an important factor in determining the response to turbulence, some military aircraft with a requirement for very-low-altitude high-speed flight tolerate the expense and weight of variable-sweep wings. Compressibility effects also change the slope of the lift curve. Airfoil section theory predicts that at subsonic Mach numbers the slope should vary as $(1 - M^2)^{-1/2}$ and at supersonic Mach numbers as $(M^2 - 1)^{-1/2}$, and this kind of behavior is observed in practical wings.

Dependence of lift on sideslip is usually small until the magnitude of the sideslip reaches several degrees, and since large values of sideslip only occur at low speed, this effect will typically be modeled as a separate Mach-independent correction to the baseline lift. The dependence on altitude is small and will be neglected here, and the dependence on control surface deflection is specific to the particular surface. Therefore, we will focus on the remaining three variables.

The *thrust coefficient*, T_C, normally applies to propeller aircraft and is used to account for propeller wash over the wings, fuselage, and vertical fin. It is defined by normalizing engine thrust in the same way as the nondimensional coefficients; thus,

$$T_C = \text{thrust}/\overline{q}S_D, \tag{2.3-15}$$

where S_D is the area of the disc swept out by a propeller blade. The propeller slip stream increases the airspeed over the wings, changes the angle of downwash behind the wing (which affects the angle of attack of the horizontal tail), and changes the dynamic pressure at the tail. The effect on the airplane lift curve can be very significant; Figure 2.3-3*a* shows the lift curve of a turboprop transport aircraft with four engines mounted directly on the wing. At high thrust coefficient, the figure shows a major increase in the peak lift coefficient and a shift of the peak to higher alpha. More information on power effects can be found in the work of Perkins and Hage (1949) and Stinton (1983).

Figure 2.3-3*b* shows the effect of Mach number on the lift curve of a fighter aircraft. Note that the slope of the lift curve at first increases with Mach number and then decreases. An additional effect (not shown) is that the peak lift coefficient decreases with increasing supersonic Mach number.

The normal force coefficient is often a more convenient quantity than lift coefficient. The normal force coefficient will usually rise with alpha, nearly monotonically, all the way to 90° angle of attack, whereas lift coefficient shows the complicated stall behavior. Unfortunately, its partner, the axial force coefficient, displays very complicated behavior in the same range of alpha and may change sign a few times over the range of alpha. The rotation matrix (2.3-2) and the definitions in Table 2.3-1 give

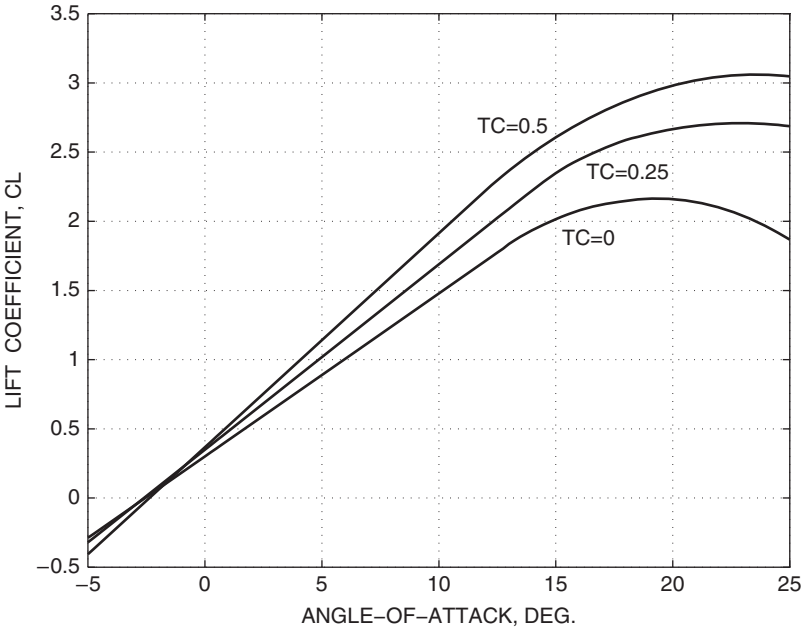

Figure 2.3-3*a* Lift coefficient of a low-speed transport aircraft.

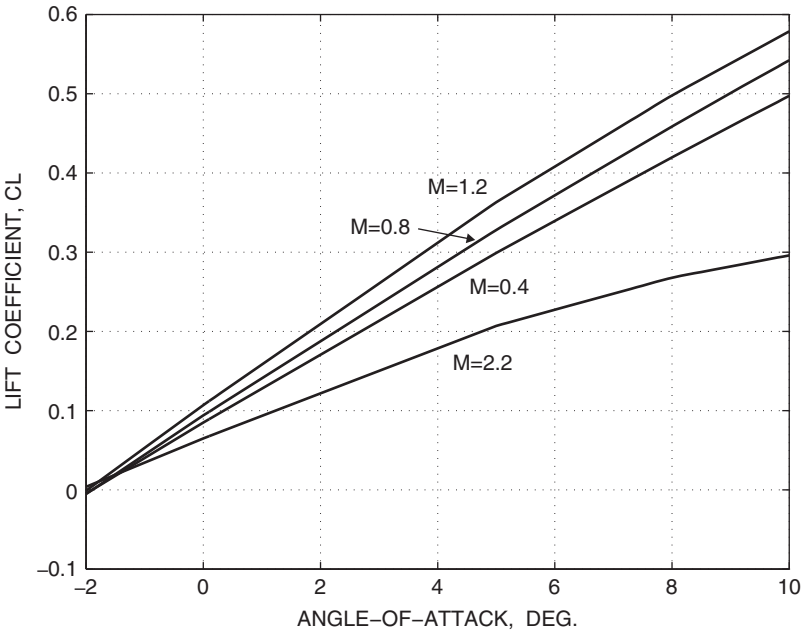

Figure 2.3-3*b* Lift coefficient of a fighter aircraft.

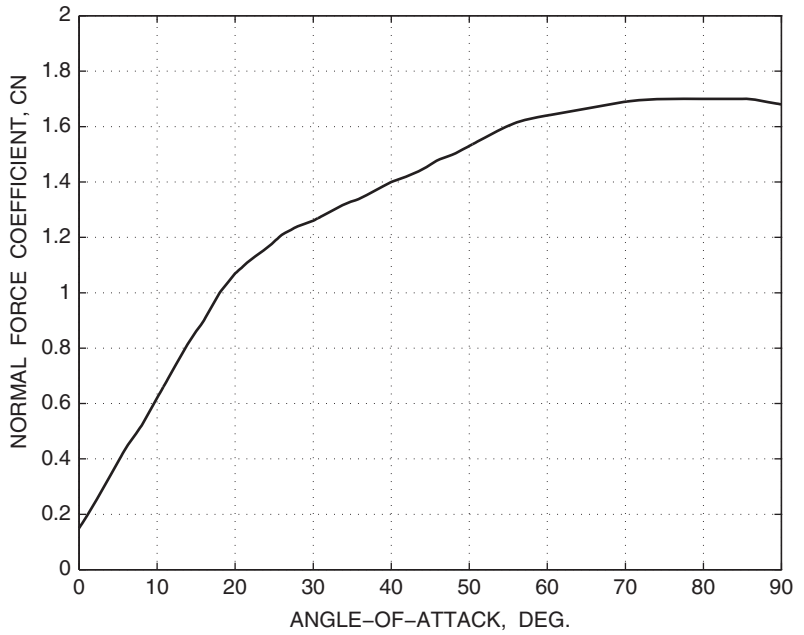

Figure 2.3-3*c* Normal force coefficient of the F-4E aircraft.

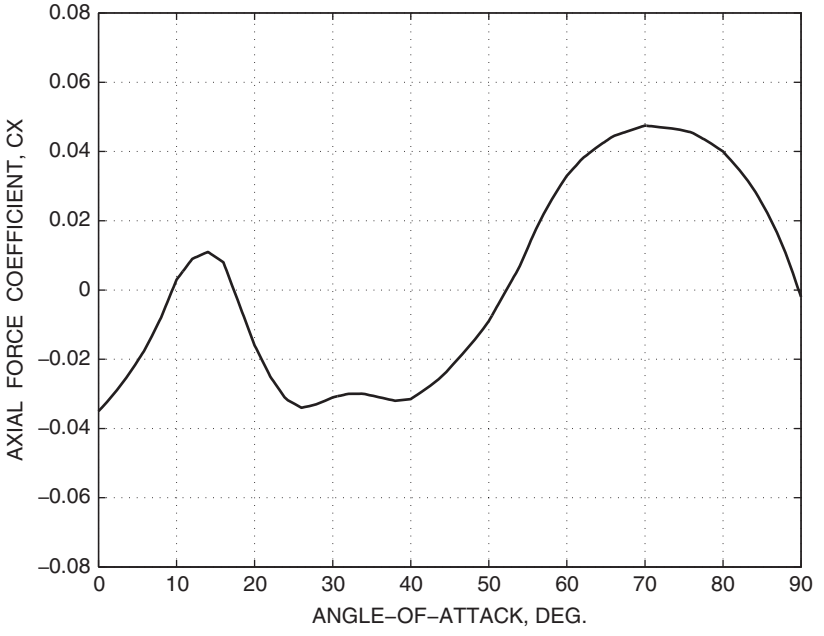

Figure 2.3-3*d* Axial force coefficient of the F-4E aircraft.

the following expressions for the lift and drag coefficients in terms of the body-axes coefficients:

$$C_D = -\cos\alpha\cos\beta\, C_X - \sin\beta\, C_Y + \sin\alpha\cos\beta\, C_N$$
$$C_L = \sin\alpha\, C_X + \cos\alpha\, C_N$$

and at low alpha $C_L \approx C_N$. Figures 2.3-3*c* and *d* show the low-Mach, high-alpha, normal and axial force coefficients for the F-4E aircraft.

A general model for lift coefficient may be of the form

$$C_L = C_L(\alpha, \beta, M, T_c) \; + \; \Delta C_L(\delta_F) + \Delta C_{L_{ge}}(h), \tag{2.3-16}$$

where $\Delta C_{L_{ge}}(h)$ is the increment of lift in ground effect.

Sideforce Coefficient, C_Y

In the case of a symmetrical aircraft, sideforce is created mainly by sideslipping motion (i.e., $\beta \neq 0$) and by rudder deflection. Figure 2.3-4 shows the sideforce coefficient for the F-4B and -C aircraft (Chambers and Anglin, 1969) for alpha equal to zero and 40° and with linear interpolation for other values of alpha. Note that positive sideslip leads to negative sideforce because positive sideslip corresponds to

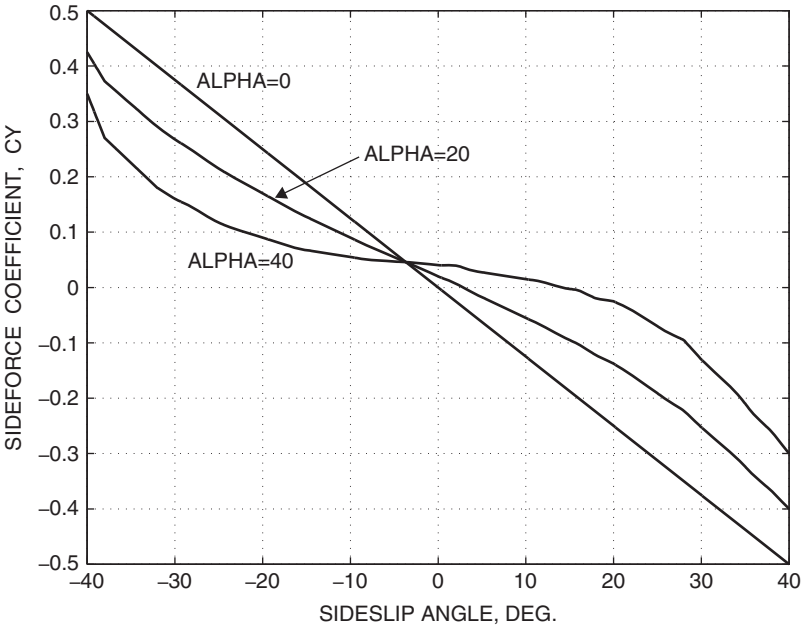

Figure 2.3-4 Sideforce coefficient of the F-4B, C aircraft.

the relative wind on the right-hand side of the nose. The high-alpha curve does not pass through the origin possibly because of asymmetry in the wind tunnel model or anomalies in the measurements. Note that at high subsonic speeds very little sideslip is possible without exceeding the hinge moment limit of the rudder or the structural limit of the vertical fin.

The sideforce model for a high-performance aircraft is typically of the form

$$C_Y = C_Y(\alpha, \beta, M) + \Delta C_{Y_{\delta r}}(\alpha, \beta, M, \delta_r) + \Delta C_{Y_{\delta a}}(\alpha, \beta, M, \delta_a) + \frac{b}{2V_T}\left[C_{Y_p}(\alpha, M)\,P + C_{Y_r}(\alpha, M)R\right] \tag{2.3-17a}$$

Additional corrections are added for flaps, gear, and the like. The last two terms are linear in the angular rates, and the other terms are linearized whenever acceptable accuracy is achieved; thus,

$$\begin{aligned} C_Y(\alpha, \beta, M) &\approx C_{Y_\beta}(\alpha, M) \times \beta \\ \Delta C_{Y_{\delta r}}(\alpha, \beta, M, \delta_r) &\approx C_{Y_{\delta r}}(\alpha, \beta, M) \times \delta_r \\ \Delta C_{Y_{\delta a}}(\alpha, \beta, M, \delta_a) &\approx C_{Y_{\delta a}}(\alpha, \beta, M) \times \delta_a \end{aligned} \tag{2.3-17b}$$

These terms have been linearized "around the origin," that is, for a symmetrical aircraft, the sideforce can be expected to go to zero when the sideslip is zero and the rudder and aileron are in their neutral positions.

Rolling Moment

Rolling moments are created by sideslip alone, by the control action of the ailerons and the rudder, and as damping moments resisting rolling and yawing motion. Consider first the effect of sideslip; if a right-wing-down roll disturbance occurs and is not corrected (stick fixed), then the effect of gravity will be to start a positive sideslip. If the aircraft aerodynamics are such that positive sideslip causes a positive rolling moment, then the roll angle will increase further. This is an unstable situation. We see that, for positive stiffness in roll, the slope of the rolling moment–sideslip curve should be negative. Therefore, it is useful to understand the aerodynamic effects that determine the behavior of the rolling moment coefficient with sideslip; this will be our baseline term in the rolling moment coefficient buildup.

The baseline rolling moment coefficient is primarily a function of sideslip, alpha, and Mach and can be written as $C_\ell(\beta, \alpha, M)$. Figure 2.3-5 is a plot of the rolling moment coefficient for the F-4B at low Mach number; it shows that, for small sideslip, the coefficient is approximately linear with beta, but changes in alpha can cause a significant change in slope. Also, at low alpha, sideslip greater than 20° can cause a loss of stability in roll. In general, the effect of sideslip is to create a lateral component of the relative wind, and there are three separate effects of this lateral component on the horizontal aerodynamic surfaces. These will now be described.

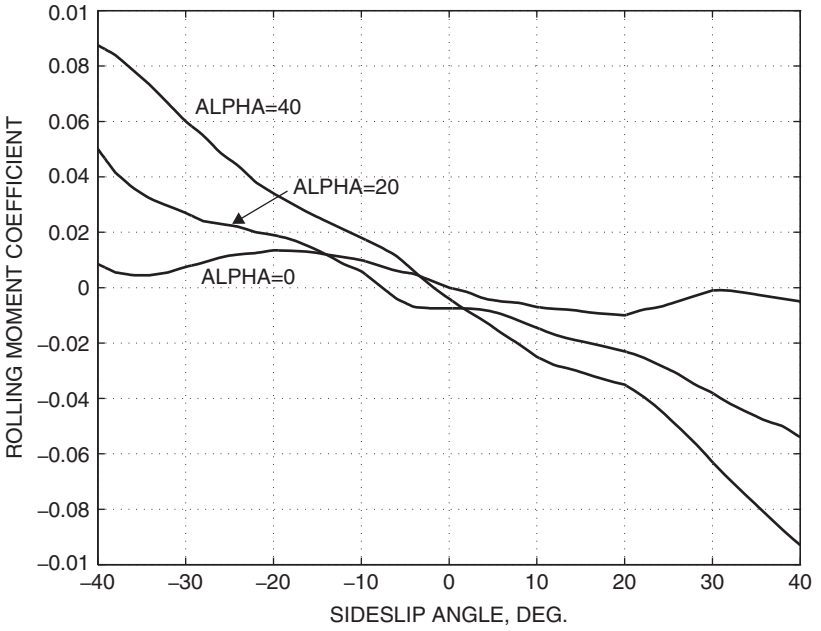

Figure 2.3-5 Rolling moment coefficient of the F-4B aircraft.

First, note that the angle by which the wings of an aircraft are canted up above the body-axes $x-y$ plane is called the *dihedral angle*, and a negative dihedral angle is called an *anhedral angle*. Dihedral is often very noticeable on small low-wing (wing root attached at the bottom of the fuselage) aircraft, while a well-known example of anhedral is the Harrier (AV-8B) aircraft. Dihedral (or anhedral) angles give one wing a positive angle of attack (in a spanwise direction) to the lateral component of the relative wind, and the other wing receives a similar negative angle of attack. Referring to Figure 2.3-1, it is easy to see that positive beta creates a negative rolling moment when the wings have positive dihedral. This same effect applies to the horizontal tail.

The second effect of sideslip on the horizontal surfaces occurs when they are swept back. In this case the relative wind is more nearly perpendicular to the leading edge of the windward wing than is the case for the leeward wing. Therefore, the windward wing develops more lift, and the outcome is again a negative rolling moment for positive beta.

The third effect of sideslip on the horizontal surfaces is that on the windward side of the fuselage some of the lateral airflow is diverted up and over the fuselage and some is diverted under the fuselage. This flow will modify the angle of attack of the wings, depending on their position on the fuselage. Above the centerline of the fuselage, the upward component of the relative wind is increased. Therefore, for a high-wing aircraft, the angle of attack of that wing is increased (assuming that it was operating at a positive alpha). For a low-wing aircraft the upward component of the relative wind would be reduced by the effect of the air flowing down and under the

fuselage, and the angle of attack of that wing would be reduced. Thus, for low-wing aircraft, positive sideslip creates a positive contribution to rolling moment, and for high-wing aircraft it creates a negative contribution.

Finally, the lateral component of the relative wind acting on the vertical tail will generate a rolling moment about the cm. Depending on the aircraft angle of attack and the location of the center of pressure of the vertical tail, this rolling moment could be positive or negative. Usually positive beta will produce a negative rolling moment component.

Of all the above effects, only the fuselage effect on a low-wing airplane led to a positive increment in rolling moment in response to a positive increment in beta. This can be a strong effect and is responsible for a loss of stability in roll. Low-wing airplanes usually have noticeable positive dihedral in order to provide positive roll stiffness. The airplanes will then have an inherent tendency to fly with wings level.

For a high-performance aircraft the rolling moment model will typically be of the form

$$C_{\ell} = C_{\ell}(\alpha, \beta, M) + \Delta C_{\ell_{\delta a}}(\alpha, \beta, M, \delta_r) + \Delta C_{\ell_{\delta r}}(\alpha, \beta, M, \delta_a) + \frac{b}{2V_T}\left[C_{\ell_p}(\alpha, M)\, P + C_{\ell_r}(\alpha, M) R\right], \tag{2.3-18a}$$

where C_{ℓ_p} is the *roll damping derivative*. The rolling moment dependence on β, and the aileron and rudder, can often be linearized around the origin:

$$\begin{aligned} C_{\ell}(\alpha, \beta, M) &\approx C_{\ell_\beta}(\alpha, M) \times \beta \\ \Delta C_{\ell_{\delta a}}(\alpha, \beta, M, \delta_a) &\approx C_{\ell_{\delta a}}(\alpha, \beta, M) \times \delta_a \\ \Delta C_{\ell_{\delta r}}(\alpha, \beta, M, \delta_r) &\approx C_{\ell_{\delta r}}(\alpha, \beta, M) \times \delta_r, \end{aligned} \tag{2.3-18b}$$

where C_{ℓ_β} is the *dihedral derivative* that determines static stability in roll and $C_{\ell_{\delta a}}$ and $C_{\ell_{\delta r}}$ are roll *control derivatives*.

Figure 2.3-6 shows the stability-axes, trimmed, roll damping derivative for the F-4C. The data are Mach dependent because of compressibility and altitude dependent because the trimmed angle of attack changes with altitude and because of aeroelastic changes with dynamic pressure.

Control Effects on Rolling Moment

We now briefly examine the control moment terms in Equations (2.3-18) with respect to their dependence on alpha and Mach. The rudder is intended to provide directional control (yaw), so the "cross-control" effect on rolling moment is an unwanted effect. This effect comes about because the center of pressure of the rudder is normally above the longitudinal axis.

Conventional ailerons mounted outboard on the trailing edge of the wings become ineffective and can reverse their net effect as high subsonic speeds are approached.

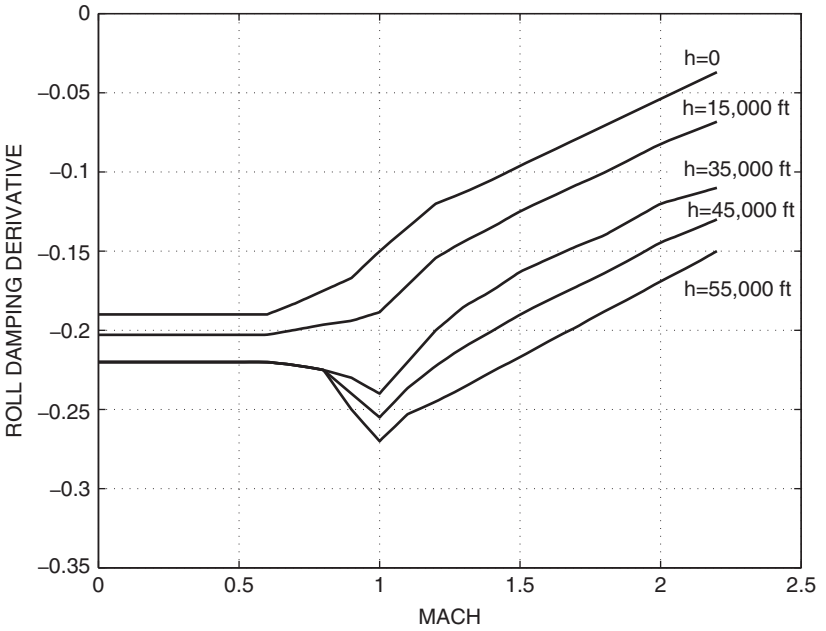

Figure 2.3-6 Roll damping derivative of the F-4C aircraft.

This is because the aileron lift component produced by a downward deflection twists the wing in the direction that reduces its angle of attack and hence reduces the wing lift component. Spoilers, which are uncambered surfaces deflected upward above the aft surface of the wing, "spoil" the lift on that portion of the wing and thus provide roll control. The twisting effect on the wing is reduced and control reversal can be avoided. Spoilers are commonly combined with ailerons in such a way that one aileron and the opposite spoiler operate simultaneously, and the ailerons deflect downward only. Mounting the ailerons farther inboard reduces the effect of wing twist but also reduces their moment arm. However, the X-29 forward-swept-wing aircraft is an example of combined inboard and outboard "flaperons" being made to work very effectively up to high alpha (Kandebo, 1988).

The effectiveness of both ailerons and spoilers is reduced by cross-flows on the wing and hence by wing sweep. Therefore, for swept-wing aircraft, an additional rolling moment is obtained by using differential control of the horizontal-tail control surfaces (e.g., most modern fighter aircraft).

Pitching Moment

The baseline pitching moment coefficient may typically be written as $C_m(\alpha, M, T_c)$ for a low-speed aircraft or $C_m(\alpha, M, h)$ for a high-speed jet aircraft where aeroelastic effects are included. Figure 2.3-7*a* illustrates the dependence of this coefficient on α and T_c for the low-speed turboprop transport aircraft. The figure shows that, as

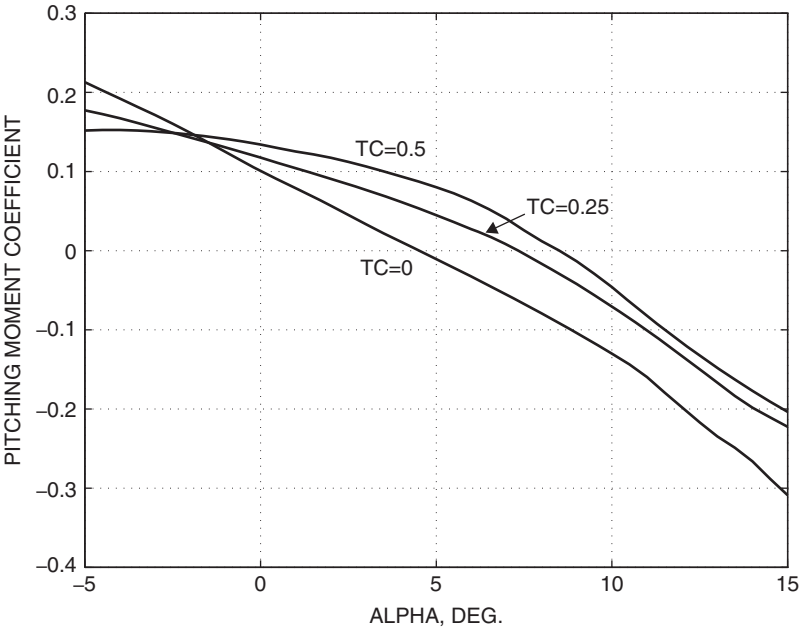

Figure 2.3-7*a* Pitching moment coefficient of a low-speed transport aircraft.

alpha increases, the nose-down (restoring) moment becomes steadily stronger. At low freestream angles of attack and high thrust coefficient, the propeller wash tends to make the effective angle of attack independent of the freestream direction, and the moment curve has only a small negative slope (reduced pitch stiffness).

Figure 2.3-7*b* shows a baseline moment coefficient that is representative of a supersonic jet-trainer. In this case the parameter is Mach number, and the slope of the moment curve gets steeper with increasing Mach because of the rearward shift of the wing-body aerodynamic center. This increasing pitch stiffness is detrimental to maneuverability and to the lift-over-drag ratio; it is discussed further in the pitch static stability section.

For a high-performance aircraft the pitching moment coefficient will be built up in the form

$$C_m = C_m(\alpha, M, h, \delta_F, T_c) + \Delta C_{m_{\delta e}}(\alpha, M, h, \delta_e) + \frac{\overline{c}}{2V_{\mathrm{T}}}[C_{m_q} Q + C_{m_{\dot{\alpha}}} \dot{\alpha}]$$
$$+ \frac{x_R}{\overline{c}} C_L + \Delta C_{m_{\mathrm{thrust}}}(\delta_t, M, h) + \Delta C_{m_{\mathrm{gear}}}(h) \qquad (2.3\text{-}19a)$$

In the baseline term, all five variables are unlikely to be present simultaneously. The M and h variables imply a high-speed aircraft, while T_c implies a low-speed propeller aircraft. Also, the effect of wing flap deflection, δ_F, may be treated as

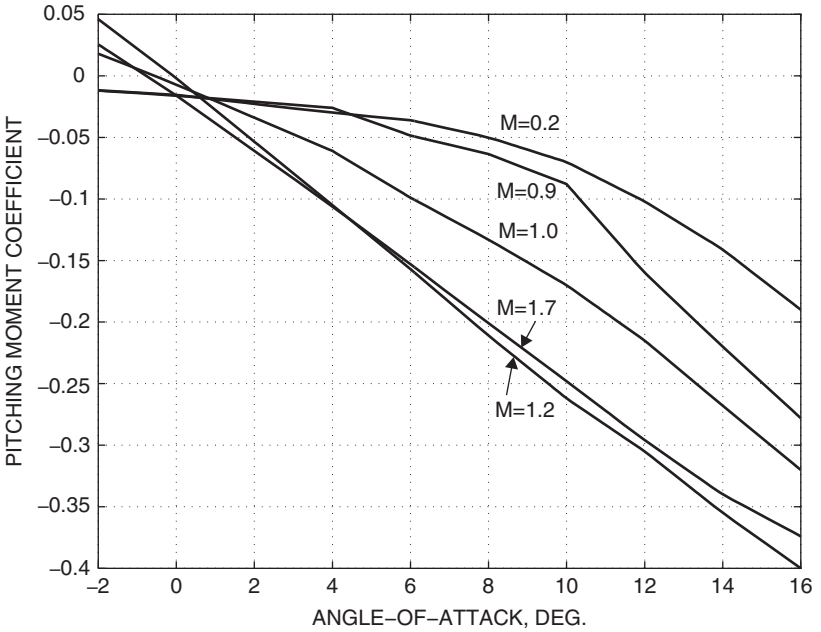

Figure 2.3-7*b* Pitching moment coefficient of a jet trainer aircraft.

a separate increment. The elevator increment term may often be linearized around the origin:

$$\Delta C_{m_{\delta e}}(\alpha, M, h, \delta_e) \approx C_{m_{\delta e}}(\alpha, M, h) \times \delta_e, \tag{2.3-19b}$$

where $C_{m_{\delta e}}$ is the *elevator control power*. The pitch damping derivative C_{m_q} and the alpha-dot acceleration derivative will also be functions of alpha, Mach, and altitude and are discussed in Section 2.6. The purpose of the term $(x_R C_L)/\overline{c}$ is to correct for any x-displacement (x_R) of the aircraft cm from the aerodynamic data reference position. If x_R is not zero, the lift force will provide a contribution to the pitching moment. This is considered in more detail in the next section. The last two terms represent, respectively, the effect of the engine thrust vector not passing through the aircraft cm and the moment due to landing gear doors and landing gear. This last term is dependent on height above ground because of ground effect.

Control Effects on Pitching Moment

A conventional elevator for a subsonic aircraft consists of a movable surface at the trailing edge of the horizontal tail. In addition, the horizontal tail may move as a whole, or a "tab" on the elevator may move, so that the elevator deflection can be trimmed to zero in various flight conditions. In transonic and supersonic

flight a shock wave attached to the horizontal tail would render this type of elevator ineffective. Therefore, on supersonic aircraft the complete horizontal stabilizer surface moves (i.e., a "stabilator") in response to control stick or trim button signals. As indicated above, elevator (or stabilator) control power is dependent on Mach and altitude because compressibility and aeroelastic effects cause the elevator effectiveness to decrease with increasing Mach number and dynamic pressure.

An aft tail experiences a downwash effect from the wing and a reduction in dynamic pressure. These are alpha-dependent effects and can be included in the control power term as implied above. However, for a propeller aircraft, the dynamic pressure at the tail is strongly dependent on thrust coefficient and may be greatly increased. This can be modeled by multiplying the elevator control power by a *tail efficiency factor*, η, which is a function of alpha, thrust coefficient, flap deflection, and ground effect:

$$\eta(\alpha, T_c, \delta_F, h) \equiv \overline{q}_{TAIL}/\overline{q} \tag{2.3-20}$$

The tail efficiency factor of a propeller aircraft may exceed 2.0 at high values of thrust coefficient.

Yawing Moment

Yawing moments are created by sideslip, by the action of the rudder, by propeller effects, by unbalanced thrust in a two-engine aircraft, and, to a lesser extent, by differences in drag between the ailerons and by asymmetric aerodynamic effects at high alpha (e.g., "vortex shedding").

The sideslip dependence has three components. A small component is created by wing sweep: Positive sideslip creates a positive yawing moment because the right wing becomes more nearly perpendicular to the freestream direction and develops more lift and drag. Second, the fuselage produces a strong negative yawing moment when in positive sideslip (see, for example, Perkins and Hage, 1949). Third, directional stability demands that the aircraft should tend to weathercock into the relative wind; therefore, it is the job of the vertical tail to provide a strong yawing moment of the same sign as beta. This moment is computed from the moment arm of the tail about the cm and the "lift" generated by the vertical tail when in sideslip. The overall result of these effects is that the yawing moment is quite linear in beta for low values of sideslip.

When the aircraft is at a high angle of attack, the fuselage yawing moment can become more adverse, and at the same time the dynamic pressure at the tail may be reduced, eventually resulting in a loss of directional stability. Figure 2.3-8*a* shows low-speed, high-alpha, yawing moment data for the F-4B, C aircraft, and clearly shows the loss of directional stability at high alpha.

A rotating propeller produces several different "power effects," which are best included in the propulsion model (Perkins and Hage, 1949; Ribner, 1943). A conventional tractor propeller has a destabilizing effect in yaw, while a pusher propeller has a stabilizing effect. The slipstream of a tractor propeller strongly affects the dynamic pressure at the tail of the airplane, and the swirl of the slipstream modifies the flow

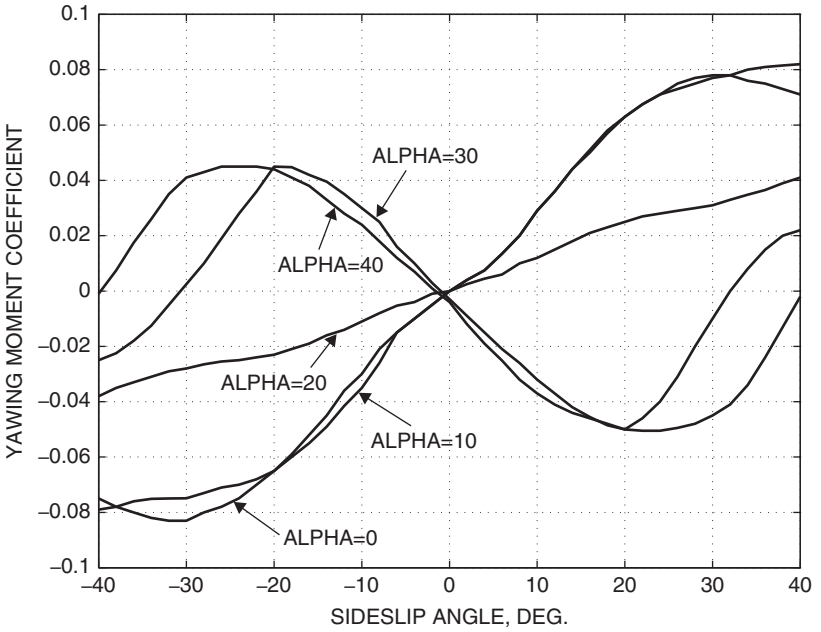

Figure 2.3-8*a* Yawing moment coefficient of the F-4B, C aircraft.

over the fuselage and tail. Thus, the baseline yawing moment can have a strong dependence on thrust coefficient.

Finally, with a high-speed aircraft, compressibility effects can cause the slope of the yawing moment–beta curve to be a function of Mach number. Figure 2.3-8*b* shows the effect of Mach on the yawing moment of the jet trainer aircraft at low alpha.

The yawing moment coefficient for a high-performance aircraft will be of the form

$$C_n = C_n(\alpha, \beta, M, T_c) + \Delta C_{n_{\delta r}}(\alpha, \beta, M, \delta_r) + \Delta C_{n_{\delta a}}(\alpha, \beta, M, \delta_a) + \frac{b}{2V_T}\left[C_{n_p}(\alpha, M)\,P + C_{n_r}(\alpha, M)R\right], \tag{2.3-21a}$$

where C_{n_r} is the *yaw damping derivative*. The thrust coefficient in the baseline term is appropriate for a propeller aircraft. The yawing moment dependence on β, and the rudder and aileron, can often be linearized around the origin:

$$\begin{aligned} C_n(\alpha, \beta, M, T_c) &\approx C_{n_\beta}(\alpha, M, T_c) \times \beta \\ \Delta C_{n_{\delta r}}(\alpha, \beta, M, \delta_r) &\approx C_{n_{\delta r}}(\alpha, \beta, M) \times \delta_r \\ \Delta C_{n_{\delta a}}(\alpha, \beta, M, \delta_a) &\approx C_{n_{\delta a}}(\alpha, \beta, M) \times \delta_a, \end{aligned} \tag{2.3-21b}$$

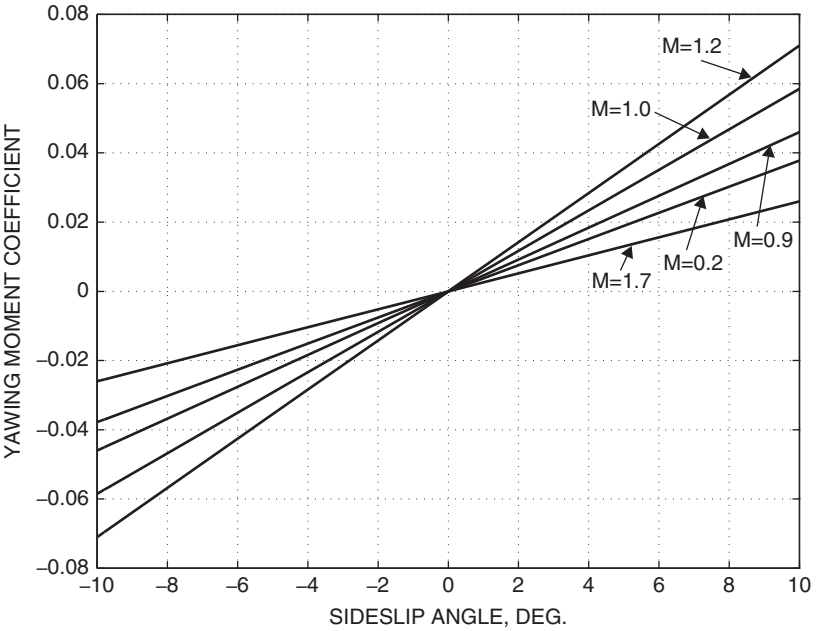

Figure 2.3-8*b* Yawing moment coefficient of a jet trainer aircraft.

where C_{n_β} is the *yaw stiffness derivative* that determines the directional stability and $C_{n_{\delta r}}$, $C_{n_{\delta a}}$ are yaw control derivatives.

Control Effects on Yawing Moment

The rudder usually forms a part of the trailing edge of the vertical tail; when deflected, it provides a strong yawing moment and some rolling moment. Its purpose is to create sideslip (e.g., for cross-wind landing) or remove sideslip (e.g., to coordinate a turn). The vertical tail is no longer a symmetric airfoil section when the rudder is deflected and then begins to produce "lift." The resulting sideforce is such that deflection of the rudder trailing edge to the right produces a positive yawing moment. All-moving vertical fins are sometimes used for rudder control, as, for example, on the SR-71, where large yawing moments can occur as a result of an engine "unstart."

Like the horizontal tail, the vertical tail and rudder can be affected by wing downwash and blanketed at high angles of attack. A tail efficiency factor can be used to model the effect, as in the pitching moment equation. Wing flap deflection can also significantly change the downwash at the rudder.

Differential deflection of the ailerons and spoilers also produces a yawing moment because of the difference in drag between the two sets. As described earlier, roll control can be obtained in a number of different ways, and the cross-control effects on yawing moment can vary.

Data Handling

It should be clear from the foregoing description of aerodynamic forces and moments that the aerodynamic database for a given aircraft can become rather large. It may range from roughly fifty data tables for a relatively simple piloted simulation model to several thousand tables for an aircraft like the Lockheed-Martin F-22. Many of the tables will have four independent variables and could contain over 10,000 data points; the whole database could contain a few million points.

A large aerodynamic database must be handled efficiently within an organization; it represents thousands of hours of planning, model testing, flight testing, and computer simulation. It must be kept current, with all changes fully documented, and be accessible to different users. The control engineer will have access to the database through a computer workstation and will be able to call up the appropriate force and moment routines for the equations of motion. An example of a small database has been given by Nguyen et al. (1979) for low-speed F-16 model data, taken at the NASA Dryden and Langley Research Centers. A three-dimensional plot made from one of the two-dimensional (two independent variables) tables of this F-16 data is shown in Figure 2.3-9. A reduced data set derived from this report is listed in the appendices and is used for the F-16 model given in Chapter 3.

Aerodynamic lookup table data are discrete, whereas aircraft models require data at arbitrary values of the independent variables. This problem is solved by using an

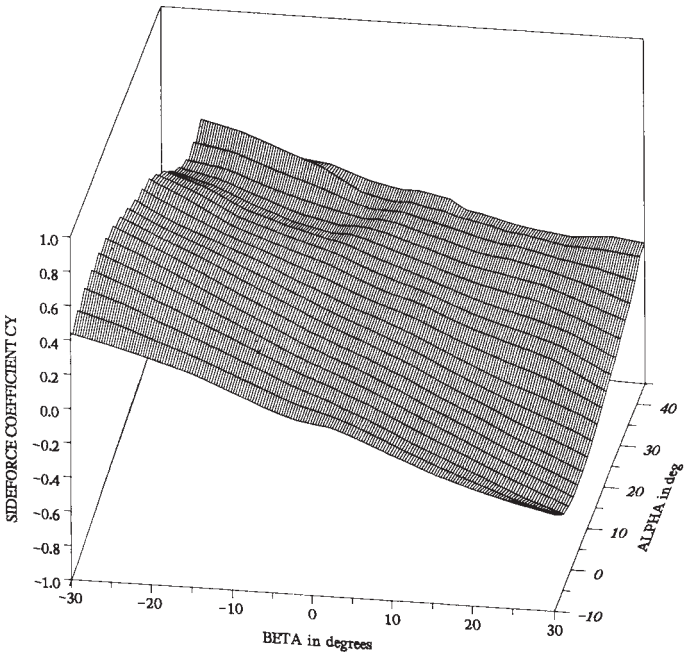

Figure 2.3-9 Sideforce coefficient of the F-16 model.

interpolation algorithm with the data. In the appendices we have provided a simple interpolation algorithm for use with the F-16 data.

Basic aerodynamic data are often rough (scattered data points). This is because of the inaccuracies associated with measuring aerodynamic data, the sensitivity to small changes in the independent variables, and fusion of data from different sources or test runs. The data can be smoothed and regenerated at new uniform increments of the independent variables as required, for example, by means of a "spline" algorithm [International Mathematical and Statistical Libraries (IMSL), 1980; Press et al., 1989].

2.4 STATIC ANALYSIS

In steady-state flight the forces and moments acting on an aircraft are constant (i.e., static) when taken in the body frame. Static analysis provides the basic information for sizing and configuring the aircraft and evaluating its performance and lays the groundwork for dynamic analysis. A "static stability" analysis is used to determine if the aircraft will return to a steady-state flight condition after being subjected to a small atmospheric disturbance. For example, an incremental increase in Mach number can produce a net increase in thrust minus drag and cause a relatively slow departure, in speed, from the equilibrium condition. In contrast, an unstable departure in pitch could be too fast for the pilot to control and could lead to structural failure. The static stability analysis is so-called because rate-dependent effects are not considered, and it is usually performed for the special case of wings-level, nonturning flight. Dynamic stability in all of the motion variables can be determined from the eigenvalues of the linearized equations of motion and is considered in Chapters 3 and 4. It can easily be performed in other steady-state flight conditions, for example, a steady turn.

Static Equilibrium

Here we consider only wings-level, zero-sideslip flight. Suitable coordinate systems for this analysis are the body-fixed axes and the stability axes (now coincident with the wind axes). We must bear in mind that the origin of these systems, the aircraft cm, is not a fixed point. The cm will move as fuel is drawn from different tanks or because of cargo movement or stores being dropped. Aerodynamic data are referred to a fixed point, typically the point inside the fuselage where a line joining the quarter-chord points, in the wing roots, intersects the plane of symmetry.

Figure 2.4-1 shows the forces and moments on the aircraft. In the figure, $R(x_R, 0, z_R)$ is the reference point for the aerodynamic moment data, C is the aircraft cm, and T is the quarter-chord point (in the plane of symmetry) of the horizontal tail. The term $\mathbf{F}_R$ is the resultant aerodynamic force on the aircraft, L and D are its lift and drag components, and $\mathbf{M}_R$ is the total aerodynamic moment at R. With respect to the aircraft cm, the position vectors of R and the quarter-chord point in the horizontal tail are, respectively, $\mathbf{r}_R$ and $\mathbf{r}_t$. The chord line of the horizontal tail has an incidence

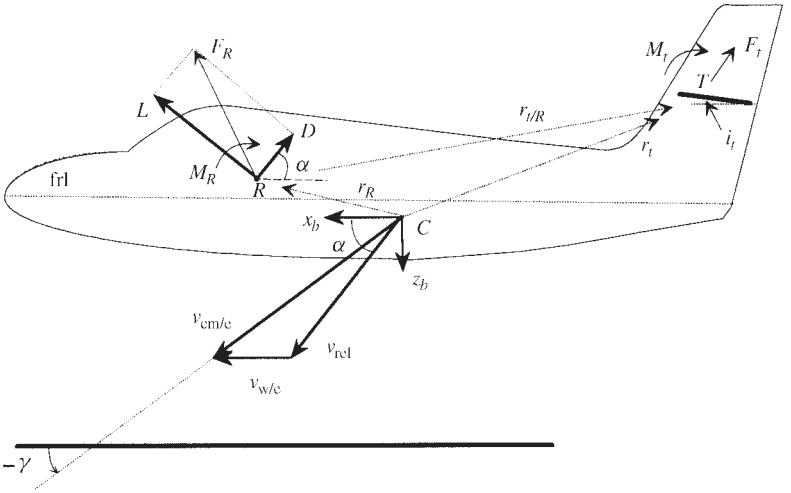

Figure 2.4-1 Diagram for calculating pitching moment.

angle i_t to the fuselage reference line. The thrust vector $\mathbf{F}_T$ (not shown) is assumed to lie in the plane of symmetry, tilted up at an angle α_T to the fuselage reference line, and does not necessarily pass through the cm.

To determine the equilibrium conditions, the direction of the gravity vector must be known relative to the aircraft. The *flight-path angle* γ shown in the figure is the angle that the velocity vector $\mathbf{v}_{CM/e}$ makes with the NE plane and is positive when the aircraft is climbing. For simplicity the wind velocity will be taken to be zero so that $\mathbf{v}_{rel} = \mathbf{v}_{CM/e}$, and alpha and the flight-path angle will determine orientation relative to the gravity vector. Then summing force components along the x and z stability axes yields

$$F_T \cos(\alpha_{frl} + \alpha_T) - D - \mathrm{m}g_D \sin\gamma = 0 \tag{2.4-1a}$$

$$F_T \sin(\alpha_{frl} + \alpha_T) + L - \mathrm{m}g_D \cos\gamma = 0 \tag{2.4-1b}$$

The moment at the cm is given by

$$\mathbf{M}_{CM} = \mathbf{M}_R + \mathbf{r}_R \times \mathbf{F}_R + \mathbf{M}_p, \tag{2.4-2}$$

where $\mathbf{M}_p$ is the pitching moment created directly by the engines. Using body-axes components in the cross-product yields the equilibrium equation

$$0 = M_{CM} = M_R + x_R F_N + z_R F_X + M_p, \tag{2.4-3}$$

where the normal force, F_N, and axial force, F_X, are given by

$$F_N = L \cos\alpha_{frl} + D \sin\alpha_{frl}$$

$$F_X = L \sin\alpha_{frl} - D \cos\alpha_{frl}$$

Now divide (2.4-3) by $(\overline{q}S\overline{c})$ to obtain dimensionless moment coefficients,

$$C_{m_{CM}} = C_{m_R} + \frac{x_R}{\overline{c}}C_N + \frac{z_R}{\overline{c}}C_X + C_{m_p}, \tag{2.4-4}$$

where C_{m_p} is thrust moment made dimensionless by dividing by $(\overline{q}S\overline{c})$, and

$$\begin{aligned} C_N &= [C_L \cos\alpha_{frl} + C_D \sin\alpha_{frl}] \approx C_L \text{ in cruise,} \\ C_X &= [C_L \sin\alpha_{frl} - C_D \cos\alpha_{frl}] \end{aligned} \tag{2.4-5}$$

In equilibrium, the left-hand side of Equation (2.4-4) is zero, and in cruise conditions, $\cos\alpha_{frl} \approx 1, \sin\alpha_{frl} \approx \alpha_{frl}, C_L \gg C_D, C_N \gg C_X$. Normally, the coordinates x_R and z_R are both small, and either one could be zero.

In *performance analysis* we solve the nonlinear equilibrium equations (2.4-1) and (2.4-4) for a given flight condition (true airspeed and altitude) using an iterative computer algorithm [(Problem (2.4-1)]. The data required are $F_T(M, h, \delta_t)$, aerodynamic data—$C_L(\alpha, M, \delta e), C_D(\alpha, M, \delta e), C_{m_R}(\alpha, M, \delta e)$—and an atmosphere model to determine mass density and the speed of sound at any altitude. Effects such as flaps and gear can be included if required. If the effect of elevator deflection on lift and drag is ignored, then the force equations are independent of the moment equation.

Effect of the Horizontal Tail

Now suppose that $\mathbf{F}_{wb}$ and $\mathbf{M}_{R,wb}$ are the aerodynamic force and moment vectors at R when the horizontal tail is removed from the aircraft. The flow over the wing-body combination creates a downwash effect at the horizontal-tail position and a change in dynamic pressure, both of which are dependent on flight conditions. These effects will be modeled later. Let $\mathbf{F}_t$ and $\mathbf{M}_{c/4,t}$ be the force and moment vectors measured at the quarter-chord point of the isolated horizontal tail when it is placed in the same flowfield that exists at the tail position of the wing-body combination. Also, assume that putting the horizontal tail back on the wing-body combination does not significantly modify the wing-body flowfield. With these assumptions, we can write

$$\mathbf{M}_{CM} = \mathbf{M}_{R,wb} + \mathbf{M}_{c/4,t} + \mathbf{r}_R \times \mathbf{F}_{wb} + \mathbf{r}_t \times \mathbf{F}_t + \mathbf{M}_p \tag{2.4-6a}$$

$$\mathbf{F}_R = \mathbf{F}_{wb} + \mathbf{F}_t \tag{2.4-6b}$$

In order to have the tail position specified in terms of a fixed vector, let

$$\mathbf{r}_t = \mathbf{r}_R + \mathbf{r}_{t/R},$$

where $\mathbf{r}_{t/R}$ is shown in the figure. Then from Equations (2.4-6a) and (2.4-6b),

$$\mathbf{M}_{CM} = \mathbf{M}_{R,wb} + \mathbf{M}_{c/4,t} + \mathbf{r}_R \times \mathbf{F}_R + \mathbf{r}_{t/R} \times \mathbf{F}_t + \mathbf{M}_p \tag{2.4-7}$$

The aerodynamic moment vector at the cm has the same y component M in either body or stability axes; other components are zero because of the symmetrical flight

condition. Equation (2.4-7) will be evaluated using the body-fixed components of the reference point and the horizontal tail. It will be assumed that the aerodynamic data reference point, tail quarter-chord point, and center of mass are at the same height in the fuselage, so that the z-components disappear from the equation. This allows conclusions to be drawn about the effect of the longitudinal position of the cm on static stability, with much less cumbersome equations; it is also usually a good approximation in practice. Equation (2.4-7) then yields the scalar equation:

$$M_{CM} = M_{R,wb} + M_{c/4,t} + x_R[L\ \cos(\alpha_{frl}) + D\ \sin(\alpha_{frl})] + (x_t - x_R)\ [L_t \cos(\alpha_{frl} - \varepsilon) + D_t\ \sin(\alpha_{frl} - \varepsilon)] + M_p \tag{2.4-8}$$

In this equation ε is the *downwash angle* at the horizontal tail and is usually positive with a magnitude of a few degrees. It represents the effect of the wings and fuselage on the direction of flow at the tail and is a function of the aircraft angle of attack and thrust effects (Roskam, 1979). The tail lift, L_t, and drag, D_t, are defined relative to the direction $(\alpha_{frl} - \varepsilon)$. In addition to the downwash effect at the tail, the airflow over the tail is modified in speed by the effect of the wings and body. This effect is modeled by the tail efficiency [η, Equation (2.3-20)].

The tail lift and drag are computed from $\overline{q}_t$ and tail reference area S_t. Therefore, dividing Equation (2.4-8) by $(\overline{q}\,\overline{c}S)$ yields

$$C_{m_{CM}} = C'm_R + \frac{x_R}{\overline{c}}[C_L\ \cos(\alpha_{frl}) + C_D\ \sin(\alpha_{frl})] - \eta\overline{V}_H[C_{L_t}\ \cos(\alpha_{frl} - \varepsilon) + C_{D_t}\ \sin(\alpha_{frl} - \varepsilon)] + C_{m_p}, \tag{2.4-9}$$

where

$$C'_{m_R} = C_{m_{R,wb}} + \eta\frac{\overline{c}_t S_t}{\overline{c}S} C_{m_{c/4,t}} \tag{2.4-10}$$

and $\overline{V}_H$ is a modification of the *horizontal-tail volume ratio* [Equation (2.6-35)], given by

$$\overline{V}_H = -\frac{(x_t - x_R)S_t}{\overline{c}S} \tag{2.4-11}$$

$\overline{V}_H$ is constant and positive for an aft tail because its numerator contains the distance of the reference point ahead of the tail. Note that, in the normal range of alpha, the drag terms in (2.4-9) can be discarded. A study of the moment equation will tell us how much elevator deflection is required to trim the aircraft and the effect of movement of the aircraft cm on trimmed elevator deflection.

Static Stability Analysis in Pitch

We focus here on the pitching moment equation and the requirements on the aircraft configuration for static stability in pitch. Static directional and rolling stability are considered in Section 2.6, in conjunction with the stability derivatives.

The moment balance around the pitch axis of the aircraft is critical to both performance and stability. If the lift force generated by the wings and body creates a large moment about the cm, the horizontal tail must carry a significant load. If this is a download, the overall effect is additional drag with a net reduction in lift and reduced load-carrying efficiency. In Section 2.2 we saw that the moment about the airfoil aerodynamic center was constant and relatively small, and for positive pitch stiffness, the axis about which the airfoil pivoted needed to be ahead of the ac. Therefore, the cm of the aircraft should be ahead of the ac of the wing-body combination, and the pitch stiffness of the complete aircraft must be analyzed. We also saw in Section 2.2 that the zero-alpha moment M_0 needed to be positive in order to obtain equilibrium with a positive angle of attack (and therefore provide the design lift). For a conventional aircraft this is achieved by giving the horizontal tail a negative incidence, so that it provides a positive contribution to the total pitching moment. Efficiency can be improved by reducing the pitch stiffness [this is done in relaxed static stability (RSS) designs], but then the movement of the cm must be more carefully controlled and the flight control system may need to be designed to provide artificial stability.

As in Section 2.2, to determine the static stability in pitch we need to find the slope of the pitching moment–alpha curve. Therefore, we must differentiate, with respect to α_{frl}, the total pitching moment at the center of mass as given by (2.4-9). In this equation each trigonometric function is multiplied by an aerodynamic coefficient that is also a function of alpha. In addition, tail efficiency and downwash angle are functions of alpha, and differentiation produces a very cumbersome expression. Nevertheless, the expression can be simplified by making use of the relationships

$$\begin{aligned} \alpha_t &= \alpha_{frl} + i_t - \varepsilon \\ \partial\alpha_t/\partial\alpha_{frl} &= 1 - \partial\varepsilon/\partial\alpha_{frl} \end{aligned} \tag{2.4-12a}$$

and, for the wing and body, the approximations

$$\left.\begin{matrix} C_L \sin\alpha_{frl} \\ C_D \cos\alpha_{frl} \\ C_{D_\alpha} \sin\alpha_{frl} \end{matrix}\right\} \ll C_{L_\alpha} \cos\alpha_{frl} \tag{2.4-12b}$$

and for the tail

$$\left.\begin{matrix} (\partial\varepsilon/\partial\alpha_{frl})\, C_{L_t} \sin(\alpha_{frl} - \varepsilon) \\ (\partial\varepsilon/\partial\alpha_{frl})\, C_{D_t} \cos(\alpha_{frl} - \varepsilon) \\ (1 - \partial\varepsilon/\partial\alpha_{frl})\, C_{D_{\alpha,t}} \sin(\alpha_{frl} - \varepsilon) \end{matrix}\right\} \ll (1 - \partial\varepsilon/\partial\alpha_{frl})\, C_{L_{\alpha,t}} \cos(\alpha_{frl} - \varepsilon) \tag{2.4-12c}$$

These are normally very good approximations. Equation (2.4-9) can now be differentiated with respect to α_{frl}, and the above approximations applied, leading to

$$C_{m_\alpha} = \frac{\partial C'_{m_R}}{\partial \alpha} + \frac{x_R}{\bar{c}} C_{L_\alpha} \cos(\alpha_{frl}) - \overline{V}_H \left[\eta \left(1 - \frac{\partial \varepsilon}{\partial \alpha} \right) C_{L_{\alpha,t}} + \frac{\partial \eta}{\partial \alpha} C_{L_t} \right] \cos(\alpha_{frl} - \varepsilon) + \frac{\partial C_{m_p}}{\partial \alpha}, \tag{2.4-13}$$

where the first term in this equation is given by

$$\frac{\partial C'_{m_R}}{\partial \alpha} = \frac{\partial C_{m_{R,wb}}}{\partial \alpha} + \frac{\bar{c}_t S_t}{\bar{c} S} \left[\frac{\partial \eta}{\partial \alpha} C_{m_{c/4,t}} + \eta \frac{\partial C_{m_{c/4,t}}}{\partial \alpha} \right] \tag{2.4-14}$$

We will also make use of (2.4-9) with the drag terms neglected:

$$C_{m_{CM}} \approx C'_{m_R} + \frac{x_R}{\bar{c}} C_L \cos(\alpha_{frl}) - \eta \overline{V}_H C_{L_t} \cos(\alpha_{frl} - \varepsilon) + C_{m_p} \tag{2.4-15}$$

For positive stiffness in pitch, of a conventional aircraft, Equation (2.4-13) must yield a negative value for C_{m_α}, and this must occur in equilibrium [$C_{m_{CM}} = 0$ in Equation (2.4-15)] at a positive angle of attack. An examination of the terms in these equations will show how this is possible.

On the right-hand side of Equation (2.4-15), the first term (C'_{m_R}) will be small and negative for a normally cambered airfoil, the second term will be negative when the cm is forward of the reference point (which is a requirement for $C_{m_\alpha} < 0$), and so the third term must be chosen to overcome these negative contributions. The volume coefficient $\overline{V}_H$ is positive, and so C_{L_t} is made negative by giving the tail a negative incidence and/or using an upside-down cambered airfoil. The incidence is chosen so that the total pitching moment is positive at small angles of attack and becomes zero at the desired positive value of α_{frl}. Trim adjustments are made with an elevator "tab" or by using an "all-flying" tail, and control adjustments are made by using the elevator to effectively change the camber of the horizontal-tail airfoil. The remaining term C_{m_p} will be variable with flight conditions, but the thrust line must be kept close enough to the cm to keep it small.

In the C_{m_α} equation (2.4-13), the first term on the right-hand side is small because the reference points are close to aerodynamic centers. The second term is of major importance; if the cm is aft of the aerodynamic reference point, x_R is positive and this term provides a positive (destabilizing) contribution to C_{m_α}.

The third term contains tail efficiency (always positive) and the complement of the "downwash slope." A good deal of information is available about the derivative of the downwash angle with respect to alpha (Roskam, 1979). Its value depends on the distance of the tail from the wing and on Mach number and is typically about 0.5 at low subsonic Mach numbers. Since the lift-curve slope is always positive below the stall, the term will provide a negative contribution to C_{m_α}.

The fourth term contains the derivative of tail efficiency with respect to α_{frl}. Tail efficiency can be strongly dependent on alpha, thrust coefficient, and flap setting. For

example, the four-engine, turboprop heavy transport aircraft, whose pitching moment is given in Figure 2.3-7*a*, has the tail at the same height on the fuselage as the wing and relatively close to the wing. For this aircraft the tail efficiency rises rapidly to a peak at several degrees alpha and then falls rapidly. The height of the peak increases strongly with thrust coefficient and can be higher than $\eta = 2.0$ but is reduced by increasing amounts of flap. The slope $\partial\eta/\partial\alpha$ can be greater than 10/rad, with no flaps, high T_c, and at a few degrees alpha. At zero thrust coefficient, the tail efficiency is slightly less than unity, and the slope $\partial\eta/\partial\alpha$ is approximately constant and slightly negative. Since C_{L_t} had to be made negative, this fourth term is destabilizing for normal thrust coefficients and alpha. This could have been observed from physical reasoning, since we know that the tail efficiency behavior makes the tail more effective at producing a download as alpha increases.

The fifth term in (2.4-13) is the derivative of the propulsion system moment coefficient with angle of attack. Power effects are very complex, especially for propeller aircraft. The existing mathematical models do not necessarily give very good results, and experimental data from powered models are needed. The reader is referred to the literature for more details (Perkins and Hage, 1949; Ribner, 1943; Stinton, 1983).

In summary, an aft-tail aircraft will become statically unstable in pitch if the cm is moved too far aft by incorrect loading. Conversely, if we regard the aerodynamic data reference point as movable and at the aircraft aerodynamic center, then as the aerodynamic center moves aft with increasing subsonic Mach number, an aircraft will become more stable in pitch. The lift-to-drag penalty becomes worse as the aerodynamic center moves aft, and for high-performance military aircraft there is a strong incentive to use "relaxed static stability."

Neutral Point

The *neutral point* is the cm position for which $C_{m_\alpha} = 0$. It is therefore an "aerodynamic center" for the whole aircraft. To find a relationship involving the neutral point, we return to the tail-on moment equation, Equation (2.4-4). If we now differentiate this equation with respect to α_{frl}, we obtain

$$C_{m_\alpha} = \frac{\partial C_{m_R}}{\partial \alpha} + \frac{x_R}{\overline{c}} C'_N(\alpha) + \frac{z_R}{\overline{c}} C'_X(\alpha) + \frac{\partial C_{m_P}}{\partial \alpha}, \tag{2.4-16}$$

where the primes on C_N and C_X denote their derivatives with respect to alpha, which can be calculated by differentiating Equations (2.4-5).

Let $x_{R/np}$ and $z_{R/np}$ be the coordinates of the reference point when the body-fixed coordinate system has its origin at the neutral point. Then by definition of the neutral point, C_{m_α} becomes zero when we insert these coordinates into Equation (2.4-16). If we solve the resulting equation for the derivative of C_{m_R} and substitute it into Equation (2.4-16), we obtain

$$C_{m_\alpha} = \frac{(x_R - x_{R/np})}{\overline{c}} C'_N(\alpha) + \frac{(z_R - z_{R/np})}{\overline{c}} C'_X(\alpha) \tag{2.4-17}$$

This equation for C_{m_α} holds over the complete range of alpha and Mach. An additional independent equation is needed if we require a solution for the coordinates of the neutral point. A universally used approximation is obtained by neglecting the z-component in this equation and using the approximations (2.4-12) in C'_N. The result is

$$C_{m_\alpha} = \frac{(x_R - x_{R/np})}{\overline{c}} C_{L_\alpha} \cos(\alpha_{frl}) \tag{2.4-18}$$

The x-difference in this equation is the position of the aerodynamic data reference point with respect to the neutral point. It can be written in terms of distances measured in the aft direction, from the leading edge of the wing mean aerodynamic chord (mac) to the cm and to the neutral point. Thus, let distance measured aft from the leading edge be divided by $\overline{c}$ and denoted by h. Then, Equation (2.4-18) becomes

$$C_{m_\alpha} = -(h_{np} - h_{cm}) C_{L_\alpha} \cos(\alpha_{frl}) \tag{2.4-19}$$

In this equation the h-difference in parentheses is called the *static margin*; h_{cm} might typically be 0.25 (chords), and h_{np} might typically be 0.30 (chords), and then the static margin would be 0.05.

A conventionally balanced aircraft is usually designed to have a minimum (worst-case loading) positive static margin of between 3 and 5% (0.03 to 0.05). This is for safety reasons and to allow some margin for cm variations with load conditions. Aircraft that operate into the transonic and supersonic regions pay a price for this low-speed static stability. The aerodynamic center of an airfoil tends to shift aft from $0.25\overline{c}$ toward $0.5\overline{c}$ in going from high subsonic speeds to supersonic speeds (see Section Basic Aerodynamics). This causes a corresponding movement in the aircraft neutral point and a large increase in the static margin. The undesirable consequences are increased trim drag (and therefore reduced range or fuel economy) and reduced maneuverability. Some modern military aircraft (notably the F-16) have minimized these penalties by using a reduced, or negative, static margin at subsonic speeds. Since negative pitch stiffness normally leads to dynamic instability in pitch, these aircraft use an automatic control system to restore pitch stability. This is described in later chapters.

2.5 THE NONLINEAR AIRCRAFT MODEL

In this section the aerodynamic force and moment models will be combined with the vector equations of motion to obtain aircraft models for simulation and for analytical purposes. For simplicity, the treatment will be limited to the flat-Earth equations of motion. First, the vector equations will be expanded with the translational velocity state equation expressed in terms of velocity components in the aircraft body-fixed system. The resulting equations are well conditioned when all of these components become zero (e.g., hovering motion or sitting on the runway), and body-axes equations are the best choice for general flight simulation.

On the other hand, for the purposes of linearizing the equations of motion and studying the dynamic behavior, it is better to have the velocity equation in terms of stability or wind-axes variables: airspeed and aerodynamic angles. A convenient way to introduce these variables is to treat the stability and wind axes as being fixed to frames that are rotating relative to the vehicle-body frame. The angular velocity vector then involves alpha-dot or beta-dot, and these become state derivatives in the state-space model. In addition, the drag, lift, and cross-wind force each appear in separate state equations and, under certain conditions, the equations decouple into two sets describing, separately, the *longitudinal motion* (pitching and translation in the geographic vertical plane) and *lateral-directional motion* (rolling, sideslipping, and yawing). The "stability" or "wind-axes" equations are therefore useful for deriving simpler, small perturbation models that can be used for linear analysis and design.

Model Equations

(i) ***Body-Axes Equations*** For convenience the flat-Earth equations of motion (1.7-18) are repeated here:

$$
\begin{aligned}
C_{frd/tp} &= fn(\Phi) \\
\dot{\Phi} &= H(\Phi)\,\boldsymbol{\omega}_{b/e}^{frd} \\
{}^{e}\dot{\mathbf{p}}_{cm/Q}^{tp} &= C_{tp/frd}\,\mathbf{v}_{cm/e}^{frd} \\
{}^{b}\dot{\mathbf{v}}_{cm/e}^{frd} &= \frac{1}{\mathrm{m}}\mathbf{F}^{frd} + C_{frd/tp}\mathbf{g}^{tp} - \tilde{\boldsymbol{\omega}}_{b/e}^{frd}\,\mathbf{v}_{cm/e}^{frd} \\
{}^{b}\dot{\boldsymbol{\omega}}_{b/e}^{frd} &= \left(J^{frd}\right)^{-1}\left[\mathbf{M}^{frd} - \tilde{\boldsymbol{\omega}}_{b/e}^{frd} J^{frd}\boldsymbol{\omega}_{b/e}^{frd}\right]
\end{aligned}
\tag{2.5-1}
$$

with the auxiliary equation

$$
\mathbf{v}_{rel}^{frd} = \mathbf{v}_{cm/e}^{frd} - C_{frd/tp}\,\mathbf{v}_{W/e}^{tp} \tag{2.5-2}
$$

Let the tangent-plane components of the position vector and the *frd* components of the velocity vector be given by, respectively,

$$
\mathbf{p}_{cm/Q}^{tp} \equiv [p_N \;\; p_E \;\; p_D]^T, \qquad \mathbf{v}_{cm/e}^{frd} \equiv [U \;\; V \;\; W]^T
$$

The body-axes components of the angular velocity vector and the Euler angles are

$$
\boldsymbol{\omega}_{b/e}^{frd} \equiv [P \;\; Q \;\; R]^T, \qquad \Phi \equiv [\phi \;\; \theta \;\; \psi]^T
$$

Therefore, the state vector for the body-axes equations is

$$
X = \begin{bmatrix} p_N & p_E & p_D & \phi & \theta & \psi & U & V & W & P & Q & R \end{bmatrix}^T \tag{2.5-3}
$$

Given a value for the state vector, the Euler angle and position derivatives can be evaluated immediately. They are shown in expanded form in Table 2.5-1, with the substitution $\dot{h} = -\dot{p}_D$ for vertical velocity.

The remaining translational and angular velocity state equations require the aerodynamic forces and moments and therefore a calculation of the relative wind. Let the wind have tangent-plane components

$$\mathbf{v}_{W/e}^{tp} = [W_N \;\; W_E \;\; W_D]^T$$

Then (2.5-2) can be used to find the vehicle velocity relative to the surrounding air:

$$\mathbf{v}_{rel}^{frd} = [U' \;\; V' \;\; W']^T$$

For lack of a convenient alternative, let the wind enter the model through the control vector, so a typical control vector will be

$$\overline{U} = [\delta_t, \delta_e, \delta_a, \delta_r, W_N, W_E, W_D]^T \tag{2.5-4}$$

Additional inputs can be created as needed for flaps, gear, speed brake, and so on, and for derivatives of wind velocity components.

The dynamic pressure, Mach number, and aerodynamic angles must now be calculated from the true airspeed (Table 2.3-1):

$$V_T = |\mathbf{v}_{rel}| \tag{2.5-5a}$$

$$\overline{q} = \frac{1}{2}\rho(h)\, V_T^2 \tag{2.5-5b}$$

$$M = M(V_T,\ h) \tag{2.5-5c}$$

$$\alpha = \tan^{-1}\,(W'/U') \tag{2.5-5d}$$

$$\beta = \sin^{-1}\,(V'/V_T), \tag{2.5-5e}$$

where a model of the standard atmosphere is used to calculate $\rho(h)$ and $M(V_T, h)$. Next compute installed thrust and the body-axes aerodynamic coefficients, transforming from stability or wind axes, as necessary, and using the component buildup equations from Section 2.3. The state derivatives alpha-dot and beta-dot cannot yet be calculated, so we must either neglect $C_{L_{\dot{\alpha}}}$ and $C_{Y_{\dot{\beta}}}$ or use approximate values of alpha-dot and beta-dot (e.g., from the last simulation time step). Control surface deflections must come either directly from the pilot via the control vector or from additional state-variable models representing actuator dynamics. The aerodynamic and thrust forces can now be calculated (subcripts A and T will be used, respectively, to denote aerodynamic and thrust components):

$$C_{(\ )} = C_{(\ )}(\alpha, \beta, M, h, \delta_S, P, Q, R) \tag{2.5-6a}$$

$$\mathbf{F}_{A,T}^{frd} = \mathbf{F}_T^{frd} + \overline{q}S[C_X \;\; C_Y \;\; C_Z]^T \tag{2.5-6b}$$

and the translational velocity state equation can be expanded as shown in Table 2.5-1.

The aerodynamic angle rates, alpha-dot, and beta-dot [(Equations (2.3-10)] must now be found. If the gust response of the aircraft must be modeled, then the relative wind equation (2.5-2) must be differentiated, and the derivative of the direction cosine matrix can be found from Poisson's kinematical equations (Section 1.8). Otherwise, when studying the dynamics of the aircraft, it is usual to set the wind to zero and use the derivatives of U, V, and W to find the aerodynamic angle rates. The aerodynamic and thrust moments can be calculated in the form

$$C_{(\,)} = C_{(\,)}(\alpha, \beta, M, h, \delta_S, \dot{\alpha}, \dot{\beta}, P, Q, R) \tag{2.5-7a}$$

$$\mathbf{M}_{A,T}^{frd} = \mathbf{M}_{T}^{frd} + \overline{q}S[\mathrm{b}C_{\ell} \;\; \overline{c}C_m \;\; bC_n]^T \tag{2.5-7b}$$

and the angular velocity state equation can be evaluated. The expansion of this "moment equation" is repeated in Table 2.5-1. This completes the body-axis 6-DoF equations.

(ii) ***Wind- or Stability-Axes Equations*** A nonlinear model in terms of the state variables

$$X^T = [V_T \;\; \beta \;\; \alpha \;\; \phi \;\; \theta \;\; \psi \;\; P_s \;\; Q \;\; R_s] \tag{2.5-8}$$

will be constructed here and, as described in the Section 2.5 introduction, will be found to have advantages for linearization and decoupling. Equations (1.7-20) show that the flat-Earth force equations (velocity state equations) are dependent only on the relative velocity, $\mathbf{v}_{rel}$, and they are an appropriate starting point here.

TABLE 2.5-1 The Flat-Earth, Body-Axes 6-DoF Equations

Force equations

$$\dot{U} = RV - QW - g_D \sin\theta + (X_A + X_T)/\mathrm{m}$$
$$\dot{V} = -RU + PW + g_D \;\; \sin\phi \;\; \cos\theta + (Y_A + Y_T)/\mathrm{m}$$
$$\dot{W} = QU - PV + g_D \;\; \cos\phi \;\; \cos\theta + (Z_A + Z_T)/\mathrm{m}$$

Kinematic equations

$$\dot{\phi} = P + \tan\theta \;\; (Q \;\; \sin\phi + R \;\; \cos\phi)$$
$$\dot{\theta} = Q \;\; \cos\phi - R \;\; \sin\phi$$
$$\dot{\psi} = (Q \;\; \sin\phi + R \;\; \cos\phi)/\cos\theta$$

Moment equations

$$\Gamma\dot{P} = J_{xz}\,[J_x - J_y + J_z]\,PQ - [J_z(J_z - J_y) + J_{xz}^2]\,QR + J_z\ell + J_{xz}n$$
$$J_y\dot{Q} = (J_z - J_x)PR - J_{xz}(P^2 - R^2) + m$$
$$\Gamma\dot{R} = [(J_x - J_y)J_x + J_{xz}^2]\,PQ - J_{xz}[J_x - J_y + J_z]\,QR + J_{xz}\ell + J_x n$$
$$\cdot\;\; \Gamma = J_x J_z - J_{xz}^2$$

Navigation equations

$$\dot{p}_N = U\mathrm{c}\theta\mathrm{c}\psi + V\,(-\mathrm{c}\phi\mathrm{s}\psi + \mathrm{s}\phi\mathrm{s}\theta\mathrm{c}\psi) + W(\mathrm{s}\phi\mathrm{s}\psi + \mathrm{c}\phi\mathrm{s}\theta\mathrm{c}\psi)$$
$$\dot{p}_E = U\mathrm{c}\theta\mathrm{s}\psi + V(\mathrm{c}\phi\mathrm{c}\psi + \mathrm{s}\phi\mathrm{s}\theta\mathrm{s}\psi) + W(-\mathrm{s}\phi\mathrm{c}\psi + \mathrm{c}\phi\mathrm{s}\theta\mathrm{s}\psi)$$
$$\dot{h} = U\mathrm{s}\theta - V\mathrm{s}\phi\mathrm{c}\theta - W\mathrm{c}\phi\mathrm{c}\theta$$

(a) *Force Equations*: As an expedient way of deriving these equations, imagine the stability axes as fixed in a new "stability frame" with angular velocity vector $-\dot{\alpha}\,\mathbf{j}$ with respect to the body frame. Similarly, imagine the wind axes as fixed in a new "wind frame" with angular velocity $\dot{\beta}\,\mathbf{k}$ with respect to the stability frame. The flat-Earth force equation (1.7-20), with steady wind, reduces to

$$^{b}\dot{\mathbf{v}}_{rel} = (1/\mathrm{m})\mathbf{F}_{A,T} + \mathbf{g} - \boldsymbol{\omega}_{b/e} \times \mathbf{v}_{rel} \tag{2.5-9}$$

Let the derivative taken in the body frame be replaced with a derivative taken in the wind frame:

$$^{w}\dot{\mathbf{v}}_{rel} + \boldsymbol{\omega}_{w/b} \times \mathbf{v}_{rel} = (1/\mathrm{m})\mathbf{F}_{A,T} + \mathbf{g} - \boldsymbol{\omega}_{b/e} \times \mathbf{v}_{rel} \tag{2.5-10}$$

Resolving these vectors in wind axes gives the matrix equation

$$^{w}\dot{\mathbf{v}}^{w}_{rel} + \widetilde{\boldsymbol{\omega}}^{w}_{w/b}\mathbf{v}^{w}_{rel} = (1/\mathrm{m})\mathbf{F}^{w}_{A,T} + C_{w/b}C_{b/n}\mathbf{g}^{n} - \widetilde{\boldsymbol{\omega}}^{w}_{b/e}\mathbf{v}^{w}_{rel} \tag{2.5-11}$$

The cross-product matrix on the left-hand side can be determined as follows. If alpha-dot is greater than zero, the angle of attack is increasing and the stability frame is undergoing a left-handed rotation about the body y-axis, relative to the body frame. Also, if beta-dot is greater than zero, the wind frame is undergoing a right-handed rotation around the stability z-axis, relative to the stability frame. Therefore,

$$\boldsymbol{\omega}^{s}_{s/b} = \boldsymbol{\omega}^{b}_{s/b} = \begin{bmatrix} 0 & -\dot{\alpha} & 0 \end{bmatrix}^{T} \tag{2.5-12a}$$

$$\boldsymbol{\omega}^{w}_{w/s} = \boldsymbol{\omega}^{s}_{w/s} = \begin{bmatrix} 0 & 0 & \dot{\beta} \end{bmatrix}^{T} \tag{2.5-12b}$$

Now

$$\boldsymbol{\omega}_{w/b} = \boldsymbol{\omega}_{w/s} + \boldsymbol{\omega}_{s/b} \tag{2.5-13}$$

and so

$$\boldsymbol{\omega}^{w}_{w/b} = \begin{bmatrix} 0 \\ 0 \\ \dot{\beta} \end{bmatrix} + \begin{bmatrix} \mathrm{c}\beta & \mathrm{s}\beta & 0 \\ -\mathrm{s}\beta & \mathrm{c}\beta & 0 \\ 0 & 0 & 1 \end{bmatrix} \begin{bmatrix} 0 \\ -\dot{\alpha} \\ 0 \end{bmatrix} = \begin{bmatrix} -\dot{\alpha}\mathrm{s}\beta \\ -\dot{\alpha}\mathrm{c}\beta \\ \dot{\beta} \end{bmatrix} \tag{2.5-14}$$

Then the left-hand side of the force equation becomes

$$^{w}\dot{\mathbf{v}}^{w}_{rel} + \widetilde{\boldsymbol{\omega}}^{w}_{w/b}\mathbf{v}^{w}_{rel} = \begin{bmatrix} \dot{V}_T \\ \dot{\beta} V_T \\ \dot{\alpha} V_T \cos\beta \end{bmatrix} \tag{2.5-15}$$

This array contains the derivatives of the first three state variables in (2.5-8).

The aerodynamic and thrust force term can now be calculated as follows. Again, for simplicity, assume that the thrust vector lies in the x_b-z_b plane but is inclined at an angle α_T to the fuselage reference line (so that positive α_T corresponds to a component of thrust in the negative z_b direction). Then it is easy to write the stability-axis components of thrust and transform to wind axes:

$$\mathbf{F}_{A,T}^{w} = \begin{bmatrix} c\beta & s\beta & 0 \\ -s\beta & c\beta & 0 \\ 0 & 0 & 1 \end{bmatrix} \begin{bmatrix} \mathbf{F}_T \cos\left(\alpha + \alpha_T\right) \\ 0 \\ \mathbf{F}_T \sin(\alpha + \alpha_T) \end{bmatrix} - \begin{bmatrix} D \\ C \\ L \end{bmatrix} \tag{2.5-16}$$

where

$$F_T = |\mathbf{F}_T|$$

In wind axes the gravity term is given by

$$\mathbf{g}^{w} = C_{w/b} C_{b/n} \begin{bmatrix} 0 \\ 0 \\ g_D \end{bmatrix} \equiv \begin{bmatrix} g_1 \\ g_2 \\ g_3 \end{bmatrix},$$

where the components are

$$\begin{aligned} g_1 &= g_D(-\mathrm{c}\alpha\ \mathrm{c}\beta\ \mathrm{s}\theta + \mathrm{s}\beta\ \mathrm{s}\phi\ \mathrm{s}\theta + \mathrm{s}\alpha\ \mathrm{c}\beta\ \mathrm{c}\phi\ \mathrm{c}\theta) = -g_D \sin(\gamma) \\ g_2 &= g_D(\mathrm{c}\alpha\ \mathrm{s}\beta\ \mathrm{s}\theta + \mathrm{c}\beta\ \mathrm{s}\phi\ \mathrm{c}\theta - \mathrm{s}\alpha\ \mathrm{s}\beta\ \mathrm{c}\phi\ \mathrm{c}\theta) \\ \mathrm{g}_3 &= g_D(\mathrm{s}\alpha\ \mathrm{s}\theta + \mathrm{c}\alpha\ \mathrm{c}\phi\ \mathrm{c}\theta) \end{aligned} \tag{2.5-17}$$

[See (3.6-2) to introduce γ into the first equation.] The remaining cross-product is given by

$$\boldsymbol{\omega}_{b/e}^{w} \mathbf{v}_{rel}^{w} = [0 \quad V_T R_w \quad -V_T Q_w]^T, \tag{2.5-18}$$

where $R_\omega = R_s$ and $Q_w = (-P_s \sin\beta + Q \cos\beta)$.

When all of these terms are assembled, the force equations are

$$\begin{aligned} \mathrm{m}\dot{V}_T &= F_T \cos(\alpha + \alpha_T) \cos\beta - D + \mathrm{m}\, g_1 \\ \mathrm{m}\dot{\beta} V_T &= -F_T \cos(\alpha + \alpha_T) \sin\beta - C + \mathrm{m}\, g_2 - \mathrm{m}\, V_T R_s \\ \mathrm{m}\dot{\alpha} V_T \cos\beta &= -F_T \sin(\alpha + \alpha_T) - L + \mathrm{m}\, g_3 + \mathrm{m}\, V_T (Q\cos\beta - P_s \sin\beta) \end{aligned} \tag{2.5-19}$$

It is evident that, if lift and cross-wind force include a linear dependence on the state derivatives alpha-dot and beta-dot, respectively, the equations can be solved for these state derivatives. Unfortunately, this requires a nonzero airspeed V_T. However, we will show that these equations are useful for constructing a small-perturbation model of aircraft dynamics.

(b) *Moment Equations*: In the moment equation (2.5-1*e*) the derivative taken in the body frame can be replaced with a derivative taken in the stability or wind frame; the

form of the equation is the same in either case. The stability frame will be shown later to be a more convenient choice; thus,

$$ {}^{s}\dot{\boldsymbol{\omega}}^{bf}_{b/e} + (\boldsymbol{\omega}_{s/b} \times \boldsymbol{\omega}_{b/e})^{bf} = (J^{bf})^{-1}[\mathbf{M}^{bf}_{A,T} - \widetilde{\boldsymbol{\omega}}^{bf}_{b/e} J^{bf} \boldsymbol{\omega}^{bf}_{b/e}] \tag{2.5-20} $$

Now change from body-axes to stability-axes components, insert a cross-product matrix for $(\boldsymbol{\omega}\times)^s$, and solve for the derivatives:

$$ {}^{s}\dot{\boldsymbol{\omega}}^{s}_{b/e} = -\widetilde{\boldsymbol{\omega}}^{s}_{s/b} \boldsymbol{\omega}^{s}_{b/e} + (J^{s})^{-1}[\mathbf{M}^{s}_{A,T} - \widetilde{\boldsymbol{\omega}}^{s}_{b/e} J^{s} \boldsymbol{\omega}^{s}_{b/e}] \tag{2.5-21} $$

where the stability-axes inertia matrix is

$$ J^{s} = C_{s/b} J^{b} C_{b/s} \tag{2.5-22} $$

Equation (2.5-22) has an extra term compared to the body-axes moment equation and offers no advantages for simulation. It does have advantages for deriving a small-perturbation model because it introduces alpha-dot into the small-perturbation moment equations in a formal manner, as will be shown in the next section. If we had wished to introduce beta-dot, it would have been necessary to convert to wind axes (Stevens and Lewis, 1992).

Consider the terms in the stability-axes moment equation; starting with the inertia matrix. We will restrict ourselves to aircraft having a plane of symmetry, so that the body-axes inertia matrix is given by Equation (1.7-9). When the transformation (2.5-22) is performed, the matrix is found to have the same structure in stability axes:

$$ J^{s} = \begin{bmatrix} J'_x & 0 & -J'_{xz} \\ 0 & J'_y & 0 \\ -J'_{xz} & 0 & J'_z \end{bmatrix}, \tag{2.5-23} $$

where

$$ \begin{aligned} J'_x &= J_x \cos^2\alpha + J_z \sin^2\alpha - J_{xz} \sin 2\alpha \\ J'_y &= J_y \\ J'_z &= J_x \sin^2\alpha + J_z \cos^2\alpha + J_{xz} \sin 2\alpha \\ J'_{xz} &= \frac{1}{2}(J_x - J_y) \sin 2\alpha + J_{xz} \cos 2\alpha \end{aligned} $$

Furthermore, the inverse of this matrix is easily found and is again of the same form:

$$ (J^{s})^{-1} = \frac{1}{\Gamma} \begin{bmatrix} J'_z & 0 & J'_{xz} \\ 0 & \Gamma/J'_y & 0 \\ J'_{xz} & 0 & J'_x \end{bmatrix} \tag{2.5-24} $$

with

$$ \Gamma = J'_x J'_z - J'^{2}_{xz} \quad (= J_x J_z - J^2_{xz}, \quad \text{Problem 2.5-3}) $$

Note that in wind axes J^w is a full matrix, so that working in stability axes is considerably more convenient, provided that we can neglect beta-dot derivatives in the moment equations. Other terms in the moment equation are

$$\begin{aligned} {}^s\dot{\boldsymbol{\omega}}^s_{b/e} &= [\dot{P}_s \;\; \dot{Q} \;\; \dot{R}]^T \\ \boldsymbol{\omega}^s_{s/b} &= [0 \;\; -\dot{\alpha} \;\; 0]^T \\ \widetilde{\boldsymbol{\omega}}^s_{s/b}\boldsymbol{\omega}^s_{b/e} &= \dot{\alpha}[-R_s \;\; 0 \;\; P_s]^T \end{aligned} \tag{2.5-25}$$

The stability-axes moment equations (2.5-21) can now be written in component form as

$$\begin{bmatrix} \dot{P}_s \\ \dot{Q} \\ \dot{R}_s \end{bmatrix} = -\dot{\alpha}\begin{bmatrix} -R_s \\ 0 \\ P_s \end{bmatrix} + \frac{1}{\Gamma}\begin{bmatrix} J'_z & 0 & J'_{xz} \\ 0 & \Gamma/J'_y & 0 \\ J'_{xz} & 0 & J'_x \end{bmatrix}\left(\begin{bmatrix} \ell_s \\ m \\ n_s \end{bmatrix} - \widetilde{\boldsymbol{\omega}}^s_{b/e}J^s\boldsymbol{\omega}^s_{b/e}\right) \tag{2.5-26}$$

The last term is of the same form as the corresponding term in the body-axes moment equations; it will not need to be expanded.

Decoupling of the Nonlinear Equations/3-DOF Longitudinal Model

Most aircraft spend most of their flying time in a wings-level steady-state flight condition and, since the model of the 3-DoF motion in a vertical plane is much simpler than the 6-DoF model, it is worthwhile investigating the equations of motion under the wings-level flight condition. Referring to the force equations (2.5-19), if the roll angle ϕ is zero, the gravity terms are greatly simplified:

$$\begin{aligned} g_1 &= -g_D \sin\gamma = -g_D \cos\beta \sin(\theta-\alpha) \\ g_2 &= g_D[\sin\theta\cos\alpha - \cos\theta\sin\alpha]\sin\beta = g_D \sin\beta \sin(\theta-\alpha) \\ g_3 &= g_D\,[\sin\alpha\sin\theta - \cos\alpha\cos\theta] = g_D\cos(\theta-\alpha) \end{aligned} \tag{2.5-27}$$

When the sideslip is small, the flight-path angle is given by the difference between pitch attitude and angle of attack, and so the gravity terms become

$$\begin{aligned} g_1 &= -g_D \sin(\gamma) \\ g_2 &= \beta\, g_D \sin(\gamma) \\ g_3 &= g_D\cos(\gamma) \end{aligned} \tag{2.5-28}$$

and the force equations (2.5-19) reduce to

$$\begin{aligned} \mathrm{m}\,\dot{V}_T &= F_T\cos(\alpha+\alpha_T) - D - \mathrm{m}\,g_D\sin\gamma \\ \mathrm{m}\,\dot{\beta}\,V_T &= -\beta F_T\cos(\alpha+\alpha_T) - C + \beta\,\mathrm{m}\,g_D\sin\gamma - \mathrm{m}\,V_T R_s \\ \mathrm{m}\,\dot{\alpha}\,V_T &= -F_T\sin(\alpha+\alpha_T) - L + \mathrm{m}\,g_D\cos\gamma + \mathrm{m}\,V_T(Q-\beta P_s) \end{aligned} \tag{2.5-29}$$

The first and third equations describe longitudinal motion and, when beta is negligible, are independent of the second (sideslip) equation.

Decoupling of the longitudinal motion also occurs in the attitude equations and the moment equations. It can be seen from the kinematic equations in Table 2.5-1 that when the roll angle is zero,

$$\dot{\theta} = Q \tag{2.5-30}$$

The body-axes moment equations in Table 2.5-1 show that, if the roll and yaw rates (P and R) are small, the pitching moment equation is not coupled to the rolling and yawing moment equations, and

$$J_Y \dot{Q} = m \tag{2.5-31}$$

Therefore, we can obtain a model for pure longitudinal motion by adding Equations (2.5-30) and (2.5-31) to the decoupled longitudinal force equations:

$$\begin{aligned} \mathrm{m}\dot{V}_T &= F_T \cos(\alpha + \alpha_T) - D - \mathrm{m}\, g_D \sin(\theta - \alpha) \\ \mathrm{m}\dot{\alpha} V_T &= -F_T \sin(\alpha + \alpha_T) - L + \mathrm{m}\, g_D \cos(\theta - \alpha) + \mathrm{m} V_T Q \\ \dot{\theta} &= Q \\ \dot{Q} &= m/J_y \end{aligned} \tag{2.5-32}$$

The state vector for these equations is

$$X = \begin{bmatrix} V_T & \alpha & \theta & Q \end{bmatrix}^T \tag{2.5-33}$$

A common alternative model uses flight-path angle as a state variable in place of pitch attitude:

$$\begin{aligned} \mathrm{m}\dot{V}_T &= F_T \cos(\alpha + \alpha_T) - D - \mathrm{m}\, g_D \sin\gamma \\ \mathrm{m}\dot{\gamma} V_T &= F_T \sin(\alpha + \alpha_T) + L - \mathrm{m}\, g_D \cos\gamma \\ \dot{\alpha} &= Q - \dot{\gamma} \\ \dot{Q} &= m/J_y \end{aligned} \tag{2.5-34}$$

These longitudinal models are used for a variety of purposes, from performance analysis to automatic control system design. If the lift and drag forces are linearized for small perturbations from a specified flight condition, we obtain linear longitudinal equations that are the same as those derived in the next section by a formal linearization of the complete 6-DoF equations followed by decoupling.

2.6 LINEAR MODELS AND THE STABILITY DERIVATIVES

When we perform a computer simulation to evaluate the performance of an aircraft with its control systems, we almost invariably use a nonlinear model. Also, the linear equations needed for control systems design will mostly be derived by numerical

methods from the nonlinear computer model. Because the nonlinear state models are difficult to handle without the use of a digital computer, most of the early progress in understanding the dynamics of aircraft and the stability of the motion came from studying linear algebraic small-perturbation equations. G. H. Bryan (1911) introduced the idea of perturbed forces and moments with respect to a "steady-state" flight condition, and this approach is still in use. The small-perturbation equations are linear equations derived algebraically from nonlinear equations like those of Section 2.5. In these equations the nonlinear aerodynamic coefficients are replaced by terms involving the aerodynamic derivatives described briefly in Section 2.3.

There are two good reasons, apart from their historical importance, for algebraically deriving the small-perturbation equations. First, the aerodynamic derivatives needed for the linear equations can be estimated relatively quickly (Hoak et al., 1970) before nonlinear aerodynamic data become available. Second, the algebraic small-perturbation equations provide a great deal of insight into the relative importance of the various aerodynamic derivatives under different flight conditions and their effect on the stability of the aircraft motion. In preparation for deriving the linear equations we now examine the concept of a steady-state flight condition.

Singular Points and Steady-State Flight

In the preceding section, when the body-axes force equations were used, alpha-dot or beta-dot force dependence created a difficulty in that the state equations became implicit in the derivatives of the states alpha and beta. This problem was solved in an ad hoc manner by using the wind-axes equations and collecting linear alpha-dot or beta-dot terms on one side of the equations. In this section where the goal is to derive linear equations algebraically, we take a more general approach, starting with *implicit state equations* in the general form

$$f(\dot{X}, X, \overline{U}) = 0, \tag{2.6-1}$$

where f is an array of n scalar nonlinear functions f_i, as in (1.1-1).

In the theory of nonlinear systems (Vidyasagar, 1978) the concept of a *singular point*, or *equilibrium point*, of an autonomous (no external control inputs) time-invariant system is introduced. The coordinates of a singular point of the implicit nonlinear state equations are given by a solution, $X = X_e$, which satisfies

$$f(\dot{X}, X, \overline{U}) = 0, \quad \text{with } \dot{X} \equiv 0;\ \overline{U} \equiv 0 \text{ or constant} \tag{2.6-2}$$

This idea has strong intuitive appeal; the system is "at rest" when all of the derivatives are identically zero, and then one may examine the behavior of the system near the singular point by slightly perturbing some of the variables. If, in the case of an aircraft model, the state trajectory departs rapidly from the singular point in response to a small perturbation in, say, pitch attitude, the human pilot is unlikely to be able to control this aircraft.

Steady-state aircraft flight can be defined as a condition in which all of the force and moment components in the body-fixed coordinate system are constant or zero.

It follows that the aerodynamic angles and the angular rate components must be constant, and their derivatives must be zero. It must be assumed that the aircraft mass remains constant. In the case of the round-Earth equations, minor circles (and the major circle around the equator) are the only trajectories along which gravity remains constant in magnitude.

Assuming that the flat-Earth equations are satisfactory for all of our control system design purposes, the definition allows steady wings-level flight and steady turning flight. Furthermore, if the change in atmospheric density with altitude is neglected, a wings-level climb and a climbing turn are permitted as steady-state flight conditions. In this case the *ned* position equations do not couple back into the equations of motion and need not be used in finding a steady-state condition. Therefore, the steady-state conditions that are important to us for control system design can be defined in terms of the remaining nine state variables of the flat-Earth equations as follows:

Steady-State Flight

$$\dot{P}, \dot{Q}, \dot{R}, \text{and } \dot{U}, \dot{V}, \dot{W} \text{ (or } \dot{V}_T, \dot{\beta}, \dot{\alpha}) \equiv 0, \text{controls fixed} \tag{2.6-3a}$$

with the following additional constraints according to the flight condition:

$$\begin{aligned}
\text{STEADY WINGS-LEVEL FLIGHT:} &\quad \phi, \dot{\phi}, \dot{\theta}, \dot{\psi} \equiv 0 \qquad (\therefore P, Q, R \equiv 0) \\
\text{STEADY TURNING FLIGHT :} &\quad \dot{\phi}, \dot{\theta} \equiv 0, \qquad \dot{\psi} \equiv \text{TURN RATE} \\
\text{STEADY PULL-UP :} &\quad \phi, \dot{\phi}, \dot{\psi} \equiv 0, \qquad \dot{\theta} \equiv \text{PULL-UP RATE} \\
\text{STEADY ROLL :} &\quad \dot{\theta}, \dot{\psi} \equiv 0, \qquad \dot{\phi} \equiv \text{ROLL RATE}
\end{aligned} \tag{2.6-3b}$$

The steady-state conditions $\dot{P}, \dot{Q}, \dot{R} \equiv 0$ require the angular rates to be zero or constant (as in steady turns), and therefore the aerodynamic and thrust moments must be zero or constant. The conditions $\dot{U}, \dot{V}, \dot{W} \equiv 0$ require the airspeed, angle of attack, and sideslip angle to be constant, and hence the aerodynamic forces must be zero or constant. Therefore, the steady-state pull-up (or push-over) and steady-state roll conditions can only exist instantaneously. However, it is useful to be able to linearize the aircraft dynamics in these flight conditions since the control systems must operate there.

While a pilot may not find it very difficult to put an aircraft into a steady-state flight condition, the mathematical model requires the solution of the simultaneous nonlinear equations (2.6-2). In general, because of the nonlinearity, a steady-state solution can only be found by using a numerical method on a digital computer. Multiple solutions can exist, and a feasible solution will emerge only when practical constraints are placed on the variables. We consider this problem in Chapter 3 and assume here that a solution X_e, $\overline{U}_e$ is known for the desired flight condition.

Linearization

The implicit nonlinear equations will be written as

$$\begin{aligned} f_1(\dot{X}, X, \overline{U}) &= 0 \\ f_2(\dot{X}, X, \overline{U}) &= 0 \\ \vdots \qquad & \quad \vdots \\ f_9(\dot{X}, X, \overline{U}) &= 0 \end{aligned} \tag{2.6-4}$$

and will be obtained from the wind-axes force equations, kinematic equations, and stability-axes moment equations, by moving all nonzero terms to the right-hand side of the equations. The reduced state vector is

$$X = [V_T \ \beta \ \alpha \ \phi \ \theta \ \psi \ P_s \ Q_s R_s]^T \tag{2.6-5a}$$

The control vector, given by (2.5-4), is reduced here to

$$\overline{U} = [\delta_t \ \delta_e \ \delta_a \ \delta_r]^T \tag{2.6-5b}$$

We now consider small perturbations from the steady-state condition X_e, $\overline{U}_e$ and derive a set of linear constant-coefficient state equations. If we expand the nonlinear state equations (2.6-4) in a Taylor series about the equilibrium point $(X_e, \overline{U}_e)$ and keep only the first-order terms, we find that the perturbations in the state, state derivative, and control vectors must satisfy

$$\begin{aligned} \nabla_{\dot{X}} f_1 \ \delta\dot{X} + \nabla_X f_1 \ \delta X + \nabla_U f_1 \ \delta\overline{U} &= 0 \\ \vdots \quad \vdots \qquad \vdots \quad \vdots \qquad \vdots \quad \vdots & \\ \nabla_{\dot{X}} f_9 \ \delta\dot{X} + \nabla_X f_9 \ \delta X + \nabla_U f_9 \ \delta\overline{U} &= 0 \end{aligned} \tag{2.6-6}$$

In this equation, ∇ (del, or nabla) represents a row array of first partial derivative operators, for example,

$$\nabla_X f_i \equiv \left[\frac{\partial f_i}{\partial X_1} \ \frac{\partial f_i}{\partial X_2} \quad \cdots \quad \frac{\partial f_i}{\partial X_n} \right]$$

Each term in (2.6-6) is a scalar product; thus, $\nabla_X f_1 \, \delta X$ is the total differential of f_1 due to simultaneous perturbations in all the elements of the state vector.

Equations (2.6-6) can now be written in implicit linear state-variable form as

$$E\dot{x} = Ax + Bu \tag{2.6-7}$$

Lowercase notation has been used to indicate that x and u are perturbations from the equilibrium values of the state and control vectors. The coefficient matrices

$$E = -\begin{bmatrix} \nabla_{\dot{X}} f_1 \\ \vdots \\ \nabla_{\dot{X}} f_9 \end{bmatrix}_{\substack{U=U_e \\ X=X_e}} \quad A = \begin{bmatrix} \nabla_x f_1 \\ \vdots \\ \nabla_x f_9 \end{bmatrix}_{\substack{U=U_e \\ X=X_e}} \quad B = \begin{bmatrix} \nabla_U f_1 \\ \vdots \\ \nabla_U f_9 \end{bmatrix}_{\substack{U=U_e \\ X=X_e}} \tag{2.6-8}$$

are called *Jacobian matrices* and must be calculated at the equilibrium point. If E is nonsingular, (2.6-7) can be rewritten as an explicit set of linear state equations, but we will see later that this is not necessarily the most convenient way to use the implicit state equations.

The Jacobian matrices E, A, B will be evaluated three rows at a time, corresponding, respectively, to the wind-axes force equations (f_1 to f_3), kinematic equations (f_4 to f_6), and moment equations (f_7 to f_9). The evaluation will be for the steady, level flight condition, with the additional constraint of no sideslip ($\beta = 0$). The latter condition greatly simplifies the algebra involved in the linearization and leads to "lateral-longitudinal" decoupling. Therefore, the equilibrium (steady-state) conditions are

STEADY-STATE CONDITIONS FOR LINEARIZATION:

$$\begin{aligned} &\beta,\ \phi,\ P,\ Q,\ R \equiv 0 \\ &\text{All derivatives} \equiv 0 \\ &V_T = V_{T_e},\ \alpha = \alpha_e,\ \theta = \theta_e,\ \psi \equiv 0,\ \ \gamma_e \equiv 0 \end{aligned} \tag{2.6-9}$$

The algebra can be further reduced by taking advantage of some features of the equations. Thus, when differentiating products containing $\cos\beta$ or $\cos\phi$, all of the resulting $\sin\beta$ or $\sin\phi$ terms will disappear when we apply the $\beta = 0$ and $\phi = 0$ equilibrium conditions. Therefore, the $\cos\beta$ or $\cos\phi$ terms can be set to unity before differentiation. Similarly, a $\cos\beta$ or $\cos\phi$ in the denominator of a quotient term can be set to unity. Also, if two or more terms with equilibrium values of zero (e.g., $\sin\beta$, $\sin\phi$) occur in a product term, this product can be discarded before differentiation.

The Linearized Force Equations The first three rows of the linear equations (2.6-7) will now be obtained by performing the gradient operations, shown in (2.6-8), on the nonlinear force equations (2.5-19). All of the terms in (2.5-19) will be moved to the right-hand side of the equations. First, we find the partial derivatives with respect to $\dot{X}$ and use the steady-state condition (2.6-9). The thrust is assumed to be independent of the state derivatives; this gives

$$-\begin{bmatrix} \nabla_{\dot{X}} f_1 \\ \nabla_{\dot{X}} f_2 \\ \nabla_{\dot{X}} f_3 \end{bmatrix}_{X=X_e} = \begin{bmatrix} \mathrm{m}\nabla_{\dot{X}}\dot{V}_T + \nabla_{\dot{X}} D \\ \mathrm{m}V_T\nabla_{\dot{X}}\dot{\beta} + \nabla_{\dot{X}} C \\ \mathrm{m}V_T\nabla_{\dot{X}}\dot{\alpha} + \nabla_{\dot{X}} L \end{bmatrix} \tag{2.6-10}$$

A term such as $\nabla_{\dot{X}}\dot{V}_T$ is simply a row array with unity in the position corresponding to the $\dot{V}_T$ state derivative and zeros elsewhere. The other terms, such as $\nabla_{\dot{X}}L$, are row arrays containing all of the partial derivatives of the forces with respect to the state derivatives.

The partial derivatives of the aerodynamic forces and moments with respect to other variables are the *aerodynamic derivatives*, first introduced in Section 2.3. Table 2.6-1 defines the derivatives that are normally significant in the force equations. These derivatives are called the *dimensional derivatives*, and later we will introduce a related set of derivatives that have been made dimensionless in the same way that the aerodynamic coefficients are made dimensionless. The dimensional derivatives are given the symbols X, Y, and Z to indicate which force component is involved (the symbols D, C, and L are also used). Their subscripts indicate the quantity with respect to which the derivative is taken [subscripts for the controls were defined in (2.6-5*b*)].

For the purpose of deriving the linear equations, only the derivatives shown in the table will be assumed to be nonzero. Therefore, the terms $\nabla_{\dot{X}}D$ and $\nabla_{\dot{X}}C$ in (2.6-10) will now be dropped (additional terms will be dropped later). Note that the components involved in the partial derivatives are wind-axes components, except for the engine thrust F_T. This force belongs naturally to the aircraft-body axes, and it only appears in the wind-axes equations in conjunction with trigonometric functions of the aerodynamic angles.

We will interpret (2.6-10) in terms of the dimensional derivatives. The array $\nabla_{\dot{X}}L$ contains only the derivative $Z_{\dot{\alpha}}$ (multiplied by m) in the $\dot{\alpha}$ position, so (2.6-10) can now be rewritten as

$$-\begin{bmatrix}\nabla_{\dot{X}}f_1\\ \nabla_{\dot{X}}f_2\\ \nabla_{\dot{X}}f_3\end{bmatrix}_{X=X_e} = \mathrm{m}\begin{bmatrix}1 & 0 & 0 & 0 & 0 & 0 & 0 & 0 & 0\\ 0 & V_{T_e} & 0 & 0 & 0 & 0 & 0 & 0 & 0\\ 0 & 0 & V_{T_e}-Z_{\dot{\alpha}} & 0 & 0 & 0 & 0 & 0 & 0\end{bmatrix} \tag{2.6-11}$$

TABLE 2.6-1 The Force Dimensional Derivatives

X-AXIS	Y-AXIS	Z-AXIS
$X_V = \dfrac{-1}{\mathrm{m}}\dfrac{\partial D}{\partial V_T}$	$Y_\beta = -\dfrac{1}{\mathrm{m}}\left(\dfrac{\partial C}{\partial \beta} + D_e\right)$	$Z_V = \dfrac{-1}{\mathrm{m}}\dfrac{\partial L}{\partial V_T}$
$X_{T_V} = \dfrac{1}{\mathrm{m}}\dfrac{\partial F_T}{\partial V_T}$	$Y_p = -\dfrac{1}{\mathrm{m}}\dfrac{\partial C}{\partial P_s}$	$Z_\alpha = \dfrac{-1}{\mathrm{m}}\left(D_e + \dfrac{\partial L}{\partial \alpha}\right)$
$X_\alpha = \dfrac{1}{\mathrm{m}}\left(L_e - \dfrac{\partial D}{\partial \alpha}\right)$	$Y_r = -\dfrac{1}{\mathrm{m}}\dfrac{\partial C}{\partial R_s}$	$Z_{\dot{\alpha}} = \dfrac{-1}{\mathrm{m}}\dfrac{\partial L}{\partial \dot{\alpha}}$
$X_{\delta e} = \dfrac{-1}{\mathrm{m}}\dfrac{\partial D}{\partial \delta_e}$	$Y_{\delta r} = -\dfrac{1}{\mathrm{m}}\dfrac{\partial C}{\partial \delta_r}$	$Z_q = \dfrac{-1}{\mathrm{m}}\dfrac{\partial L}{\partial Q}$
$X_{\delta t} = \dfrac{1}{\mathrm{m}}\dfrac{\partial F_T}{\partial \delta_t}$	$Y_{\delta a} = -\dfrac{1}{\mathrm{m}}\dfrac{\partial C}{\partial \delta_a}$	$Z_{\delta e} = \dfrac{-1}{\mathrm{m}}\dfrac{\partial L}{\partial \delta_e}$

Next, using (2.5-19), form the partial derivatives with respect to X and apply the steady-state conditions (2.6-9). The result is

$$\begin{bmatrix} \nabla_X f_1 \\ \nabla_X f_2 \\ \nabla_X f_3 \end{bmatrix} =$$

$$\begin{bmatrix} -F_T \sin\left(\alpha_e + \alpha_T\right) \nabla_X \alpha + \cos(\alpha_e + \alpha_T) \nabla_X F_T - \mathrm{m} g_D \cos\gamma_e \nabla_X(\theta - \alpha) - \nabla_X D \\ -F_T \cos(\alpha_e + \alpha_T) \nabla_X \beta + \mathrm{m} g_D (\sin\gamma_e \nabla_X \beta + \cos\theta_e \nabla_X \phi) - \nabla_X C - \mathrm{m} V_{T_e} \nabla_X R_s \\ -F_T \cos(\alpha_e + \alpha_T) \nabla_X \alpha - \sin(\alpha_e + \alpha_T) \nabla_X F_T + \mathrm{m} g_D \sin\gamma_e \nabla_X(\alpha - \theta) - \nabla_X L + \mathrm{m} V_{T_e} \nabla_X Q \end{bmatrix} \tag{2.6-12}$$

This result can be further reduced by using the steady-state conditions, obtained by setting the left-hand side of (2.5-19) to zero, to replace some groups of terms by the steady-state lift and drag forces. Thus, the partial derivatives evaluated at the equilibrium point are

$$\begin{bmatrix} \nabla_X f_1 \\ \nabla_X f_2 \\ \nabla_X f_3 \end{bmatrix}_{\substack{\overline{U}=\overline{U}_e \\ X=X_e}} = \begin{bmatrix} \cos\left(\alpha_e + \alpha_T\right) \nabla_X F_T - \nabla_X D + L_e \nabla_X \alpha - \mathrm{m} g_D \cos\gamma_e \nabla_X \theta \\ -\nabla_X C - D_e \nabla_X \beta + \mathrm{m} g_D \cos\theta_e \nabla_X \phi - \mathrm{m} V_{T_e} \nabla_X R_s \\ -\sin(\alpha_e + \alpha_T) \nabla_X F_T - \nabla_X L - D_e \nabla_X \alpha - \mathrm{m} g_D \sin\gamma_e \nabla_X \theta + \mathrm{m} V_{T_e} \nabla_X Q \end{bmatrix} \tag{2.6-13}$$

where α_e, θ_e, γ_e, L_e, and D_e are the steady-state values. Note that there is no steady-state sideforce. If this expression is interpreted in terms of the derivatives from Table 2.6-1, we obtain for the right-hand side:

$$\mathrm{m} \begin{bmatrix} X_V + X_{T_V} \cos\left(\alpha_e + \alpha_T\right) & 0 & X_\alpha & 0 & -g_D \cos\gamma_e & 0 & 0 & 0 & 0 \\ 0 & Y_\beta & 0 & g_D \cos\theta_e & 0 & 0 & Y_p & 0 & Y_r - V_{T_e} \\ Z_V - X_{T_V} \sin(\alpha_e + \alpha_T) & 0 & Z_\alpha & 0 & -g_D \sin\gamma_e & 0 & 0 & V_{T_e} + Z_q & 0 \end{bmatrix} \tag{2.6-14}$$

This matrix constitutes the top three rows of A in (2.6-7).

It only remains to obtain the partial derivatives of the force equations with respect to the control vector $\overline{U}$. The partial derivatives are

$$\begin{bmatrix} \nabla_U f_1 \\ \nabla_U f_2 \\ \nabla_U f_3 \end{bmatrix} = \begin{bmatrix} \cos\left(\alpha + \alpha_T\right) \nabla_U F_T - \nabla_U D \\ \nabla_U Y \\ -\sin(\alpha + \alpha_T) \nabla_U F_T - \nabla_U L \end{bmatrix} \tag{2.6-15}$$

Now, inserting the relevant dimensional derivatives and the equilibrium values of the angles, we obtain

$$\begin{bmatrix} \nabla_U f_1 \\ \nabla_U f_2 \\ \nabla_U f_3 \end{bmatrix}_{\substack{X=X_e \\ \overline{U}=\overline{U}_e}} = \mathrm{m} \begin{bmatrix} X_{\delta t} \cos\left(\alpha_e + \alpha_T\right) & X_{\delta e} & 0 & 0 \\ 0 & 0 & Y_{\delta a} & Y_{\delta r} \\ -X_{\delta t} \sin(\alpha_e + \alpha_T) & Z_{\delta e} & 0 & 0 \end{bmatrix} \tag{2.6-16}$$

and these are the top three rows of B in (2.6-7).

This completes the linearization of the force equations. Note that the positions of the zero elements correspond to the beginnings of the anticipated decoupling in (2.6-7). One of the assumptions contributing to this decoupling is that the partial derivatives of drag with respect to the lateral-directional controls (ailerons and rudder) can be neglected. In practice aileron and rudder deflections do cause nonnegligible changes in drag, but this assumption does not have any significant consequences on the linearized dynamics.

The Linearized Kinematic Equations We will now determine the second block of three rows in (2.6-7). The nonlinear kinematic relationship between the Euler angle rates and the stability-axes rates P_s, Q, and R_s is obtained from Table 2.5-1 and the transformation matrices $C_{bf/s}$. Thus,

$$\dot{\Phi} = H(\Phi)\, C_{bf/s}\, \omega^s_{b/e} \tag{2.6-17}$$

There are no aerodynamic forces or moments involved in these equations, and it is easy to see that the contribution to the E-matrix is given by

$$-\begin{bmatrix} \nabla_{\dot{X}} f_4 \\ \nabla_{\dot{X}} f_5 \\ \nabla_{\dot{X}} f_6 \end{bmatrix} = \begin{bmatrix} 0 & 0 & 0 & 1 & 0 & 0 & 0 & 0 & 0 \\ 0 & 0 & 0 & 0 & 1 & 0 & 0 & 0 & 0 \\ 0 & 0 & 0 & 0 & 0 & 1 & 0 & 0 & 0 \end{bmatrix} \tag{2.6-18}$$

Next we determine the contributions of the kinematic equations to the A-matrix. Equations (2.6-17) are linear in P_s, Q, and R_s, so all partial derivatives of the coefficient matrix elements will be eliminated when we set $P_s = Q = R_s = 0$. It only remains to evaluate the coefficient matrices under the steady-state conditions. The result is

$$H(\Phi)\, C_{bf/s} = \begin{bmatrix} c\alpha + t\theta c\varphi s & \mathrm{t}\theta \mathrm{s}\varphi & -s\alpha + t\theta c\varphi c\alpha \\ -s\varphi s\alpha & c\varphi & -s\varphi c\alpha \\ c\varphi s\alpha / c\theta & s\varphi / c\theta & c\varphi c\alpha / c\theta \end{bmatrix} \tag{2.6-19}$$

Inserting the steady-state conditions in this matrix and applying some trigonometric identities, we see that

$$\begin{bmatrix} \nabla_X f_4 \\ \nabla_X f_5 \\ \nabla_X f_6 \end{bmatrix}_{\substack{U=U_e \\ X=X_e}} = \begin{bmatrix} 0 & 0 & 0 & 0 & 0 & 0 & c\gamma_e / c\theta_e & 0 & s\gamma_e / c\theta_e \\ 0 & 0 & 0 & 0 & 0 & 0 & 0 & 1 & 0 \\ 0 & 0 & 0 & 0 & 0 & 0 & s\alpha_e / c\theta_e & 0 & c\alpha_e / c\theta_e \end{bmatrix} \tag{2.6-20}$$

The partial derivatives of the kinematic variables with respect to the control vector are all zero, so this completes the linearization of the kinematic equations. Note that the force and moment equations are independent of the heading angle ψ in the *ned* tangent plane, so the third kinematic equation is not really needed in the linear model.

The Linearized Moment Equations Here we determine the last three rows of the linear state equations (2.6-7). The starting point for this linearization is the stability-axes moment equations (2.5-26), with all terms moved to the right-hand side. The moment partial derivatives that are normally considered important are contained in Table 2.6-2; the table defines the moment dimensional derivatives. These dimensional derivatives are given the symbols L, M, and N to denote, respectively, rolling, pitching, and yawing moments, and their subscripts indicate the quantity with respect to which the derivative is taken. These include all six of the state variables that determine the translational and rotational rates, the four control variables, and the angular rate alpha-dot. The derivatives with respect to beta-dot have been omitted from the table because they are usually unimportant and are difficult to measure. The effect of beta-dot on yawing moment may sometimes be important, and the derivative can be estimated with methods given in the USAF DATCOM (Hoak et al., 1970). It is convenient to include the moment of inertia for the corresponding axis in the definition of the dimensionless coefficient. Therefore, each derivative has the dimensions of angular acceleration divided by the independent variable dimensions (s^{-1}, s^{-2}, $ft^{-1}s^{-1}$, or none).

We will assume, as in Section 2.5, that the engine thrust vector lies in the x_b-z_b plane and therefore contributes only a pitching moment $m_{y,T}$ to the stability-axes moment equations. This is not an accurate assumption for a propeller aircraft, and

TABLE 2.6-2 The Moment Dimensional Derivatives

ROLL	PITCH	YAW
$L_\beta = \frac{1}{J'_X}\frac{\partial \mathscr{L}}{\partial \beta}$	$M_V = \frac{1}{J'_Y}\frac{\partial m_A}{\partial V_T}$	$N_\beta = \frac{1}{J'_Z}\frac{\partial n_A}{\partial \beta}$
$L_P = \frac{1}{J'_X}\frac{\partial \mathscr{L}}{\partial P}$	$M_\alpha = \frac{1}{J'_Y}\frac{\partial m_A}{\partial \alpha}$	$N_p = \frac{1}{J'_Z}\frac{\partial n_A}{\partial P}$
$L_r = \frac{1}{J'_X}\frac{\partial \mathscr{L}}{\partial R}$	$M_{\dot\alpha} = \frac{1}{J'_Y}\frac{\partial m_A}{\partial \dot\alpha}$	$N_r = \frac{1}{J'_Z}\frac{\partial n_A}{\partial R}$
$L_{\delta a} = \frac{1}{J'_X}\frac{\partial \mathscr{L}}{\partial \delta_a}$	$M_q = \frac{1}{J'_Y}\frac{\partial m_A}{\partial Q}$	$N_{\delta a} = \frac{1}{J'_Z}\frac{\partial n_A}{\partial \delta_a}$
$L_{\delta r} = \frac{1}{J'_X}\frac{\partial \mathscr{L}}{\partial \delta_r}$	$M_{\delta e} = \frac{1}{J'_Y}\frac{\partial m_A}{\partial \delta_e}$	$N_{\delta r} = \frac{1}{J'_Z}\frac{\partial n_A}{\partial \delta_r}$
	$M_{T_V} = \frac{1}{J'_Y}\frac{\partial m_T}{\partial V_T}$	$N_{T_\beta} = \frac{1}{J'_Z}\frac{\partial n_T}{\partial \beta}$
	$M_{T_\alpha} = \frac{1}{J'_Y}\frac{\partial m_T}{\partial \alpha}$	
	$M_{\delta t} = \frac{1}{J'_Y}\frac{\partial m_T}{\partial \delta_t}$	

there will be a number of power effects (Stinton, 1983; Ribner, 1943). These include a rolling moment due to propeller torque reaction, which is a function of throttle setting, and moments and forces that depend on the total angle of attack of the propeller, which is a function of alpha and beta. The table shows derivatives for thrust moment varying with speed, alpha, throttle position, and sideslip. For simplicity, the derivatives with respect to alpha and beta will be omitted from our equations.

The stability-axes moment equations (2.5-26) are repeated here, with all nonzero terms moved to the right-hand side:

$$0 = \begin{bmatrix} f_7 \\ f_8 \\ f_9 \end{bmatrix} = \begin{bmatrix} -\dot{P}_s + \dot{\alpha} R_s \\ -\dot{Q} \\ -\dot{R}_s - \dot{\alpha} P_s \end{bmatrix} + \frac{1}{\Gamma} \begin{bmatrix} J'_z & 0 & J'_{xz} \\ 0 & \Gamma/J'_y & 0 \\ J'_{xz} & 0 & J'_x \end{bmatrix} \left(\begin{bmatrix} \ell_s \\ m \\ n_s \end{bmatrix} - \tilde{\boldsymbol{\omega}}^s_{b/e} J^s \boldsymbol{\omega}^s_{b/e} \right) \tag{2.6-21}$$

To find the block of E-matrix terms, all the moment equation terms that involve state derivatives must be examined. These are

$$\dot{P}_s, \dot{Q}, \dot{R}_s, \dot{\alpha} R_s, \dot{\alpha} P_s, m$$

The two alpha-dot terms are of degree 2 in the variables that are set to zero in the steady state. Therefore, the corresponding partial derivatives vanish from the E-matrix, leaving only four terms:

$$-\begin{bmatrix} \nabla_{\dot{X}} f_7 \\ \nabla_{\dot{X}} f_8 \\ \nabla_{\dot{X}} f_9 \end{bmatrix}_{\substack{\overline{U}=\overline{U}_e \\ X=X_e}} = \begin{array}{c} \begin{matrix} \dot{v}_T & \dot{\beta} & \dot{\alpha} & \dot{\phi} & \dot{\theta} & \dot{\psi} & \dot{P}_s & \dot{Q} & \dot{R}_s \end{matrix} \\ \begin{bmatrix} 0 & 0 & 0 & 0 & 0 & 0 & 1 & 0 & 0 \\ 0 & 0 & -M_{\dot{\alpha}} & 0 & 0 & 0 & 0 & 1 & 0 \\ 0 & 0 & 0 & 0 & 0 & 0 & 0 & 0 & 1 \end{bmatrix} \end{array} \tag{2.6-22}$$

The contributions of the moment equations to the A- and B-matrices must now be found. In Equation (2.6-21), on the right, the derivatives of the angular rates are constants for the purposes of partial differentiation; the alpha-dot terms are of degree 2 in the variables of the steady-state condition, as is the last term on the right. This leaves only the term comprising the product of the inertia matrix and the moment array. The stability-axes inertia matrix is a function of alpha, but its derivative will be multiplied by a moment array that is null in steady-state nonturning flight. Therefore, the only partial derivatives that are of interest are given by the inertia matrix terms multiplied by the partial derivatives of the moments:

$$\begin{bmatrix} \nabla_{\dot{X}} f_7 \\ \nabla_{\dot{X}} f_8 \\ \nabla_{\dot{X}} f_9 \end{bmatrix}_{\substack{\overline{U}=\overline{U}_e \\ X=X_e}} = \begin{bmatrix} \left(J'_Z \nabla_X \ell_s + J'_{XZ} \nabla_X n_s \right) / \Gamma \\ (\nabla_X m) / J'_Y \\ (J'_{XZ} \nabla_X \ell_s + J'_X \nabla_X n_s) / \Gamma \end{bmatrix} \tag{2.6-23}$$

and

$$\begin{bmatrix} \nabla_U f_7 \\ \nabla_U f_8 \\ \nabla_U f_9 \end{bmatrix}_{\substack{\overline{U}=\overline{U}_e \\ X=X_e}} = \begin{bmatrix} \left(J'_Z \nabla_U \mathscr{l}_s + J'_{XZ} \nabla_U n_s\right)/\Gamma \\ (\nabla_U m)/J'_Y \\ (J'_{XZ} \nabla_U \mathscr{l}_s + J'_X \nabla_U n_s)/\Gamma \end{bmatrix} \tag{2.6-24}$$

When the partial derivatives in (2.6-23) and (2.6-24) are interpreted in terms of the dimensional derivatives in Table 2.6-2, we obtain the last three rows of the A-matrix,

$$\begin{bmatrix} \nabla_X f_7 \\ \nabla_X f_8 \\ \nabla_X f_9 \end{bmatrix}_{\substack{\overline{U}=\overline{U}_e \\ X=X_e}} =$$

$$\begin{bmatrix} 0 & \mu L_\beta + \sigma_1 N_\beta & 0 & 0 & 0 & 0 & \mu L_p + \sigma_1 N_p & 0 & \mu L_r + \sigma_1 N_r \\ M_V + M_{T_V} & 0 & M_\alpha + M_{T\alpha} & 0 & 0 & 0 & 0 & M_q & 0 \\ 0 & \mu N_\beta + \sigma_2 L_\beta & 0 & 0 & 0 & 0 & \mu N_p + \sigma_2 L_p & 0 & \mu N_r + \sigma_2 L_r \end{bmatrix} \tag{2.6-25}$$

and the last three rows of the B-matrix,

$$\begin{bmatrix} \nabla_U f_7 \\ \nabla_u f_8 \\ \nabla_u f_9 \end{bmatrix}_{\substack{\overline{U}=\overline{U}_e \\ X=X_e}} = \begin{bmatrix} 0 & 0 & \mu L_{\delta a} + \sigma_1 N_{\delta a} & \mu L_{\delta r} + \sigma_1 N_{\delta r} \\ M_{\delta t} & M_{\delta e} & 0 & 0 \\ 0 & 0 & \mu N_{\delta a} + \sigma_2 L_{\delta a} & \mu N_{\delta r} + \sigma_2 L_{\delta r} \end{bmatrix} \tag{2.6-26}$$

In these equations, the constants μ and σ_i are given by

$$\mu = (J'_Z J'_X)/\Gamma \quad \sigma_1 = (J'_Z J'_{XZ})/\Gamma \quad \sigma_2 = (J'_X J'_{XZ})/\Gamma \tag{2.6-27}$$

The cross-product of inertia is normally small in magnitude compared to the moments of inertia, so the parameter μ is quite close to unity, and the σ_i are much smaller than unity.

The Decoupled Linear State Equations

All of the information for the coefficient matrices of the linear state equations (2.6-7) has now been obtained. An inspection of the coefficient blocks shows that the longitudinal- and lateral-directional equations are decoupled (although the lateral-directional equations do depend on steady-state longitudinal quantities such as γ_e and θ_e). Therefore, rather than attempt to assemble the complete equations, we will collect the longitudinal- and lateral-directional equations separately.

If the longitudinal state and control variables are ordered as follows, additional potential decoupling will become apparent. Thus, we choose the longitudinal state and input vectors as

$$x = [\alpha \quad q \quad v_T \quad \theta]^T \quad u = [\delta_e \quad \delta_t]^T \tag{2.6-28}$$

The longitudinal equations are obtained from the first and last rows of (2.6-11), (2.6-14), and (2.6-16) (divided through by m); the middle rows of (2.6-18) and (2.6-20); and the middle rows of (2.6-22), (2.6-25), and (2.6-26). The longitudinal coefficient matrices are now given by

$$E = \begin{bmatrix} V_{T_e} - Z_{\dot{\alpha}} & 0 & 0 & 0 \\ -M_{\dot{\alpha}} & 1 & 0 & 0 \\ 0 & 0 & 1 & 0 \\ 0 & 0 & 0 & 1 \end{bmatrix} \quad B = \begin{bmatrix} Z_{\delta e} & -X_{\delta t} \sin\left(\alpha_e + \alpha_T\right) \\ M_{\delta e} & M_{\delta t} \\ X_{\delta e} & X_{\delta t} \cos(\alpha_e + \alpha_T) \\ 0 & 0 \end{bmatrix}$$

$$A = \begin{bmatrix} Z_\alpha & V_{T_e} + Z_q & Z_V - X_{T_V} \sin\left(\alpha_e + \alpha_T\right) & -g_D \sin\gamma_e \\ M_\alpha + M_{T_\alpha} & M_q & M_V + M_{T_V} & 0 \\ X_\alpha & 0 & X_V + X_{T_V} \cos(\alpha_e + \alpha_T) & -g_D \cos\gamma_e \\ 0 & 1 & 0 & 0 \end{bmatrix} \tag{2.6-29}$$

We see that E is block diagonal and does not contribute to any coupling between the α, q, and v_T, θ pairs of variables. Furthermore, E is nonsingular for nonhovering flight because, although $Z_{\dot{\alpha}}$ can be positive, it is normally much smaller in magnitude than V_T.

The A-matrix has several null elements and, in level flight, the (1, 4) element is zero. In trimmed flight, at low Mach numbers, the moment derivatives in element (2, 3) are zero (see next section). Finally, the (1, 3) element is small compared to the other elements of the first row and can often be neglected. Under the above conditions, the angle-of-attack and pitch-rate differential equations have no dependence on the speed, pitch-attitude perturbations (but not vice-versa). The solution of these equations, with the elevator and throttle inputs fixed, is a "stick-fixed" mode of oscillation known as the short-period mode (Chapter 3).

In the same vein, the (3, 1) element of the B-matrix (drag due to elevator deflection) is usually negligible, and the pitching moment due to throttle inputs, element (2, 2), is zero if the x-z plane component of the engine thrust vector passes through the aircraft center of mass [this is not true for aircraft such as the B-747 and B-767 (Roskam, 1979)]. Also, the (1, 2) element of B may often be neglected because of the small sine component. Under these conditions, the elevator input controls only the alpha-pitch-rate dynamics, the throttle input controls only the speed-pitch-attitude dynamics, and transfer function analysis is simplified (Chapter 4).

The lateral-directional states and controls are

$$x = [\beta \quad \phi \quad p_s \quad r_s]^T \quad u = [\delta_a \quad \delta_r]^T, \tag{2.6-30}$$

where the state ψ has been dropped. The state equations are obtained from the second rows of (2.6-11), (2.6-14), and (2.6-16); the first rows of (2.6-18) and (2.6-20); and

the first and third rows of (2.6-22), (2.6-25), and (2.6-26). The resulting coefficient matrices are

$$E = \begin{bmatrix} V_{T_e} & 0 & 0 & 0 \\ 0 & 1 & 0 & 0 \\ 0 & 0 & 1 & 0 \\ 0 & 0 & 0 & 1 \end{bmatrix} \quad B = \begin{bmatrix} Y_{\delta a} & Y_{\delta r} \\ 0 & 0 \\ L'_{\delta a} & L'_{\delta r} \\ N'_{\delta a} & N'_{\delta r} \end{bmatrix}$$

$$A = \begin{bmatrix} Y_\beta & g_D \cos\theta_e & Y_p & Y_r - V_{T_e} \\ 0 & 0 & c\gamma_e/c\theta_e & s\gamma_e/c\theta_e \\ L'_\beta & 0 & L'_p & L'_r \\ N'_\beta & 0 & N'_p & N'_r \end{bmatrix}, \tag{2.6-31}$$

where primed moment derivatives are defined (McRuer et al., 1973) by

$$\begin{aligned} L'_\beta &= \mu L_\beta + \sigma_1 N_\beta & L'_p &= \mu L_p + \sigma_1 N_p & L'_r &= \mu L_r + \sigma_1 N_r \\ N'_\beta &= \mu N_\beta + \sigma_2 L_\beta & N'_p &= \mu N_p + \sigma_2 L_p & N_r &= \mu N_r + \sigma_2 L_r \\ L'_{\delta a} &= \mu L_{\delta a} + \sigma_1 N_{\delta a} & L'_{\delta r} &= \mu L_{\delta r} + \sigma_1 N_{\delta r} \\ N'_{\delta a} &= \mu N_{\delta a} + \sigma_2 L_{\delta a} & N'_{\delta r} &= \mu N_{\delta r} + \sigma_2 L_{\delta r} \end{aligned} \tag{2.6-32}$$

The inverse of the E-matrix is diagonal and exists for nonzero airspeed. Its effect is simply to divide the right-hand side of the beta-dot equation by airspeed. Therefore, although the original nonlinear equations were assumed implicit, the linear equations can now be made explicit in the derivatives. The coefficient matrices depend on the steady-state angle of attack and pitch attitude in both cases. Although they nominally apply to small perturbations about a wings-level, steady-state flight condition, the equations can be used satisfactorily for perturbed roll angles of several degrees.

In this chapter we will be content with simply deriving the coefficient matrices for the linear state equations; the equations will not be used until Chapter 3. The remainder of the chapter will be devoted to expressing the dimensional stability derivatives, used in the coefficient matrices, in terms of derivatives of the dimensionless aerodynamic coefficients defined in (2.3-8*b*). The resulting "dimensionless derivatives" have the advantage that they are less dependent on the specific aircraft and flight condition and more dependent on the geometrical configuration of an aircraft. Methods have been developed to estimate the dimensionless derivatives, and they can be used to compare and assess different design configurations.

The Dimensionless Stability and Control Derivatives

The dimensional aerodynamic derivatives are simply a convenient set of coefficients for the linear equations. We must now relate them to the *dimensionless stability*

derivatives used by stability and control engineers and found in aerodynamic data. The way in which the stability derivatives are made dimensionless depends on whether the independent variable for the differentiation is angle, angular rate, or velocity. This will be illustrated by example before we tabulate the derivatives.

Consider the derivative X_V in Table 2.6-1; this derivative is taken with respect to airspeed. The drag force depends on airspeed both through dynamic pressure and through the variation of the aerodynamic drag coefficient with airspeed. Therefore, using the definition of X_V and the drag equation from (2.3-8*b*), we have

$$X_V = \frac{-1}{\mathrm{m}} \left[\frac{\partial \overline{q}}{\partial V_T} S C_D + \overline{q} S \frac{\partial C_D}{\partial V_T} \right] = \frac{-\overline{q} S}{\mathrm{m} V_{T_e}} (2C_D + C_{D_V}),$$

where $C_{D_V} \equiv V_{T_e}(\partial C_D / \partial V_T)$ is the dimensionless speed damping derivative.

Next consider a derivative that is taken with respect to angular rate, C_{m_q}. The dimensionless rate damping derivatives were defined in Section 2.3 and can now be related to the dimensional derivatives. Making use of the definition of pitching moment coefficient in (2.3-8*b*), we have

$$M_q = \frac{\overline{q} S \overline{c}}{J'_Y} \frac{\partial C_m}{\partial Q} = \frac{\overline{q} S \overline{c}}{J'_Y} \frac{\overline{c}}{2V_{T_e}} C_{m_q}, \quad \text{where} \quad C_{m_q} \equiv \frac{2V_{T_e}}{\overline{c}} \frac{\partial C_m}{\partial Q}$$

The "dimensionless" stability derivatives taken with respect to angle actually have dimensions of deg^{-1} when expressed in degrees rather than radians.

Tables 2.6-1 and 2.6-2 include six thrust derivatives (X_{T_V}, X_{δ_t}, M_{T_V}, M_{T_α}, M_{δ_t},N_{T_β}). The corresponding dimensionless derivatives can be defined by expressing the thrust force and moment components in terms of dimensionless coefficients. For example, a pitching moment component due to thrust can be written as $M_T = \overline{q} S \overline{c} C_{m_T}$. Values for the thrust derivatives would be found by referring to the "installed thrust" data for the specific engine and determining the change in thrust due to a perturbation in the variable of interest. In the case of the derivatives with respect to V_T and throttle setting, it is probably most convenient to work directly with the dimensional derivatives. Determination of the thrust derivatives with respect to α and β is more complicated; a readable explanation is given by Roskam (1979).

Following the lines of the examples above, the longitudinal dimensionless stability and control derivatives and the lateral-directional dimensionless stability and control derivatives corresponding to Tables 2.6-1 and 2.6-2 are given in Tables 2.6-3 and 2.6-4. Some of the thrust derivatives have been omitted because of lack of space and because of their limited utility.

The dimensionless stability derivatives are in general very important to both the aircraft designer and the stability and control engineer. They provide information about the natural stability of an aircraft, about the effectiveness of the control surfaces, and about the maneuverability. They correlate with the geometrical features of the aircraft and thereby facilitate the preliminary design process. The typical variation of many of the stability derivatives with flight conditions (e.g., speed, angle of attack, sideslip angle) is known to the designer, and he or she can therefore

TABLE 2.6-3 Longitudinal Dimensional versus Dimensionless Derivatives

$X_V = \dfrac{-\overline{q}S}{\mathrm{m}V_{T_e}}(2C_{D_e} + C_{D_V})$	$C_{D_V} \equiv V_{T_e}\dfrac{\partial C_D}{\partial V_T}$
$X_{T_V} = \dfrac{\overline{q}S}{\mathrm{m}V_{T_e}}(2C_{T_e} + C_{T_V})$	$C_{T_V} \equiv V_{T_e}\dfrac{\partial C_T}{\partial V_T}$
$X_\alpha = \dfrac{\overline{q}S}{\mathrm{m}}(C_{L_e} - C_{D_\alpha})$	$C_{D_\alpha} \equiv \dfrac{\partial C_D}{\partial \alpha}$
$X_{\delta e} = \dfrac{-\overline{q}S}{\mathrm{m}}C_{D_{\delta e}}$	$C_{D_{\delta e}} \equiv \dfrac{\partial C_D}{\partial \delta_e}$
$Z_V = \dfrac{-\overline{q}S}{\mathrm{m}V_{T_e}}(2C_{L_e} + C_{L_V})$	$C_{L_V} \equiv V_{T_e}\dfrac{\partial C_L}{\partial V_T}$
$Z_\alpha = \dfrac{-\overline{q}S}{\mathrm{m}}(C_{D_e} + C_{L_\alpha})$	$C_{L_\alpha} \equiv \dfrac{\partial C_L}{\partial \alpha}$
$Z_{\dot\alpha} = \dfrac{-\overline{q}S\overline{c}}{2\mathrm{m}V_{Te}}C_{L\dot\alpha}$	$C_{L_{\dot\alpha}} \equiv \dfrac{2V_{T_e}}{\overline{c}}\dfrac{\partial C_L}{\partial \dot\alpha}$
$Z_q = \dfrac{-\overline{q}S\overline{c}}{2\mathrm{m}V_{T_e}}C_{L_q}$	$C_{L_q} \equiv \dfrac{2V_{T_e}}{\overline{c}}\dfrac{\partial C_L}{\partial Q}$
$Z_{\delta e} = \dfrac{-\overline{q}S}{\mathrm{m}}C_{L_{\delta e}}$	$C_{L_{\delta e}} \equiv \dfrac{\partial C_L}{\partial \delta_e}$
$M_V = \dfrac{\overline{q}S\overline{c}}{J_Y V_{T_e}}(2C_{m_e} + C_{m_V})$	$C_{m_V} \equiv V_{T_e}\dfrac{\partial C_m}{\partial V_T}$
$M_{T_V} = \dfrac{\overline{q}S\overline{c}}{J_Y V_{T_e}}(2C_{m_T} + C_{m_{T_V}})$	$C_{m_{T_V}} \equiv V_{T_e}\dfrac{\partial C_{m_T}}{\partial V_T}$
$M_\alpha = \dfrac{\overline{q}S\overline{c}}{J_Y}C_{m_\alpha}$	$C_{m_\alpha} \equiv \dfrac{\partial C_m}{\partial \alpha}$
$M_{\dot\alpha} = \dfrac{\overline{q}S\overline{c}}{J_Y}\dfrac{\overline{c}}{2V_{T_e}}C_{m_{\dot\alpha}}$	$C_{m_{\dot\alpha}} \equiv \dfrac{2V_{T_e}}{\overline{c}}\dfrac{\partial C_m}{\partial \dot\alpha}$
$M_q = \dfrac{\overline{q}S\overline{c}}{J_Y}\dfrac{\overline{c}}{2V_{T_e}}C_{m_q}$	$C_{m_q} \equiv \dfrac{2V_{T_e}}{\overline{c}}\dfrac{\partial C_m}{\partial Q}$
$M_{\delta e} = \dfrac{\overline{q}S\overline{c}}{J_Y}C_{m_{\delta e}}$	$C_{m_{\delta e}} \equiv \dfrac{\partial C_m}{\partial \delta_e}$

anticipate the design problems in different parts of the flight envelope. Information on the importance of the stability derivatives, the accuracy with which they can be estimated, and their variation with flight conditions can be found in stability and control textbooks (Roskam, 1979; Etkin, 1972; Perkins and Hage, 1949) and in the USAF DATCOM (Hoak et al., 1970). Stability derivatives at certain flight conditions, for a number of different aircraft, are also given in these books, by Blakelock (1965), by McRuer et al. (1973), and in various other texts.

TABLE 2.6-4 Lateral-Directional Dimensional versus Dimensionless Derivative

$Y_\beta = \frac{\overline{q}S}{\mathrm{m}} C_{Y_\beta}$	$C_{Y_\beta} = -\left(\frac{\partial C_C}{\partial \beta} + C_{D_e}\right)$
$Y_p = \frac{\overline{q}Sb}{2\mathrm{m}V_{T_e}} C_{Y_p}$	$C_{Y_p} \equiv -\frac{2V_{T_e}}{b}\frac{\partial C_C}{\partial P_S}$
$Y_r = \frac{\overline{q}Sb}{2\mathrm{m}V_{T_e}} C_{Y_r}$	$C_{Y_r} \equiv -\frac{2V_{T_e}}{b}\frac{\partial C_C}{\partial R_S}$
$Y_{\delta r} = \frac{\overline{q}S}{\mathrm{m}} C_{Y_{\delta r}}$	$C_{Y_{\delta r}} \equiv -\frac{\partial C_C}{\partial \delta_r}$
$Y_{\delta a} = \frac{\overline{q}S}{\mathrm{m}} C_{Y_{\delta a}}$	$C_{Y_{\delta a}} \equiv -\frac{\partial C_C}{\partial \delta_a}$
$L_\beta = \frac{\overline{q}Sb}{J'_X} C_{\ell_\beta}$	$C_{\ell_\beta} \equiv \frac{\partial C_\ell}{\partial \beta}$
$L_p = \frac{\overline{q}Sb}{J'_X}\frac{b}{2V_{T_e}} C_{\ell_p}$	$C_{\ell_p} \equiv \frac{2V_{T_e}}{b}\frac{\partial C_\ell}{\partial P}$
$L_r = \frac{\overline{q}Sb}{J'_X}\frac{b}{2V_{T_e}} C_{\ell_r}$	$C_{\ell_r} \equiv \frac{2V_{T_e}}{b}\frac{\partial C_\ell}{\partial R}$
$L_{\delta a} = \frac{\overline{q}Sb}{J'_X} C_{\ell_{\delta a}}$	$C_{\ell_{\delta a}} \equiv \frac{\partial C_\ell}{\partial \delta_a}$
$L_{\delta r} = \frac{\overline{q}Sb}{J'_X} C_{\ell_{\delta r}}$	$C_{\ell_{\delta r}} \equiv \frac{\partial C_\ell}{\partial \delta_r}$
$N_\beta = \frac{\overline{q}Sb}{J'_Z} C_{n_\beta}$	$C_{n_\beta} \equiv \frac{\partial C_n}{\partial \beta}$
$N_p = \frac{\overline{q}Sb}{J'_Z}\frac{b}{2V_{T_e}} C_{n_p}$	$C_{n_p} \equiv \frac{2V_{T_e}}{b}\frac{\partial C_n}{\partial P}$
$N_r = \frac{\overline{q}Sb}{J'_Z}\frac{b}{2V_{T_e}} C_{n_r}$	$C_{n_r} \equiv \frac{2V_{T_e}}{b}\frac{\partial C_n}{\partial R}$
$N_{\delta a} = \frac{\overline{q}Sb}{J'_Z} C_{n_{\delta a}}$	$C_{n_{\delta a}} \equiv \frac{\partial C_n}{\partial \delta_a}$
$N_{\delta r} = \frac{\overline{q}Sb}{J'_Z} C_{n_{\delta r}}$	$C_{n_{\delta r}} \equiv \frac{\partial C_n}{\partial \delta_r}$

In the next subsection we briefly describe the significance of various dimensionless derivatives and their variation with flight conditions. This information will be utilized in Chapter 4 when aircraft dynamic modes are analyzed.

Description of the Longitudinal Dimensionless Derivatives

The names and relative importance of the longitudinal stability derivatives are shown in Table 2.6-5, starting with the most important.

TABLE 2.6-5 Importance of Longitudinal Stability Derivatives

C_{L_α}	Lift-curve slope (determines response to turbulence)
C_{m_α}	Pitch stiffness (< 0 for static stability)
C_{m_q}	Pitch damping (< 0 for short-period damping)
C_{m_V}	Tuck derivative (< 0 gives unstable tuck)
$C_{m_{\dot{\alpha}}}$	Alpha-dot derivative (less important than C_{m_q})
C_{D_V}	Speed damping (if > 0 can mitigate unstable C_{m_V})
C_{D_α}	Drag versus alpha slope
C_{L_v}	Lift versus speed slope
$C_{L_{\dot{\alpha}}}$	Acceleration derivative for lift
C_{L_q}	Pitch-rate-dependent lift

The stability derivatives are estimated from geometrical properties, from the slopes of the aerodynamic coefficients, or from perturbed motion of an aircraft in flight test or a model in a wind tunnel. The aerodynamic coefficients are, in general, nonlinear functions, and so for a given aircraft the stability derivatives vary with the aerodynamic angles (α, β), Mach number (compressibility effect), thrust (power effect), and dynamic pressure (aeroelastic effects). Descriptions of these variations and methods of estimating the derivatives can be found in the literature (Roskam, 1979; Perkins and Hage, 1949; Queijo, 1971). Stability derivatives obtained from flight test are usually presented in graphs that apply to trimmed-flight conditions at, for example, a given altitude with varying Mach number. Therefore, a sequence of points along a particular curve would correspond to different combinations of thrust, angle of attack, and elevator setting. This is acceptable to the flying-qualities engineer but presents a difficulty to the simulation engineer seeking to build a lookup table for that derivative.

Plots of aerodynamic coefficients, particularly those of high-speed aircraft, can exhibit both small-scale fluctuations and regimes of widely different behavior. Differentiation exaggerates such effects, and so it is easier to generalize about the behavior of aerodynamic coefficients than about the stability derivatives. Furthermore, the stability derivatives do not provide an adequate model of aircraft behavior for large-amplitude maneuvers and very nonlinear regimes such as stall. Stability derivative information is more readily available than aerodynamic coefficient data and is appropriate for linear models for stability analysis and flight control system design but is limited in its applicability to flight simulation. We now summarize the typical behavior of the most important derivatives in the normal flight regimes.

Lift-Curve Slope The derivative C_{L_α} is called the lift-curve slope; it is important because it determines how turbulent changes in alpha translate into changes in lift and hence determines the level of comfort for the pilot. In the same manner, it affects the maneuverability of the aircraft. It also affects the damping of the pitching motion of the aircraft when subjected to sudden disturbances, as will be shown in Chapter 4. This influences the pilot's opinion of the *handling qualities* of the airplane.

The lift-curve slope is approximately independent of alpha and typically in the range 1 to 8 (per radian) for the linear region of the lift curve below stall. When the wing is producing a large amount of lift, wing twist will reduce the local angle of attack of the wing panels according to distance out from the wing root. This will tend to reduce the lift-curve slope as alpha increases.

As explained in Section 2.3, compressibility effects also change C_{L_α} significantly; below the critical Mach number it increases with Mach, and at supersonic speeds it decreases with Mach. In the transonic range it may pass smoothly through a maximum (e.g., fighter-type wings) or may show a dip (thick, higher-aspect wings with no sweep). Wing sweep-back has the effect of reducing the lift-curve slope and making the curve of C_{L_α} versus Mach less peaked. The propulsion system can also have a strong effect on the C_{L_α}, as can be visualized from Figure 2.3-3*a*.

Pitch Stiffness Derivative The derivative C_{m_α} is the slope of the curve of the static pitching moment coefficient, around the cm, versus alpha, with controls neutral. Figures 2.3-7 show pitching moment–alpha curves, and Section 2.4 explains the factors that contribute to the derivative. This derivative is of critical importance for aircraft pitch stability; it also plays an important role in the dynamic behavior of pitching motion, as shown in Chapter.4.

Section 2.4 shows that the pitch stiffness will increase as the aerodynamic center moves aft with increasing Mach number and, depending on cm position, will also be affected by changes in wing C_{L_α} with Mach. The second important component of C_{m_α} contains the lift-curve slope of the horizontal tail. Again, the lift-curve slope varies with Mach, but this may not have a very great effect on C_{m_α}, particularly in the case of a thin, swept, low-aspect "all-flying" tail. The lift-curve slope is multiplied by the tail efficiency factor, and this will tend to decrease with increasing alpha, to an extent depending on the degree of coupling between wing and tail. The third component of C_{m_α} is the derivative with respect to alpha of the pitching moment at the "wing-body aerodynamic center." A true wing-body aerodynamic center may not exist, and so this term is nonzero and difficult to determine. Roskam (1979) states that C_{m_α} will normally lie in the range -3 to $+1$ rad^{-1}.

***Pitch Damping Derivative*, C_{m_q}** The pitch damping derivative, C_{m_q}, was introduced in Section 2.3. This derivative is normally negative and determines the moment that opposes any pitch rate. It provides the most important contribution to the damping of the dynamic behavior in pitch (see Chapter 4) and hence is intimately involved in aircraft handling qualities.

The pitch damping is not given by the slope of an aerodynamic coefficient; it must be estimated from oscillatory motion of the aircraft or aircraft model or calculated. The main physical mechanism involved is that pitch rate determines translational rate of the horizontal tail perpendicular to the relative wind. This changes the tail angle of attack, tail "lift," and hence the tail moment about the cm. When the induced translational rate is small compared to true airspeed, the change in tail angle of attack will

be linearly related to pitch rate. Therefore, the pitch damping moment is invariably modeled as linearly proportional to pitch rate through C_{m_q}.

A very simple expression for the pitch damping derivative C_{m_q} can be obtained by calculating the horizontal-tail increment in lift due to a pitch-rate-induced translational velocity at the tail. Equation (2.3-9*a*) gives this derivative as

$$C_{m_q} = \frac{2V_{T_e}}{\overline{c}} \frac{\Delta C_m}{Q} \tag{2.6-33}$$

Let the moment arm of the tail ac about the aircraft cm be ℓ_t. The increment in lift of the tail is, in dimensionless form,

$$\Delta C_{L_t} = C_{L_{\alpha,t}} \tan^{-1}(Q\ell_t / V_{T_e}) \approx C_{L_{\alpha,t}} (Q\ell_t / V_{T_e}) \tag{2.6-34}$$

Now remember that the dimensional pitching moment coefficient is obtained by multiplying the dimensionless moment coefficient by $(S\overline{c})$. Therefore, this lift must be converted to a nondimensional pitching moment by multiplying by the *horizontal-tail volume ratio*,

$$V_H = (S_t \ell_t)/(S\overline{c}) \tag{2.6-35}$$

From the above three equations, noting that a positive pitch rate gives the tail a downward motion, a positive lift component, and therefore a negative contribution to aircraft pitching moment, we obtain

$$C_{m_q} = -2V_H C_{L_{\alpha,t}} (\ell_t / \overline{c}) \tag{2.6-36}$$

This equation neglects any pitch damping effect from the wings and fuselage, applies only for small alpha, and does not model any compressibility, aeroelastic, or thrust-dependent effects. It can be made to include some thrust and wing-downwash effects by including the tail efficiency factor [Equation (2.3-20)].

Figure 2.6-1 shows the variation of the pitch damping and acceleration derivatives for the jet trainer. These derivatives change quite dramatically with Mach in the transonic region, they are independent of alpha until stall is approached, and the pitch damping is somewhat dependent on altitude through aeroelastic effects. They can also be expected to be dependent on elevator deflection and movement of the tail aerodynamic center.

Tuck Derivative The effect of speed variations on pitching moment is contained in the "tuck derivative," C_{m_V}. This derivative can also be written in terms of Mach:

$$C_{m_V} = \frac{V_{T_e}}{a} \frac{\partial C_m}{\partial (V_T / a)} = M \frac{\partial C_m}{\partial M} \tag{2.6-37}$$

The derivative will be negligible at low subsonic speeds when compressibility effects are absent and at supersonic speeds when the aerodynamic center has ceased to

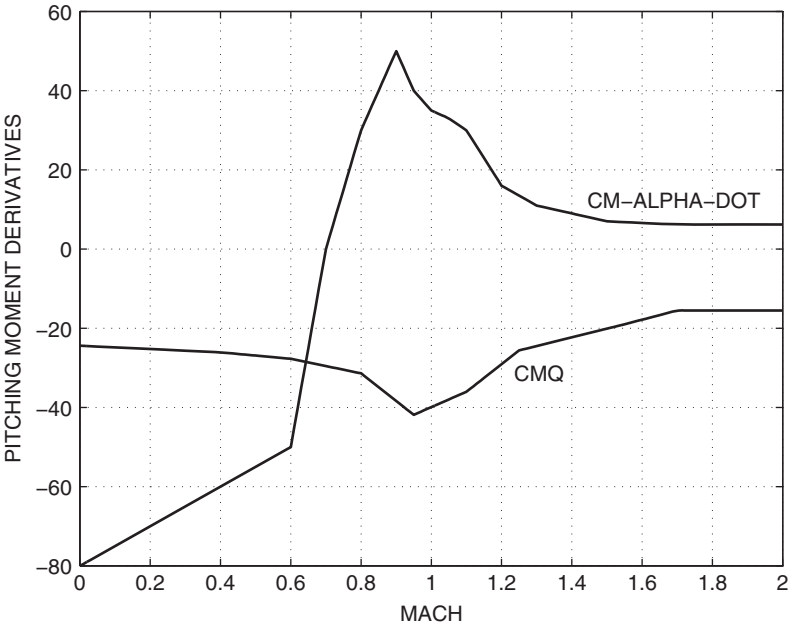

Figure 2.6-1 Pitching moment derivatives of a jet trainer aircraft.

move. In the transonic region we would expect to find a negative value as the ac moves aft but, in fact, C_{m_V} can be positive for some aircraft. The derivative changes quite abruptly as the transonic regime is reached and, if it is negative, the aircraft will tend to pitch down as speed increases. Gravity will then tend to further increase the speed, leading to an unstable pitch-down or "tuck-under" effect. The tuck may be particularly troublesome if the elevator control effectiveness is simultaneously decreasing with Mach. The transonic drag rise helps to mitigate an unstable tuck characteristic. Values of the tuck derivative range between about −0.4 and +0.6 (Roskam, 1979).

Speed Damping Derivative The speed damping derivative, C_{D_V}, can also be written in terms of Mach:

$$C_{D_V} = \frac{V_T}{a}\frac{\partial C_D}{\partial (V_T/a)} = M\frac{\partial C_D}{\partial M} \tag{2.6-38}$$

Like the tuck derivative, the speed damping derivative is a compressibility effect. It is negligible at low Mach numbers, rises to a peak with the transonic drag rise, then changes rapidly to negative values as the drag coefficient peaks and falls off with Mach, after the transonic regime. Values typically lie in the range −0.01 to +0.30 (Roskam, 1979).

TABLE 2.6-6 Importance of Lateral-Directional Derivatives

C_{ℓ_β}	Dihedral derivative (< 0 for positive stiffness)
C_{n_β}	Yaw stiffness (> 0 for positive stiffness)
C_{ℓ_p}	Roll damping (< 0 for roll damping)
C_{n_r}	Yaw damping (< 0 for yaw damping)
C_{n_p}	Yawing moment due to roll rate
C_{ℓ_r}	Rolling moment due to yaw rate
C_{Y_β}	Sideforce due to sideslip
C_{Y_r}	Sideforce due to yaw rate
C_{Y_p}	Sideforce due to roll rate
$C_{n_{\dot\beta}}$	Yawing moment due to sideslip rate
$C_{Y_{\dot\beta}}$	Sideforce due to sideslip rate
$C_{\ell_{\dot\beta}}$	Rolling moment due to sideslip rate

Description of the Lateral-Directional Dimensionless Derivatives

The lateral-directional stability derivatives are shown in Table 2.6-6, starting with the most important. The more important derivatives are discussed below.

Dihedral Derivative The *dihedral derivative*, C_{l_β}, is the slope of the rolling moment versus sideslip curve. Section 2.3 showed that this slope should be negative to achieve positive stiffness in roll and that positive wing dihedral could provide this. However, too much positive stiffness in roll tends to reduce the damping of the aircraft dynamic behavior in a yawing-rolling motion (the dutch roll mode, see Chapter 4), and the designer must find a compromise in the value of C_{l_β}. In some aircraft, wing sweep produces a C_{l_β} that is too negative and the aircraft may have negative dihedral (anhedral) of the wings or horizontal tail to offset this effect (e.g., F-4 and AV8-B aircraft). The value of C_{l_β} is typically in the range -0.4 to $+0.1$ per radian (Roskam, 1979) and may change significantly with Mach number in the transonic range.

Yaw Stiffness Derivative The *yaw stiffness derivative*, C_{n_β}, is the slope of the curve of yawing moment due to sideslip (Section 2.3), and it is associated with weathercock stability (tendency to head into the relative wind). It must be positive for positive stiffness in yaw, and it is principally determined by the size of the vertical tail. Weathercock stability can be lost at high dynamic pressure, due to structural deformation of the vertical tail, and aircraft have been known to "swap ends" in flight.

C_{n_β} plays a major role in the aircraft dutch roll mode (Chapter 4). Its value is typically in the range 0 to 0.4 rad^{-1} (Roskam, 1979), tending to fall off and possibly even become negative at transonic to supersonic Mach numbers. It may also become

negative at high angles of attack when the vertical tail becomes immersed in the wake from the wings and body. Achieving a suitable value of C_{n_β} is a consideration in the initial sizing of the vertical tail of an aircraft.

Roll Damping Derivative The *roll damping derivative*, C_{ℓ_p}, was introduced in Section 2.3 and is chiefly due to the variation of angle of attack along the wing span when the aircraft is rolling. The rolling moment produced by the differential lift between the two wings will be linearly proportional to roll rate until stall begins on the outer wing panels. This derivative is positive, except possibly in a spin, and usually lies in the range -0.8 to -0.1 per radian. It thus provides a moment that damps rolling motion, plays the major roll in the response of the aircraft to aileron inputs (see roll time constant, Chapter 4), and determines the associated handling qualities. It is determined from small-amplitude rolling motion measurements. When considering maximum roll rate, the helix angle (Section 2.3) is the more important parameter. In general, C_{ℓ_p} is a function of Mach number, altitude (because of aeroelastic effects), and alpha.

Yaw Damping Derivative The *yaw damping derivative*, C_{n_r}, was introduced in Section 2.3 and assumes a linear relationship between yaw rate and the yawing moment it produces. It is mainly determined by the vertical tail and is always negative except possibly in a spin. A simple calculation, analogous to the calculation of pitch damping, gives

$$C_{n_r} = -2V_v C_{L_{\alpha,vt}}(\ell_t/b), \tag{2.6-39}$$

where V_v is a volume ratio for the vertical tail. It is the most important parameter in the airplane dutch roll mode (Chapter 4), and many aircraft must use an automatic control system to augment C_{n_r} (Chapter 4) because of inadequate dutch roll damping.

2.7 SUMMARY

In this chapter we have described how the aerodynamic forces and moments acting on an aircraft are created, how they are modeled mathematically, and how the data for the models are gathered. We have related these forces and moments to the equations of motion of a rigid aircraft that were derived in Chapter 1. The transformation of the equations of motion into a different set of coordinates has been demonstrated and also the derivation of a nonlinear model for longitudinal motion only. Steady-state flight conditions have been defined. It has been shown that the equations of motion can be linearized around a steady-state condition and that they can then be separated into two decoupled sets. One of these sets describes the longitudinal motion of an aircraft, and the other describes the lateral-directional motion. The linear equations have been expressed in terms of the aerodynamic derivatives, and the significance of these derivatives has been explained. In Chapter 3 we develop a number of powerful analytical and computational tools and use them in conjunction with the aircraft models developed here.

REFERENCES

Anderson, F. *Northrop: An Aeronautical History*. Los Angeles: Northrop Corporation, 1976.

Anderson, J. D., Jr. *Fundamentals of Aerodynamics*. 2d ed. New York: McGraw-Hill, 1991.

——— *Aircraft Performance and Design*. New York: McGraw-Hill, 1999.

Babister, A. W. *Aircraft Stability and Control*. Oxford: Pergamon, 1961.

Blakelock, J. H. *Automatic Control of Aircraft and Missiles*. New York: Wiley, 1965.

Bryan, G. H. *Stability in Aviation*. London: Macmillan, 1911.

Chambers, J. R., and E. L. Anglin. "Analysis of Lateral-Directional Stability Characteristics of a Twin-Jet Fighter Airplane at High Angles of Attack." *NASA Technical Note D-5361*. Washington, D.C.: NASA, 1969.

DeCamp, R. W., R. Hardy, and D. K. Gould. "Mission Adaptive Wing." *Paper 872419*, Society of Automotive Engineers, 1987.

Dommasch, D. O., S. S. Sherby, and T. F. Connolly. *Airplane Aerodynamics*. 4th ed. New York: Pitman, 1967.

Drendel, L. *SR-71 Blackbird in Action*. Carrollton, Tex.: Squadron/Signal Publications, 1982.

Droste, C. S., and J. E. Walker. "The General Dynamics Case Study on the F-16 Fly-by-Wire Flight Control System." *AIAA Professional Case Studies*, no date.

Duncan, W. J. *The Principles of the Control and Stability of Aircraft*. Cambridge: Cambridge University Press, 1952.

Etkin, B. *Dynamics of Atmospheric Flight*. New York: Wiley, 1972.

Goman, M., and A. Khrabrov. "State-Space Representation of Aerodynamic Characteristics of an Aircraft at High Angles of Attack." *Journal of Aircraft* 31, no. 5 (September–October 1994): 1109–1115.

Hoak, D. E., et al. *USAF Stability and Control DATCOM*. Wright Patterson Air Force Base, Ohio: Flight Control Division, Air Force Flight Dynamics Laboratory, September 1970.

IMSL. *Library Contents Document*. 8th ed. Houston, Tex.: International Mathematical and Statistical Libraries, 1980.

Kandebo, S. W. "Second X-29 Will Execute High-Angle-of-Attack Flights." *Aviation Week and Space Technology* (October 31, 1988): 36–38.

Kuethe, A. M., and C. Y. Chow. *Foundations of Aerodynamics*. 4th ed. New York: Wiley, 1984.

Maine, R. E., and K. W. Iliffe. "Formulation and Implementation of a Practical Algorithm for Parameter Estimation with Process and Measurement Noise." Paper 80-1603. *AIAA Atmospheric Flight Mechanics Conference*, August 11–13, 1980, pp. 397–411.

McCormick, B. W. *Aerodynamics, Aeronautics, and Flight Mechanics*. New York: Wiley, 1995.

McFarland, R. E. "A Standard Kinematic Model for Flight Simulation at NASA Ames." *NASA CR-2497*. Washington, D.C.: NASA, January 1975.

McRuer, D., I. Ashkenas, and D. Graham. *Aircraft Dynamics and Automatic Control*. Princeton, N.J.: Princeton University Press, 1973.

Nguyen, L. T., et al. "Simulator Study of Stall/Post-Stall Characteristics of a Fighter Airplane with Relaxed Longitudinal Static Stability." *NASA Technical Paper 1538*. Washington, D.C.: NASA, December 1979.

Perkins, C. D., and R. E. Hage. *Airplane Performance Stability and Control*. New York: Wiley, 1949.

Pope, A. *Wind Tunnel Testing*. New York: Wiley, 1954.

Press, W. H., B. P. Flannery, S. A. Teukolsky, and W. T. Vetterling. *Numerical Recipes: The Art of Scientific Computing*. New York: Cambridge University Press, 1989.

Queijo, M. J. "Methods of Obtaining Stability Derivatives." *Performance and Dynamics of Aerospace Vehicles*. Washington, D.C.: NASA-Langley Research Center, NASA, 1971.

Rech, J., and C. S. Leyman. "A Case Study by Aerospatiale and British Aerospace on the Concorde." *AIAA Professional Case Studies*, no date.

Ribner, H. S. *NACA Reports 819*, *820*. Langley, Va.: NACA, 1943.

Roskam, J. *Airplane Flight Dynamics and Automatic Flight Controls*. Lawrence, Kans.: Roskam Aviation and Engineering Corp., 1979.

Scott, W. B. "X-28 Proves Viability of Forward-Swept Wing." *Aviation Week and Space Technology* (October 31, 1988): 36–42.

Stevens, B. L., and F. L. Lewis. *Aircraft Control and Simulation*. 1st ed. New York: Wiley, 1992.

Stinton, D. *Design of the Airplane*. Washington, D.C.: AIAA, 1983.

——— *Flying Qualities and Flight Testing of the Airplane*. AIAA Educational Series. Washington, D.C.: AIAA, 1996.

U.S. Standard Atmosphere. *U.S. Extensions to the ICAO Standard Atmosphere*. Washington, D.C.: U.S. Government Printing Office, 1976.

Vidyasagar, M. *Nonlinear Systems Analysis*. Englewood Cliffs, N.J.: Prentice Hall, 1978.

Whitford, R. *Design for Air Combat*. London: Jane's, 1987.

Yuan, S. W. *Foundations of Fluid Mechanics*. Englewood Cliffs, N.J.: Prentice Hall, 1967.

PROBLEMS

Section 2.2

2.2-1 An airfoil is tested in a subsonic wind tunnel. The lift is found to be zero at a geometrical angle of attack $\alpha = -1.5°$. At $\alpha = 5°$, the lift coefficient is measured as 0.52. Also, at $\alpha = 1°$ and 7.88°, the moment coefficients about the center of gravity are measured as -0.01 and 0.05, respectively. The center of gravity is located at $0.35c$. Calculate the location of the aerodynamic center and the value of Cm_{ac}.

Section 2.3

2.3-1 An aircraft is flying wings level at constant altitude, at a speed of 500 ft/s, with an angle of attack of 8° and a sideslip angle of $-5°$, when it runs into gusty wind conditions. Determine the new "instantaneous" angles of attack and sideslip angle for the following cases:

(i) A horizontal gust of 20 ft/s from *left to right* along the body y-axis

(ii) A horizontal gust of 50 ft/s from dead astern

(iii) A gust of 30 ft/s, *from the right*, with velocity vector in the y-z plane, and at an angle of 70° below the x-y plane

2.3-2 Derive expressions for the derivatives of V_T, alpha, and beta, in terms of U', V', and W' and their derivatives. Check the results against Equations (2.3-10).

2.3-3 Consult the literature to find information on the significance and numerical values of the helix angle achieved by different types of fighter aircraft. Find some graphs of roll rate versus equivalent airspeed and calculate some values of helix angle. Explain the shape of the graph.

2.3-4 Program the functions for the body-axes force coefficients *CX* and *CZ*, as given in Appendix A, for the F-16 model. Write another program to use these data and plot a set of curves of lift coefficient as a function of alpha (for $-10° \leq \alpha \leq 50°$), with elevator deflection as a parameter (for $\delta e = -25°, 0°, 25°$). Determine the angle of attack at which maximum lift occurs.

2.3-5 Program the body-axes moment coefficient *CM*, as given in Appendix A, for the F-16 model. Write another program to plot a set of curves of pitching moment as a function of alpha (for $-10° \leq \alpha \leq 50°$), with elevator deflection as a parameter (for $\delta e = -25°, 0°, 25°$). Comment on the pitch stiffness and on the elevator control power.

2.3-6 Program the F-16 engine thrust model, function THRUST, in Appendix A. Write a program to plot the thrust as a function of power setting (0 to 100%), with altitude as a parameter (for $h = 0.$ 25 kft, 50 kft), at Mach 0.6. Also, plot thrust against Mach number, at 100% power, with altitude as a parameter (for $h = 0.$ 25 kft, 50 kft). Comment on these characteristics of the jet engine.

Section 2.4

2.4-1 Solve numerically the nonlinear longitudinal-equilibrium equations to determine the angle of attack and elevator deflection (both in degrees) of the following small airplane, for level ($\gamma = 0$) steady-state flight at 90 ft/s. Assume $g = 32.2$ ft/s.

Atmospheric density = $2.377 * 10^{-3}$ slugs/ft^3 (assumed constant)

Weight = 2300 lb, inertia (slug-ft^2): $I_{yy} = 2094$

Wing reference area, $S = 175$ ft^2

Mean aerodynamic chord, $\bar{c} = 4.89$ ft

Thrust angle, $\alpha_T = 0$

Lift: $C_L = 0.25 + 4.58 * \alpha$ (alpha in radians)

Drag: $C_D = 0.038 + 0.053 * C_L * C_L$

Pitch: $C_m = 0.015 - 0.75 * \alpha - 0.9 * \delta_e$ (alpha, δ_e, in radians)

Pitch damping coefficient, $C_{m_q} = -12.0$ (per rad/s)

2.4-2 Derive Equation (2.4-13), including all of the missing steps.

2.4-3 An aircraft is flying at 30,000 ft ($\rho = 8.9068 * 10^{-4}$) and has a wing lift coefficient of 1.0 and a tail lift coefficient of 1.2. The wing surface area and tail surface area are 600 ft^2 and 150 ft^2, respectively. The mean aerodynamic chord of the wing is 10 ft. The mean aerodynamic center of the wing is 10 ft ahead of the cm. The pitching moment coefficient about the aerodynamic center of the wing is -0.05. The tail is made up of a symmetric airfoil cross section; take the tail efficiency as $\eta = 1.0$. Determine the distance of the tail aerodynamic center from the cm for trimmed flight. If the aircraft weighs 50,000 lb, calculate the air speed for trimmed level flight.

Section 2.5

2.5-1 Make a block diagram of the flat-Earth vector equations of motion (2.5-1), including wind inputs, pilot control inputs, and terrestrial position calculations. Blocks included should be vector integration, moment generation, force generation, atmosphere model with Mach and dynamic pressure calculation, addition, subtraction, and cross product. The diagram should show all of the variables that would be needed in a high-fidelity simulation.

2.5-2 Repeat Problem 2.5-1 for the oblate rotating-Earth equations of motion.

2.5-3 Show that the quantity Γ in Equation (2.5-24) can be calculated from either body-axes or wind-axes quantities, with the same formula.

2.5-4 Expand the flat-Earth vector form equations of motion, Equations (2.5-1), into scalar equations. Check the results against Table 2.5-1.

Section 2.6

2.6-1 Work through the derivation of the coefficient matrices for the linearized force equations (2.6-11), (2.6-14), and (2.6-16), filling in all of the steps.

2.6-2 Fill in all of the steps in the derivation of the coefficient matrix, Equation (2.6-20), for the linearized kinematic equations.

2.6-3 Fill in all of the steps in the derivation of the coefficient matrices for the linearized moment equations (2.6-22), (2.6-25), and (2.6-26).

2.6-4 Write a program to calculate (approximately) the derivative of a function of a single variable (assumed to be continuous), given discrete values of the function. Use the program with the lookup table from Problem 2.3-5 to estimate the derivative C_{m_α} at the values of $\alpha = 0°, 10°, 20°$, and $30°$ (when $\delta e = 0°$). Determine whether the aircraft has positive pitch stiffness at these angles of attack.